

Alma Mater Studiorum – Università di Bologna

**DOTTORATO DI RICERCA IN
SCIENZE MEDICHE GENERALI E SCIENZE
DEI SERVIZI**

Ciclo 33^o

Settore Concorsuale: 06/A1

Settore Scientifico Disciplinare: MED/03

**UNDERSTANDING THE EFFECT OF MITOCHONDRIAL
COMPLEX I DEFICIENCY IN CANCER CELLS AND
THEIR MICROENVIRONMENT**

Presentata da: Nikkitha Umesh Ganesh

Coordinatore Dottorato
Prof. Fabio Piscaglia

Supervisore
Prof Giuseppe Gasparre

Co-supervisore
Dr.ssa Ivana Kurelac

Esame finale anno 2021

Acknowledgements

I would like to extend my sincere gratitude to my supervisors Prof. Giuseppe Gasparre and Dr Ivana Kurelac whose understanding, generous guidance and support made it possible for me to complete this project.

I would also express my gratitude to Camelia (my light in the lab), Laura, Giulia and Monica for being so kind and for giving their precious advice, help and motivation to help me finish this project.

I would like to acknowledge my friends and lab partners Maria, Licia, Sara, Greta and Stefano for making my life in Italy so much better and for keeping me entertained throughout the project.

To my fellow TRANSMITers for having my back. I had an absolute blast being part of this amazing group.

A special thanks to Prof Anna Maria, Dr Luisa Iommarini, Maurizio Baldassarre, Milena Pariali for their valuable inputs throughout the course of my project.

A big thanks to my family back home for always being there during the tough times and for their unconditional love and blessing.

To my best friend Taniya, thank you for always encouraging me and bringing out the best in me. The distance cannot keep us apart.

Lastly, my deepest admiration to my life partner and soul mate Manish. Without you, life would have been impossible. Thank you for just being you.

Abstract

For cancer cells, metabolic reprogramming is important for balancing energy, maintaining redox homeostasis, and synthesizing biosynthetic precursors. Thus, targeting metabolism has become a valid anticancer strategy to pursue. Among others, respiratory complex I (CI) has been identified as a valid target. In this context, a genetic ablation of mitochondrial CI enzyme in colorectals (HCT) and osteosarcomas (143B) was associated with the lack of HIF-1 α stabilization and subsequent inability to adapt to hypoxic environment, suggesting this may contribute to the anti-tumorigenic effect of CI deficiency. However, most recent data imply that, despite the lack of HIF-1 α , the progression of CI-deficient tumors seems to be supported by components of tumor microenvironment (TME), in particular tumor associated macrophages (TAMs). Thus, the aim of this thesis was (i) to prove that the lack of HIF-1 α stabilization and subsequent inability to adapt to hypoxic environment is a generalized phenomenon in murine, human cancers and in an orthotopic system and may contribute to the anti-tumorigenic effect of CI deficiency; (ii) to prove that the CI-deficient tumors activate macrophages to progress despite HIF-1 α destabilization; (iii) to identify common targetable factors responsible for macrophage recruitment among the CI deficient 143B and HCT models. By introducing a non degradable form of HIF-1 α (HIF-TM) in CI deficient models, we demonstrated that HIF-TM rescued their tumorigenic potential, mature vasculature and vessel size. Moreover, in 143B CI deficient model, lack of HIF-1 activity correlated with macrophage migration inhibitory factor (MIF) downregulation and macrophage abundance. This indicated that the disruption of HIF-1-MIF axis leading to vasculature remodeling and TAM recruitment is one of the adaptive mechanisms activated by the CI defective 143B tumors. However, this mechanism may not be generalized to the epithelial HCT model. Large-scale omics approach on CI deficient and CI competent 143B and HCT xenografts derived supernatants identified nine common metabolites secreted specifically from both the CI deficient models, allowing to hypothesize a potential cytokine-like function of these metabolites in attracting TAMs.

Table of contents

List of figures	ix
List of tables	xi
1 INTRODUCTION	3
1.1 HALLMARKS OF CANCER AND TUMOR MICROENVIRONMENT . . .	3
1.1.1 CELL POPULATIONS OF THE TUMOR MICROENVIRONMENT	3
1.1.2 HYPOXIA AS THE KEY CONDITION IN TUMOR MILIEU	5
1.2 CANCER METABOLISM	6
1.2.1 MITOCHONDRIA	8
1.2.2 MITOCHONDRIAL METABOLIC ALTERATIONS IN CANCER . .	10
1.2.3 TARGETING CANCER METABOLISM	11
1.2.4 TARGETING MITOCHONDRIAL COMPLEX I (CI) AND ITS CON- SEQUENCES ON CANCER PROGRESSION	12
1.3 METABOLIC CROSS TALK BETWEEN CANCER CELLS AND THEIR TUMOR MICROENVIRONMENT	15
1.3.1 METABOLIC COMPETITION AND COOPERATION	16
1.3.2 METABOLIC BY-PRODUCTS AS SIGNALLING MOLECULES IN TME	16
1.3.3 TARGETING MITOCHONDRIAL COMPLEX I (CI) AND ITS CON- SEQUENCES ON TME	18
1.3.4 TARGETING MITOCHONDRIAL COMPLEX I (CI) AND ITS CON- SEQUENCES ON MACROPHAGES	24
2 AIMS	25
3 EXPERIMENTAL PROCEDURES	27
3.1 CELL LINES MAINTENANCE	27
3.2 GENERATION OF TM-HIF-1 α	27

3.3	GENOME EDITING FOR GENERATION OF NDUFS3 KNOCK-OUT	28
3.4	MITOCHONDRIA ISOLATION	29
3.5	CN-PAGE	29
3.6	SDS-PAGE AND WESTERN BLOT ANALYSIS	30
3.7	CELL VIABILITY	30
3.8	RNA EXTRACTIONS, qRT-PCR	31
3.9	P53 TRANSFECTION	31
3.10	<i>IN VIVO</i> TUMOR GROWTH	32
3.11	ESTABLISHING PSEUDO-ORTHOTOPIC OSTEOSARCOMAS	32
3.12	CYTOKINE ARRAY	33
3.13	IMMUNOFLUORESCENT (IF) AND IMMUNOHISTOCHEMICAL (IHC) STAINING	34
	3.13.1 IHC	34
	3.13.2 IF	34
3.14	FLOW CYTOMETRY ANALYSIS	35
3.15	METABOLOMICS	35
3.16	PROTEOMICS	36
3.17	STATISTICAL ANALYSIS	37
4	RESULTS	39
4.1	HIF-1 α IS ACCOUNTABLE FOR LOW TUMORIGENIC POTENTIAL OF CI DEFICIENT CANCER CELLS	39
	4.1.1 INTRODUCING THE HIF-TM IN CI DEFICIENT CELLS RESCUES THEIR TUMORIGENIC POTENTIAL AND VESSEL MATURATION	39
	4.1.2 INDUCING NDUFS3 KO IN B16F10 MURINE MELANOMA MODEL LEADS TO CI INACTIVATION, INABILITY TO PERFORM OX- IDATIVE PHOSPHORYLATION AND PREVENTS HIF-1 α STABI- LIZATION IN HYPOXIA	43
4.2	MACROPHAGE ABUNDANCE IN CI DEFICIENT OSTEOSARCOMAS IS ASSOCIATED WITH DOWNREGULATION OF HIF-1-MIF AXIS	48
	4.2.1 MACROPHAGE ABUNDANCE IS ASSOCIATED WITH CI DEFI- CIENCY IN 143B XENOGRAFTS	48
	4.2.2 HIF-1-MIF AXIS CONTRIBUTES TO MACROPHAGE ABUNDANCE IN 143B CI DEFICIENT TUMORS	50
	4.2.3 MACROPHAGE ABUNDANCE IS ASSOCIATED WITH CI DEFI- CIENCY AND HIF-1-MIF DOWNREGULATION IN THE ORTHO- TOPIC OSTEOSARCOMA MODEL	54

4.3	MACROPHAGE ABUNDANCE IN COLORECTAL CI DEFICIENT TUMORS IS NOT ASSOCIATED WITH DEREGLATION OF HIF-1-MIF AXIS, REGARDLESS OF P53 STATUS	58
4.3.1	MIF IS NOT DOWNREGULATED IN HCT CI DEFICIENT TUMORS, DESPITE LACKING HIF-1 ACTIVITY	59
4.3.2	HIF-1 IS NOT ACCOUNTABLE FOR MACROPHAGE ABUNDANCE IN HCT CI DEFICIENT TUMORS	61
4.3.3	LACK OF MIF DOWNREGULATION IN CI DEFICIENT TUMORS DOES NOT DEPEND ON p53	63
4.4	NINE METABOLITES IDENTIFIED AS POSSIBLE FACTORS DRIVING MACROPHAGE ABUNDANCE IN CI DEFICIENT TUMORS	65
4.4.1	PROTEOMICS DOES NOT IDENTIFY COMMON SECRETED PROTEINS BETWEEN CI-DEFICIENT 143B AND HCT CELLS	65
4.4.2	METABOLOMICS ANALYSIS IDENTIFIES NINE METABOLITES SPECIFICALLY SECRETED BY CI-DEFICIENT MODELS	67
5	DISCUSSION	75
6	CONCLUSIONS	83
7	REFERENCES	85

List of figures

1.1	Illustration of the ten hallmarks of cancer as proposed by Hanahan and Weinberg. (Adapted from Hanahan and Weinberg, 2011).	4
1.2	The cells of tumor microenvironment: A schematic image of the components of the tumour microenvironment. Most developed solid cancers are normally surrounded by a large number of stromal cells and immune cells that infiltrate.	5
1.3	A schematic image of the mechanisms by which transcription factor HIF-1 α regulates the levels of genes involved in aerobic glycolysis, angiogenesis, erythropoiesis and pH regulation in hypoxic tumors. p- HIF-1 α is hydroxylated to proline residue in normoxia and targeted for proteasome degradation (PHD- prolyl-hydroxylase; VHL- von Hippel-lindau factor, HRE- hypoxia responsive elements (Adapted from Supuran, 2017).	7
1.4	The mitochondrial structure description. In the inner mitochondrial membrane, the ETC is embedded. The movement of the electrons through the ETC and the subsequent generation of adenosine triphosphate (ATP) is shown. Via CI or CII, electrons (e-) from reduced substrates join the ETC and are then transferred through CIII and CIV where oxygen (O ₂) has been reduced to create water (H ₂ O) (solid black lines). The inner membrane potential is decreased by protons that escape back through the mitochondrial inner membrane and into the matrix (dashed red line). Q = coenzyme Q; C = cytochrome c. (Adapted from Mcewen et al., 2011).	9
1.5	Representative image of glycolysis and TCA cycle. PPP= Pentose phosphate pathway.	11

1.6	Targeting metabolic reprogramming in cancer. In a fast proliferating cancer cell, glycolysis and TCA cycle intermediates are used for macromolecule biosynthesis (proteins, lipids and nucleotides). Energy is produced by both glycolysis and oxidative phosphorylation. Glutamine may serve for TCA cycle intermediates replenishment. Atypical accumulation of metabolites such as D-2HG may promote epigenetic remodelling. mTORC1 regulates several transcription factors to promote glycolysis and macromolecule biosynthesis. These metabolic reactions have been recognized as valid targets for cancer treatment and some of the current metabolic anti-cancer strategies are indicated in red.	13
1.7	Overview of the CI modules. In it pictured are the N-module (colored in green), iron–sulfur (Fe-S) clusters (orange spheres), Q module (in gold), Pp-proximal in violet and Pd-distal in salmon. (Giachin et al., 2016).	15
1.8	The consequences of cancer cell metabolic reprogramming on the non-malignant populations of TME. Full and dashed lines indicate respectively stimulation and inhibition. Wavy line represents metabolite exchange between cancer associated fibroblasts and cancer cells.	17
3.1	Representation of the three point mutations of the HIF-1 α ensuring a non degradable and constitutive activation of the protein, even in normoxia. . . .	28
3.2	Graphical representation of P53 transfection method in the HCT-/- cells. . . .	32
3.3	Schematic diagram representing the generation of the pseudo-orthotopic osteosarcomas in Rag1-/- FVB/n mice.	33
3.4	Experimental setting of the extraction of the conditioned media from the <i>ex vivo</i> cultures for LC-MS analysis.	36
4.1	<u>HIF-TM introduction ensures a stable, non-degradable HIF-1α protein and its translocation to the nucleus</u> (A)- Immunofluorescence of 143B-/- cells cultured <i>in vitro</i> and carrying empty vector (Mock) or HIF-TM. Magnification 200x. (B) HIF-1 α protein SDS-PAGE and Western Blot analysis of 143B-/- cells carrying empty vector (mock) and HIF-TM, cultured in 1% O ₂ and 21% O ₂ . Gamma tubulin was used as loading control.	40

- 4.2 Introducing HIF-TM in CI deficient cells rescues their tumorigenic potential
 (A) Tumor growth curves of 143B^{-/-} and HCT116^{-/-} after injection into nude mice (for each cell line: N=8, EXP=2). Data represent average tumor mass + SEM (*p<0.05, **p<0.01). Representative images of tumor masses are shown. Bars=2cm. (B) SDS-PAGE and western blot analysis of HIF-1 α protein levels. Vinculin was used as a loading control. (C) qRT-PCR analyses of xenografts for HIF-1 responsive genes SLC2A1, LDHA and VEGF. Data display mean+SEM; N=3 (*p<0.05, **p<0.01, ***p<0.001). 41
- 4.3 HIF-TM does not induce increase in the tumorigenic potential of 143B^{+/+} tumors - Tumor growth curve of the 143B^{+/+} Mock and 143B^{+/+} HIF-TM xenografts after subcutaneous injection into nude mice. Data display mean+SEM. N=6, EXP=1. 42
- 4.4 HIF-TM xenografts present with mature vessels positive for pericytes. Immunofluorescent staining analyzing vessel morphology of 143B^{-/-} Mock and 143B^{-/-} HIF-TM xenografts. SMA (green) is fibroblasts marker, Endomucin (Endo-red) is vessels marker and DAPI (blue) is nuclei marker. 43
- 4.5 Sanger sequence identifying the NDUFS3 KO clones. Electropherograms compare the wild type sequence D3-4 clone B16^{+/+} to one of the G4-2 B16^{-/-} clone carrying homozygous *c.330₃31insC* frameshift mutation. Moreover, the same clone also harbors a *c.328A > G* point mutation. The mutated nucleotides are underlined and indicated in bold black. 44
- 4.6 The identified B16^{-/-} cells from the NDUFS3 western blot cannot sustain proliferation when cultivated in low glucose or compelled to depend on OXPHOS for energy production in galactose media. (A) SDS-PAGE analysis followed by western blot identifies clones with absence of NDUFS3 protein in this representative image. Actin is used as a loading control. (B) B16^{-/-} cells cannot sustain proliferation when cultivated in low glucose or compelled to depend on OXPHOS for energy production in galactose media. Sulforhodamine B (SRB) assay was performed *in vitro* on B16F10 clones incubated for 48 hours in low glucose (5mM) or galactose (5mM). Data represent the percentage of cell proliferation (y axis) of each clone (x axis) in the stress condition normalized to time zero. The dashed red line separates the B16^{+/+} and B16^{-/-} clones. N=3, Exp=1. 45

- 4.7 The effect of NDUFS3 knock-out on CI assembly and function in selected B16-/- clones. (A) CI-in gel NADH dehydrogenase activity following clear native page in the B16+/+ and B16-/- clones. Bovine heart mitochondria (BHM) were used as a positive control and 143B-/- clone 1G5 was used as a negative control (B) Representative SDS-PAGE and Western Blot of the mitochondrial lysates isolated from the clones analyzed in (B). Succinate dehydrogenase subunit A (SDHA) was used as loading control. 46
- 4.8 B16-/- clones cannot stabilize HIF-1 α expression. SDS-PAGE and Western Blot analysis of HIF-1 α expression in B16-/- E6-1 and G4-2 clones and B16+/+ G4-5 and D3-4 clones in normoxia (N) and 1 hour and 5 hours of hypoxic conditions (h). Actin is used as a loading control. 47
- 4.9 Macrophage infiltration is a phenotype of 143B-/- tumors. Flow cytometry analysis of innate immune system populations in 143B. The contribution of macrophages (F4/80+), neutrophils (Lys6G+), dendritic cells (CD11c+F4/80-) and natural killer cells (CD49b+) is shown at day 30 post injection in ICRF nude mice. Data are mean+SEM. N= 4; (* P<0.05). (Kurelac et al., 2019) . . . 49
- 4.10 143B+/+ tumors present with necrosis. Immunohistochemistry in 143B+/+ xenograft for neutrophil marker 2b10. Scale bar: 100 μ m. 49
- 4.11 143B-/- xenografts present with higher macrophage abundance. (A) Immunofluorescence staining of 143B xenografts for macrophage marker F4/80. (B) Representative graph of the macrophage count of the 143B xenografts per field of view (FOV). Data displayed are mean \pm SEM N= 4; (* P<0.05). 50
- 4.12 MIF is one of the downregulated cytokine in HCT-/- tumors. (A) Blotting of supernatants from 143B and HCT xenograft-derived cancer cells against the human cytokine array (B) Table representing the coordinates of the cytokine in the kit and the representative graph of the cytokine array analysis. 51
- 4.13 143B-/- tumors demonstrate a higher MIF expression compared to 143B+/+. (A) qRT-PCR analysis of MIF expression in xenografts and (B) *in vitro* after 24H incubation in hypoxia (C) SDS-PAGE and Western Blot analysis of MIF expression in xenografts. Actin was used as a loading control. Data display mean \pm SEM. N = 3; (* P<0.05; ** P<0.01; ***P<0.001). 52
- 4.14 143B-/- HIF-TM tumors exhibits a higher MIF expression compared to 143B-/- Mocks due to presence of stable HIF-1 α . (A) qRT-PCR analysis of MIF expression in xenografts and (B) *in vitro* (C) SDS-PAGE and Western Blot analysis of MIF expression in xenografts. Vinculin was used as a loading control. Data display mean \pm SEM. N = 3; (* P<0.05; ** P<0.01; ***P<0.001). 53

- 4.15 143B^{-/-} HIF-TM xenografts arrest macrophage infiltration. (A) Immunofluorescence staining of 143B^{-/-} Mock and 143B^{-/-} HIF-TM xenografts for macrophage marker F480 represented in red and DAPI nuclei marker represented in blue. Magnification 40X. (B) Quantification of the macrophage count of 143B^{-/-} Mock and 143B^{-/-} HIF-TM xenografts per field of view (FOV) are represented by the graphs. Data displayed are mean \pm SEM N= 8; (***)P<0.001). 54
- 4.16 143B^{-/-} tumors had higher macrophage infiltration. Representative images of immunohistochemistry analysis for macrophage marker F4/80 in 143B xenografts at day 30 in trabecular bone (upper images) and infiltrating the tissue (lower images). Scale bars: 50 μ m. Data displayed are mean \pm SEM; (* P<0.05; ** P<0.01). 55
- 4.17 143B^{-/-} xenografts are associated with HIF-1 α destabilization and demonstrate higher immature vessels count, negative for pericytes. (A) Immunohistochemistry analysis of the HIF-1 α in 143B^{+/+} and 143B^{-/-} osteosarcomas xenografts. Scale bars: 50 μ m. (B) Immunofluorescent staining analyzing vessel morphology in CI-deficient and competent osteosarcoma xenografts. SMA (green) is fibroblasts marker, Endomucin (red) is vessels marker and DAPI (blue) is nuclei marker. Quantification of the total number of vessels per field of view (FOV), percentage of pericyte negative vessels (%Endo+SMA-) and the average vessel size in 143B^{+/+} and 143B^{-/-} tumors are represented by the graphs. Data displayed are mean \pm SEM. N=4; (* P<0.05; ** P<0.01; ***P<0.001; NS= Not significant). N=4. 56
- 4.18 143B^{-/-} xenograft derived supernatant is associated with MIF downregulation. In xenograft-derived cell culture supernatants, the results of cytokine screening. The arrows show the dot blots of the cytokine array for MIF. 57
- 4.19 143B^{-/-} pseudo-orthotopic xenografts preserved bone microenvironment. Hematoxylin and eosin staining of the trabecular bone in the 143B xenografts at day 30 and day 60 post implantation.; osteoblasts are indicated by the asterisks, osteocytes by arrows and the neoplastic cells are circled. Scale bars: 100 μ m. Quantification of osteocytes and osteoblasts in the osteosarcoma xenografts are represented by the graphs. Data displayed are mean \pm SEM; (* p < 0.05, ** p < 0.01). 58

- 4.20 Macrophage infiltration is a phenotype of HCT^{-/-} tumors. Flow cytometry analysis of innate immune system populations in HCT tumors. The contribution of macrophages (F4/80 +), neutrophils (Lys6G +), dendritic cells (CD11c + F4/80-) and natural killer cells (CD49b +) is shown at day 30 post injection in ICRF nude mice. Data are mean + SEM. (* P<0.05). 59
- 4.21 HCT^{+/+} tumors demonstrate no significant changes in MIF expression compared to HCT^{-/-} counterpart. (A) qRT-PCR analysis of MIF expression in xenografts and (B) *in vitro* after 24H incubation in hypoxia (C) SDS-PAGE and Western Blot analysis of MIF expression in xenografts. Actin was used as a loading control. Data display mean ± SEM. N = 3; (NS= not significant). . . 60
- 4.22 HCT^{-/-} HIF-TM xenografts has no significant changes in macrophage count compared to HCT^{-/-} mocks. (A) Immunofluorescence staining of HCT xenografts for macrophage marker F480 represented in red and DAPI nuclei marker represented in blue. Magnification 40X. (B) Quantification of the macrophage count of the HCT^{-/-} Mock and HCT^{-/-} HIF-TM xenografts per field of view (FOV) are represented by the graphs. Data displayed are mean ± SEM. N = 4; (NS= Not significant). 61
- 4.23 HCT^{-/-} HIF-TM tumors show similar MIF expression compared to HCT^{-/-} Mock irrespective of presence of HIF-1 α . (A) qRT-PCR analysis of MIF expression in xenografts and (B) *in vitro* (C) SDS-PAGE and Western Blot analysis of MIF expression in xenografts. Vinculin was used as a loading control. Data display mean ± SEM. N = 3; (NS= not significant). 62
- 4.24 MIF upregulation is P53-dependent and is significant in hypoxia but not normoxia in presence of a defective CI. (A) RT-PCR analysis of MIF expression in HCT^{-/-} with PMSCV mock or WT P53 or Mut P53 transfected cells after a total RNA extraction, incubated 24h in normoxia or hypoxia. HCT^{-/-} p53 PMSCV cell cultured in normoxia used as a control (B) SDS-PAGE and Western Blot analysis for MIF and p53 expression of the same cultured in normoxia or incubated in hypoxia for 24h. Actin was used as a loading control. (C) qRT-PCR analysis of P21 in HCT^{-/-} cells with either PMSCV control, WT or Mut P53 genotype incubated in normoxia (21% O₂) or hypoxia (1% O₂) for 24 hours. Data are mean ± SEM. N = 3; (* P<0.05; ** P<0.01; ***P<0.001). . . 64

- 4.25 No common secreted proteins between 143B and HCT. (A) Principal component analysis (PCA) of the proteomics data of 143B and HCT CI-deficient and CI-competent models (B) Volcano plots presenting the proteomics summary of the post *ex vivo* conditioned media of osteosarcomas 143B and colorectal HCT cancers (B) Venn diagrams using the VENNY 2.1 software showing overlap of the proteomics data of 143B and HCT secretome. 66
- 4.25 LC-MS analysis reveals nine common metabolites between 143B and HCT conditioned media. (A) Principal component analysis (PCA) of the metabolomics data of 143B and HCT CI-deficient and CI-competent models. The CI-deficient 143B and HCT is represented in green and the CI-competent 143B and HCT tumors are represented in red (B) HeatMap analysis of the metabolites after post *ex vivo* conditioned media based LC-MS analysis in 143B+/+ & 143B/- osterosarcomas and HCT+/+ & HCT/-colorectals. Data was mean normalized, log transformed and paretoscaled. The color scale indicates the relative expression levels of the metabolites across all samples(C) Venn diagrams using the VENNY 2.1 software showing overlap of the metabolomics data of 143B and HCT revealed nine secreted metabolites common to both. 70
- 4.26 Metabolites significant in both osteosarcomas 143B and colorectal HCT cancer 71
- 4.27 Summary of pathway analysis of the 143B and HCT xenograft derived supernatants showing glycolysis and selenocompound metabolism that was the most disrupted pathways. (A) The matched paths are all seen as circles. The color of each circle is dependent on p-values (in the subsequent pathway, darker colors reflect more important changes in metabolites), while the size of the circle corresponds to the impact score of the pathway. The most influenced pathways with high scores of statistical importance are annotated. The x-axis represents the pathway impact value computed from pathway topological analysis and -log of the P-value obtained from pathway enrichment analysis is represented as the y-axis. (B) Overview of the metabolite set enrichment analysis in 143B and HCT post *ex vivo* conditioned media. The intensity of the color is correlated with the degree of statistical importance of each pathway (highly significant - red, not significant - white), while the length of each bar reflects the fold enrichment of each pathway. 73

List of tables

1.1	A list of studies reporting TME-related effects of metformin and/or complex inhibition (Kurelac et al., 2019).	19
-----	--	----

LIST OF ABBREVIATIONS

AMPK: AMP activated kinase
Arg1: arginase
CAFs: Cancer associated fibroblasts
CI: Complex I
CII: Complex II
CIII: Complex III
CIV: Complex IV
CN-PAGE: Clear Native PAGE
DAB: diaminobenzidine
EDTA: ethylenediaminetetraacetic acid
ETC: Electron transport chain
GLUT1: Glucose Transporter Type 1
HIF-1: Hypoxia inducible factor 1
HRE: hypoxic responsive elements
IDH: isocitrate dehydrogenase
IMM: Inner mitochondrial membrane
IMS: Inter-membrane mitochondrial space
LDHA: lactate dehydrogenase A
MCT: Monocarboxylate transporter
MDSC: Myeloid-derived suppressor cell
mtDNA: mitochondrial DNA
mTORC1: mammalian Target of rapamycin complex I
NADH/NAD⁺: nicotinamide adenine dinucleotide
NK: Natural killer cell
OXPHOS: oxidative phosphorylation
PD-L1: Programmed death ligand 1
PHD: prolyl-hydroxylases enzymes
ROS: Reactive oxygen species

SDH: succinate dehydrogenase

TAM: Tumor associated macrophage

TCA: Tricarboxylic acid

TIL: Tumor infiltrating lymphocyte

TME: Tumor microenvironment

Treg: regulatory T-cells

VEGF: vascular endothelial growth factor

VHL: Von Hippel-Lindau

α -KG: α -ketoglutarate

Chapter 1

INTRODUCTION

1.1 HALLMARKS OF CANCER AND TUMOR MICROENVIRONMENT

Cancer is defined as an abnormal division of cells that have escaped the normal growth and survival control mechanisms, disabled by genetic mutations in their oncogenes or tumor suppressor genes (TSG). These dense complexities of cancer enabling them to transform from a normal cell to malignant cell, was organized into six major “hallmarks” by Hanahan and Weinberg in 2000, (Hanahan and Weinberg, 2000) namely: sustaining proliferative signalling, evading cell death, evading growth suppressors, enabling replicative immortality, inducing angiogenesis, and activating tissue invasion and metastasis. A decade later, the same authors added four new hallmarks: reprogramming energy metabolism, evading immune response, genome instability and mutation, and tumor-promoting inflammation (Hanahan and Weinberg, 2011) (Fig. 1.1). These hallmarks have proven to be a solid foundation for understanding the common traits acquired by cancer and rationalizes their evolution from a normal cell into malignancy and therefore in guiding their treatment.

1.1.1 CELL POPULATIONS OF THE TUMOR MICROENVIRONMENT

The tumor mass, apart from cancer cells, contains a range of infiltrating and resident cells (immune cells and stroma), extracellular matrix proteins and secreted factors cumulatively known as the tumor microenvironment (TME). The cell populations of TME include endothelial stromal cells, immune cells such, stromal fibroblasts, non-cellular extracellular matrix components such as collagen, fibronectin, hyaluron, laminin, etc; and several cell types of innate and adaptive immune cells (Fig. 1.2) (Bhagban et al., 2020). The progression of a

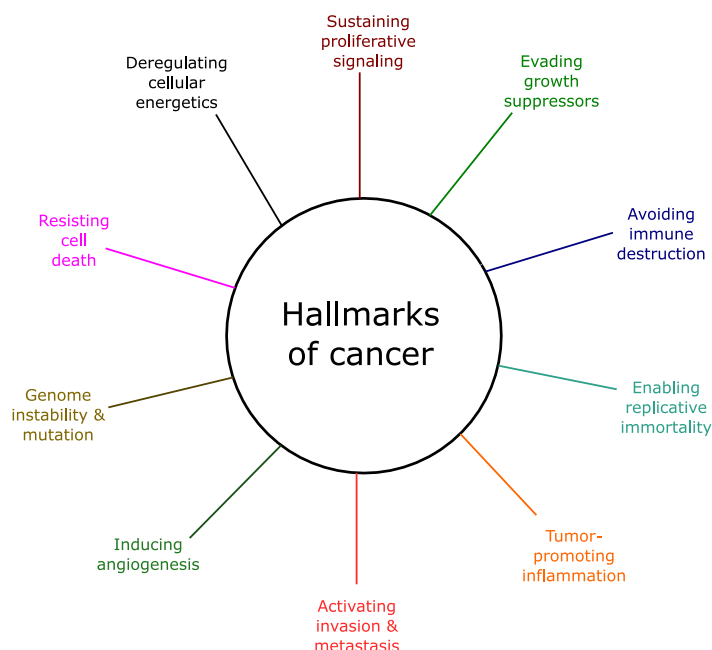
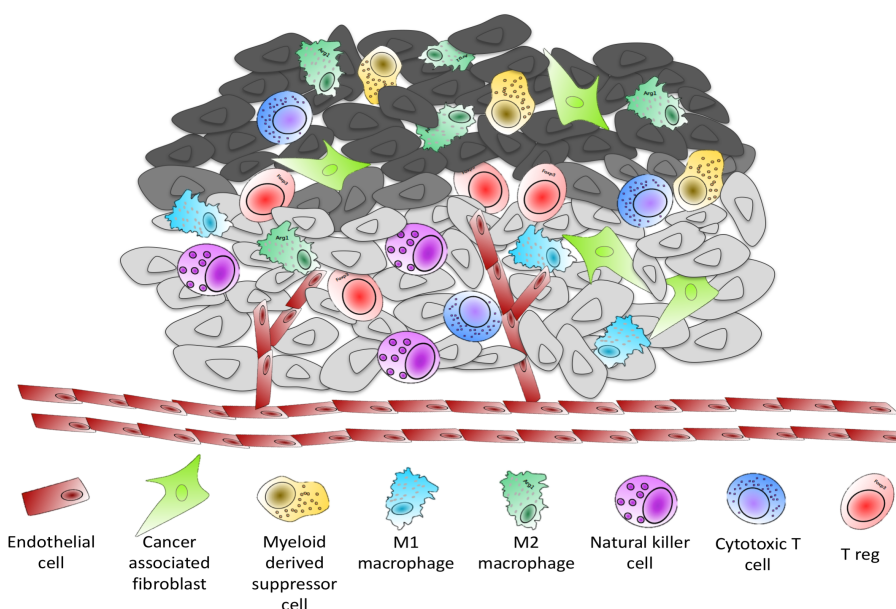


Fig. 1.1 Illustration of the ten hallmarks of cancer as proposed by Hanahan and Weinberg. (Adapted from Hanahan and Weinberg, 2011).

tumor is substantially influenced by the interactions of cancer cells with their environment, eventually determining their fate. The selection of progressing cancer cells, among other, is influenced by the cellular and non-cellular components of TME, often resulting in activation of signalling networks that promotes using non-malignant cells and their activity for tumor advantage. Tumors attract immunosuppressive (protumorigenic) myeloid-derived suppressor cells (MDSCs) and Foxp3-expressing regulatory T-cells (Tregs), while subduing immunity promoting cytotoxicity of CD4+ and CD8+ T effectors and natural killer (NK) cells (Chen and Mellman, 2017). Indeed non-malignant cells of TME are considered to facilitate tumorigenesis at all stages of cancer growth and metastasis, which is why TME has become the focus of intense research to reveal new avenues for the treatment of cancer. Depending on the tumor type and stage, the degree to which TME influences cancer cell progression varies. For example, macrophages found in tumors (TAMs) may release inhibitory cytokines such as IL-10, prostaglandins or reactive oxygen species (ROS) and are re-programmed to inhibit lymphocyte functions (Mantovani et al., 2003; Martinez et al., 2008). MDSCs may facilitate tumor development and suppress immune cell activity by copiously developing an enzyme involved in the metabolism of l-arginine, arginase 1, which synergizes with iNOS to increase the production of superoxide and NO, blunting lymphocyte responses (Ochoa et al, 2007). Stimulated cancer associated fibroblasts (CAFs) secrete stromal cell-derived factor 1 (SDF-1) to promote angiogenesis by recruiting circulating endothelial progenitor cells (EPCs) into the

tumor mass (Orimo and Weinberg, 2006). Recent evidence shows that inflammatory monocytes are recruited by tumor cells and host organ-derived chemokine chemokine (C-C motif) ligand 2 (CCL2) that differentiate into macrophages and promote efficient seeding and development of tumor cell metastases in distant metastatic lung sites (Qian et al., 2011). It has been extensively shown that signals promoting protumorigenic TME functions are cancer cell-derived. For example, tumors may produce several factors, including IL-10, VEGF, GM-CSF, which facilitate the aggregation and maturation of MDSC and Tregs and block dendritic cells (DC) as well as CD4+ and CD8+T effector functions. Furthermore, tumor cell-secreted Interleukin-4 (IL-4) facilitates macrophage polarization from pro-inflammatory (antitumorigenic) M1 to proangiogenic M2 TAMs (Vitale et al., 2019).



Tumor Microenvironment

Fig. 1.2 The cells of tumor microenvironment: A schematic image of the components of the tumour microenvironment. Most developed solid cancers are normally surrounded by a large number of stromal cells and immune cells that infiltrate.

1.1.2 HYPOXIA AS THE KEY CONDITION IN TUMOR MILIEU

Apart from harbouring different cell types, TME is characterized by a particular milieu, which due to uncontrolled fast proliferation often results in hypoxia and acidification (Petrova et al., 2018). The salient characteristic of certain tumors is that they exist in a low oxygen atmosphere (hypoxia) ranging from 0 to 2% O₂ because the rate of proliferation of tumor

cells always exceeds the rate of development of new blood vessels (angiogenesis). In a normal as well as in a cancerous cell, adaptation to hypoxia is governed by hypoxia inducible factor 1 (HIF-1), a pleiotropic transcription factor that leads to transcription of genes such as vascular endothelial growth factor (VEGF) that promotes endothelial cell formation, and glucose transporters (Glut1) which is responsible for glucose uptake and lactate dehydrogenase-A (LDHA) which regulates the conversion of pyruvate to lactate. HIF-1 are also involved in proliferation of cells, survival, and development of tumors by controlling growth promoters, oncogenes and glycolytic pathways (Masoud and Li, 2015). Moreover, HIF-1 α helps cells to monitor the decreased intracellular pH that occurs as a result of increased anaerobic glycolysis and the subsequent production of lactic acid (Weidemann and Johnson, 2008). Therefore HIF-1 mediates a transition from oxidative to glycolytic metabolism under hypoxic conditions. Hydroxylation by the prolyl hydroxylase PHD2 of a particular proline residue in HIF-1 α under well-oxygenated conditions triggers the von Hippel-Lindau (VHL) protein, which recruits an ubiquitin ligase that targets HIF-1 α for proteasomal degradation (Kaelin and Ratcliffe, 2008). In addition, HIF-1 (FIH-1) inhibiting agent represses the action of HIF-1 α transactivation using O₂ and alpha-ketoglutarate as substrates by hydroxylation an asparaginyl residue, thus preventing the interaction of HIF-1 α with the p300 protein coactivator (Lando et al., 2002). Hypoxia, on the other hand, inhibits PHDs and stabilizes HIF-1 α , which then translocates into the nucleus and dimerizes with constitutively expressed HIF-1 β , forming an active HIF-1 complex and inducing its gene transcription to facilitate glycolytic metabolism, angiogenesis and survival (Ruas and Poellinger, 2005) (Fig. 1.3). The correlation between increased HIF-1 levels and aggressive tumor growth and poor patient prognosis is supported by a large number of studies. HIF-1, which causes increase in the metabolic genes involved in glycolytic flux, coordinates the metabolic adaptation to hypoxia (Chen et al, 2014; Baba et al, 2010; Semenza, 2013).

1.2 CANCER METABOLISM

Due to their unrestrained proliferation, tumor cells have remarkably different metabolism as compared to their tissue of origin (Ward and Thomson, 2012). Considering the excess amount of nutrients utilized and excreted by the proliferating cancer cells, they undergo metabolic reprogramming that provide them with continuous supply of energy even during nutrient starvation period, allowing them to survive under severe selective pressure. Growing tumors need to generate vast amount of lipids, nucleotides, proteins and energy to maintain their growth. These anabolic processes are supported by the increase uptake of glucose and upregulation of glycolysis (Vander Heiden et al, 2009). Otto Heinrich Warburg pioneered

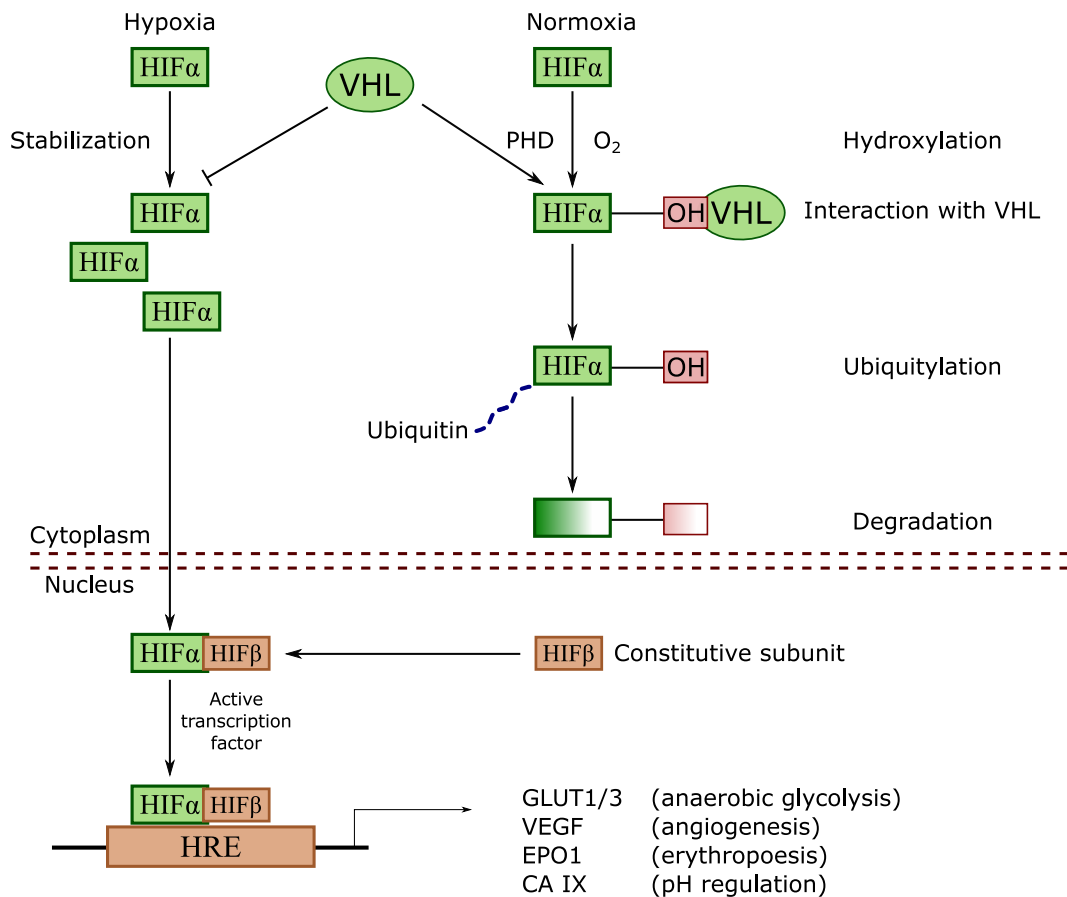


Fig. 1.3 A schematic image of the mechanisms by which transcription factor HIF-1 α regulates the levels of genes involved in aerobic glycolysis, angiogenesis, erythropoiesis and pH regulation in hypoxic tumors. p- HIF-1 α is hydroxylated to proline residue in normoxia and targeted for proteasome degradation (PHD- prolyl-hydroxylase; VHL- von Hippel-lindau factor, HRE- hypoxia responsive elements (Adapted from Supuran, 2017).

investigations of cancer cell metabolism when he described a process by which the cancer cells survived by relying on aerobic glycolysis rather than oxidative phosphorylation even in the presence of oxygen called the “Warburg effect” (Warburg, 1956). He suggested the upregulation of glycolysis is most likely due to dysfunctional mitochondria (Warburg, 1956). However, this theory has been negated over the past decade as it has been demonstrated that the upregulation of glycolysis in cancer cells is governed by oncogenic signalling (Gaude and Frezza, 2014). Moreover, it is now generally accepted that cancer cells require both glycolysis and mitochondrial respiration to survive (Koppenol et al, 2011). The molecular mechanisms involved in the metabolic reprogramming in cancer are convoluted, engaging extensive remodelling of multiple signalling pathways like the HIF-1 α , c-Myc, Ras and phosphatidylinositol-3-OH kinase (PI3K), mTOR (mammalian target of rapamycin) and AMP-activated protein kinase (AMPK) (Semenza, 2010; Shaw and Cantley, 2006; Shackelford and Shaw, 2009). During the process of glycolysis, glucose is converted into lactate to generate two ATP molecules. In cancer cells about 60% of ATP production is by glycolysis (Busk M et al, 2008). Cancer cells preferential dependence on glycolysis stems from the fact that this pathway is essential for the biosynthesis of lipids, proteins, nucleic acids, production of lactate and to maintain the NAD⁺/NADH redox balance. Presence of hypoxic core in tumors further accentuates the necessity of glycolysis (Lunt SY, Vander Heiden MG, 2011). The discerning ability of cancer cells to adapt or bypass certain metabolic process to fulfil their energy needs has been a topic of great interest to many researchers with several anti-cancer therapies being proposed to target cancer metabolism.

1.2.1 MITOCHONDRIA

Mitochondria often referred to as the powerhouse of cell are subcellular organelles inherited maternally and are essential for bioenergetics, biosynthesis, and cell signalling. Mitochondria are double lipid layered membrane organelle divided into the intermembrane space (IMS), outer mitochondrial membrane (OMM), inner mitochondrial membrane (IMM) with cristae to provide large surface area for ATP production, and the mitochondrial matrix (Fig. 1.4). Mitochondria have their own genetic system with many copies of a circular DNA (mtDNA), which is composed, of 16,569 base pairs. Only 13 proteins are encoded by the mtDNA, whereas most of the oxidative phosphorylation (OXPHOS) system is encoded by the nucleus and then translocated into mitochondria by multicomponent import machinery (Calvo and Mootha, 2010).

The most well known metabolic reaction taking place in mitochondria is OXPHOS, which results in energy production in the form of ATP. The trans-membrane electrochemical gradient that drives ATP synthesis is generated by the high pH of the mitochondrial matrix created by

Electron transport chain (ETC). The final electron acceptor is oxygen at the end of ETC, and this eventually forms water, together with ATP (Fig. 1.4). The participating ETC protein complexes include NADH dehydrogenase complex I (CI), Succinate dehydrogenase (CII), Cytochrome bc1 complex (CIII), and Cytochrome c oxidase (CIV). This generates a proton concentration gradient that is used by ATP synthase or complex V (CV), to fuel the production of ATP energy carrier molecule (Taylor and Turnbull, 2005). In addition to metabolic alterations, through their direct involvement in apoptosis and the production of reactive oxygen species (ROS), mitochondria contribute to tumorigenesis. The latter can promote oxidative stress, increase the instability of the nuclear genome, and influence signalling pathways involved in cell proliferation, differentiation, and hypoxia adaptation (Storz, 2005). In addition, mutations in mtDNA typically end up impacting protein translation or structure provided the highly compressed organization of mtDNA, which is mainly coding. Moreover, the key sites of ROS development are respiratory CI and CIII and have been designated as causative for the high mutational rate of mtDNA, especially in the context of somatic mutation generation (Leone et al., 2018). In a number of human cancers, alterations in mtDNA have also been identified. For example, subsets of hepatocellular carcinomas and prostate cancers were associated with a mutation in the D-loop region of CI (Nomoto et al., 2002).

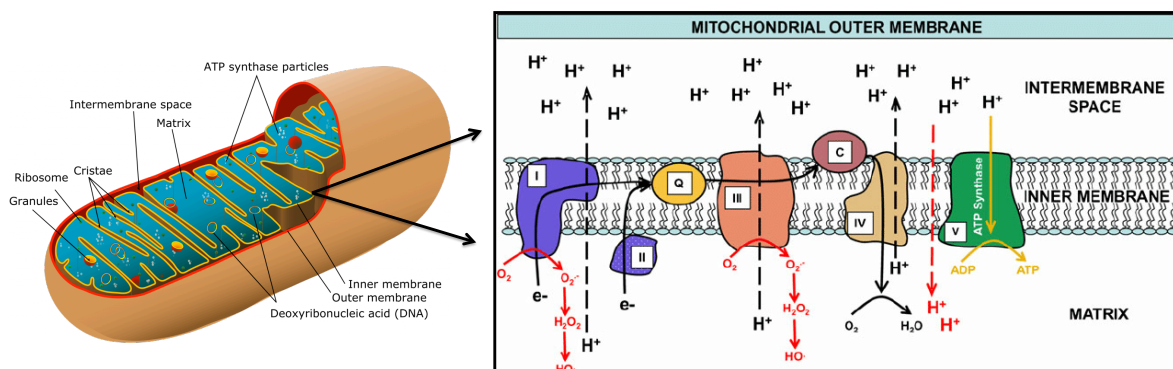


Fig. 1.4 The mitochondrial structure description. In the inner mitochondrial membrane, the ETC is embedded. The movement of the electrons through the ETC and the subsequent generation of adenosine triphosphate (ATP) is shown. Via CI or CII, electrons (e^-) from reduced substrates join the ETC and are then transferred through CIII and CIV where oxygen (O_2) has been reduced to create water (H_2O) (solid black lines). The inner membrane potential is decreased by protons that escape back through the mitochondrial inner membrane and into the matrix (dashed red line). Q = coenzyme Q; C = cytochrome c. (Adapted from Mcewen et al., 2011).

1.2.2 MITOCHONDRIAL METABOLIC ALTERATIONS IN CANCER

Although cancer cells show upregulated glycolysis, under the condition of limited nutrients, i.e, glucose deprivation, they increase the mitochondrial respiration to survive (Smolková et al., 2010). A central mechanism for the synthesis of sugars, lipids and amino acids is the TCA cycle (Fig. 1.5). It is typically viewed in a naive view of a cyclic mitochondrial pathway that continuously oxidizes the acetyl moiety of acetyl-coenzyme A to CO₂, forming nicotinamide adenine dinucleotide (NADH) and flavin adenine dinucleotide (FADH₂), whose electrons power the ATP generating mitochondrial respiratory chain (Cardaci and Ciriolo, 2012). Interestingly, we now know that a typical cellular reaction to disrupted mitochondrial metabolism is glutamine-dependent reductive carboxylation. This mechanism acts as the predominant metabolic strategy to generate lipids for the growth of cancer cells and can be acutely induced through ETC inhibition. Reductive carboxylation is induced by a disruption caused by ETC impairment in the redox ratio of the mitochondria, reducing the NAD⁺/NADH ratio and making the TCA's oxidative role less effective (Mullen et al., 2011; Gaude et al., 2018; Fendt et al., 2013). TCA is also fuelled by process called glutaminolysis, which involves catabolizing glutamine by glutaminase (GLS) to produce ATP. In order to use a significant fraction of TCA cycle intermediates as precursors for biosynthetic pathways, glutamine metabolism enables cells to retain an adequate anaplerotic flux (DeBerardinis et al., 2008). In addition, many cancers overexpress fatty acid synthase (FASN), a key biosynthetic enzyme involved in lipogenesis to synthesize fatty acids de novo, to provide lipids for membrane formation, energy production via β -oxidation and lipid modification of proteins to fulfil the requirement of the rapidly proliferating cells (Ogino et al., 2008). Therefore even with impaired mitochondrial mechanism, cancer cells implement different energy acquisition pathways to progress. Cellular metabolism reprogramming occurs both directly and indirectly as a result of oncogenic mutations. Mutations in the metabolic genes such as FH, SDH, IDH that leads to the accumulation of certain metabolites like succinate, fumarate and (R)-2-hydroxyglutarate (HG), act as oncogenic signalling molecules in variety of human tumors (Gaude and Frezza, 2014). IDH mutations are gain-of-function mutations at odds with SDH and FH loss of function mutations and confer on the enzyme the capacity to generate the oncometabolite D-2-hydroxyglutarate (D-2HG). These oncometabolites share the ability to inhibit alpha-ketoglutarate (α -KG)-dependent enzymes that regulate epigenetic gene expression, such as histone lysine demethylases of the Jumonji domain (JMJ) and ten-eleven translocation (TET) dioxygenases, resulting in the expression of a potentially oncogenic transcriptional program associated with a terminal differentiation block (Xiao et al., 2012; Xu et al., 2011; Saha et al., 2014). Interestingly, succinate and fumarate accumulation is not only caused by primary mitochondrial defects, but may also be derived from oncogenic protein signalling such as KRAS (Masgras et al., 2017). Mutations in all the

above mentioned enzymes of the TCA cycle compel cells to rely on a truncated TCA cycle that results in the stabilization of the subunits of HIF-1 α , even during presence of oxygen resulting in a pseudo-hypoxic phenotype.

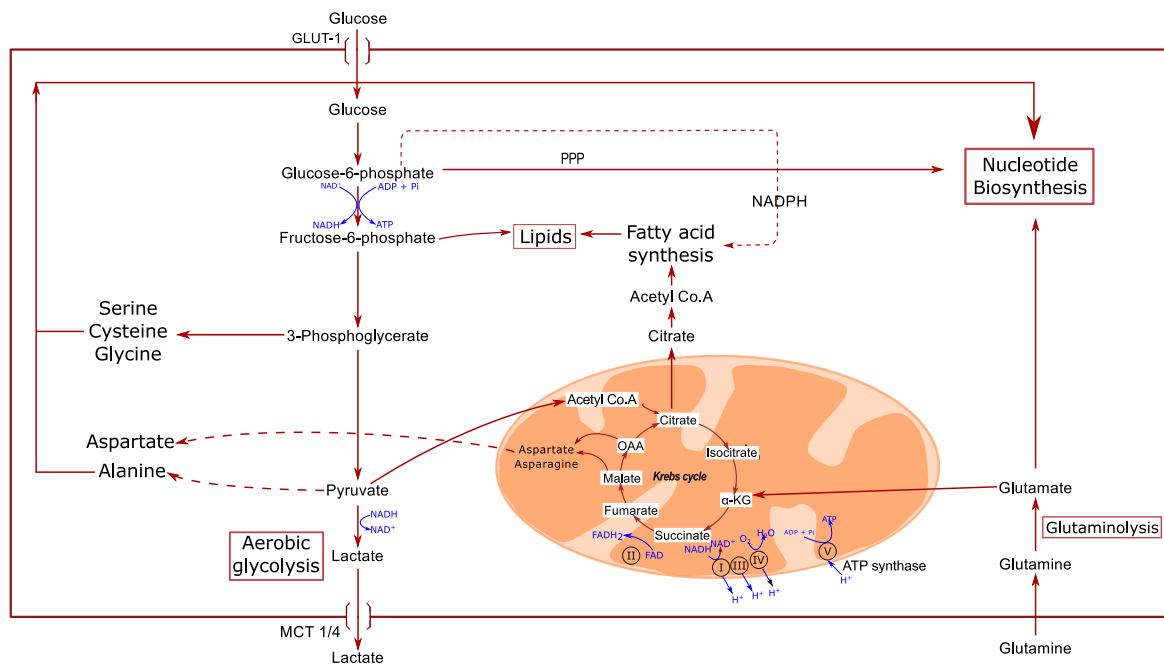


Fig. 1.5 Representative image of glycolysis and TCA cycle. PPP= Pentose phosphate pathway.

1.2.3 TARGETING CANCER METABOLISM

Through selective toxicity against proliferating cells, the earliest anticancer drugs focused on targeting cancer metabolism. Sidney Farber in 1947, found that in children with acute lymphoblastic leukemia, aminopterin (folate analog) could induce disease remission. This early therapeutic success of antifolates has since led to development of drugs called antimetabolites. Small molecules resembling nucleotide metabolites are the antimetabolites that also inhibit the function of enzymes involved in nucleotide base synthesis. For example, the 5-fluorouracil(5-FU) pyrimidine analog, a synthetic uracil analog, inhibits thymidylate synthase, limiting thymidine nucleotide supply for DNA synthesis. Today, 5-FU and the associated 5-FU-prodrug capecitabine remain frequently used in chemotherapy and are an effective medication for gastrointestinal cancer (Heidelberger et al., 1957; Wagner et al., 2007). The purine and pyrimidine antimetabolites, some of the earliest anticancer drugs, specifically attack essential metabolic pathways needed for proliferation. These include the drugs gemcitabine and cytarabine, which are integrated into DNA, resulting in DNA polymerase inhibition (Parker,

2009). Lactate has been identified in the microenvironment of almost every solid tumor type. There has been emerging evidence that argues lactate plays a fundamental role in regulating different signalling pathways to promote tumor progression. MCTs inhibitors such as α -cyano-4-hydroxy-cinnamic acid (ACCA, 4CIN, CHCA) and techniques like silencing MCTs by siRNA have already been utilized as promising cancer therapeutics (Matthew, 2010; Lee, 2016). Pharmacological agents, which inhibit IDH1 and IDH2 mutants, is developed and tested for an anti-tumor efficacy. AGI-5198, which targets mutant IDH1, for instance reduces the rate of intratumoral D-2HG, inducing expression of genes implicated in glial cells differentiation and inhibits development in IDH1-mutant human glioma cells (Rohle et al., 2013). A particular mutant IDH2 inhibitor, AG-2211 (enasidenib) provides survival advantage in a mouse model of IDH2-AML mutation (Quivoron et al., 2014; Yen et al., 2017). Present glutaminolysis targeting efforts have mainly centered on inhibiting glutaminase. In cancer trials in patients, one potent glutaminase inhibitor, CB-839, is currently being tested. (William et al., 2014). Targeting FASN has been shown to decrease tubulin palmitoylation and interrupt the organisation of microtubules, inhibiting development in tumor cells (Heuer et al., 2017). While arginine is not critical in normal tissue, some solid cancers do not produce argininosuccinate synthetase (ASS), and are instead auxotrophic to arginine and are thus susceptible to its depletion (Riess et al., 2018). Several lines of evidence indicate that autophagy mediated by PI3K / Akt / mTOR pathway may be a viable target to prevent drug resistance and increase tumour cell chemosensitivity (Xu et al., 2020). While several inhibitors have been developed (Fig. 1.5) and are currently in clinical trials, owing to their effects on mitochondrial reprogramming in cell bioenergetics and cell trafficking, they have not shown exciting results in patients (Caino et al., 2015)

1.2.4 TARGETING MITOCHONDRIAL COMPLEX I (CI) AND ITS CONSEQUENCES ON CANCER PROGRESSION

CI is the ETC 's rate limiting and first enzyme. It is crucial for the production of cellular energy, supplying about 40 percent of the proton motive force required for ATP synthesis (Sazanov, 2014). It oxidizes NADH to NAD⁺ and donates the released electrons to the coenzyme Q10 (CoQ10, also known as ubiquinone) electron carrier, linking this mechanism to the translocation from the mitochondrial matrix to the intermembrane space of four protons (Sazanov, 2014). CI is made up of 45 distinct subunits in humans, seven of which (the ND subunits) are encoded by mtDNA and the others by the nuclear (nDNA) genome (Fig. 1.7). CI contributes to the proton-motive force (PMF) needed by the FoF1-ATP-synthase (CV) to drive different mitochondrial functions, including ATP production (Koopman et al., 2010). The ETC and CV together

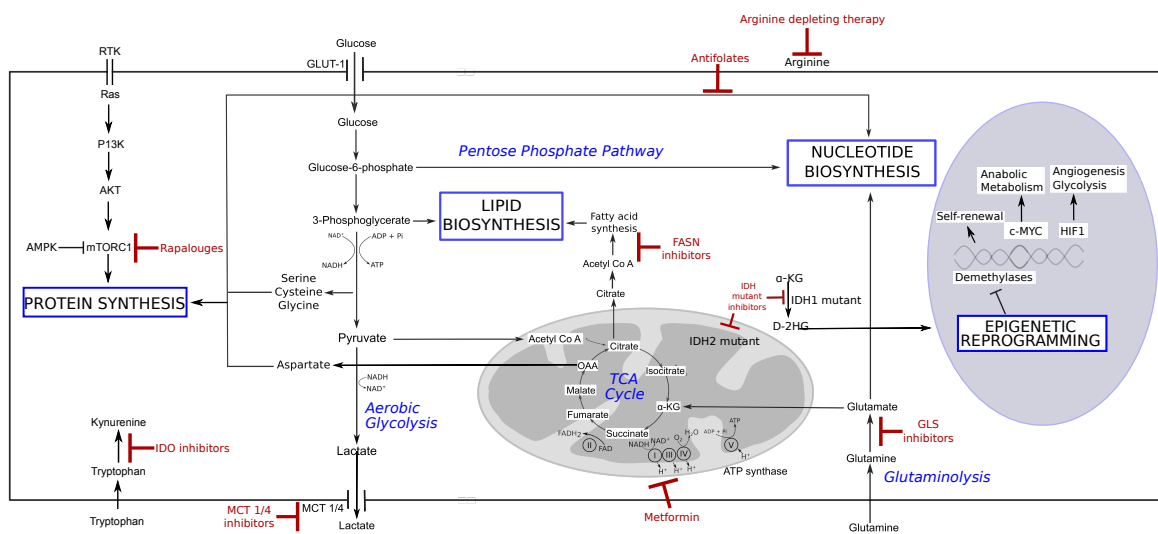


Fig. 1.6 Targeting metabolic reprogramming in cancer. In a fast proliferating cancer cell, glycolysis and TCA cycle intermediates are used for macromolecule biosynthesis (proteins, lipids and nucleotides). Energy is produced by both glycolysis and oxidative phosphorylation. Glutamine may serve for TCA cycle intermediates replenishment. Atypical accumulation of metabolites such as D-2HG may promote epigenetic remodelling. mTORC1 regulates several transcription factors to promote glycolysis and macromolecule biosynthesis. These metabolic reactions have been recognized as valid targets for cancer treatment and some of the current metabolic anti-cancer strategies are indicated in red.

constitute the system of OXPHOS. To perform the catalytic function of CI, only 14 evolutionary conserved CI core subunits are needed, seven coded by mtDNA (ND1, ND2, ND3, ND4, ND4L, ND5, ND6) and seven coded by nDNA (NDUFB1, NDUFB2, NDUFB3, NDUFB4, NDUFB5, NDUFB6, NDUFB7) (Roostenberg et al., 2011). In many pathological disorders, such as neurodegenerative diseases (Rodenberg, 2016; Marin et al., 2013), diabetes (Elango et al., 2014), and cancer (Kurelac et al., 2013; Iommarini et al., 2013), defects in nuclear and mitochondrial genes encoding CI subunits are a contributing factor. These findings are however contentious with respect to cancer. The differential effects of CI on tumor progression depend upon the severity of its impairment (Iommarini et al., 2013). Although CI gene mutations has shown to encourage prostate, thyroid, renal, lung, colorectal, breast and head and neck tumors progression (Allergra et al., 2006; Akouchekian et al., 2011; Horton et al., 1996; Kim et al., 2016, Su et al., 2016; Yu et al., 2015), multiple studies by our group show opposite effects of CI mutations on tumor progression (Iommarini et al., 2013; Calabrese et al., 2013). This emphasizes the role of CI as an “oncojanus” (Gasparre et al., 2011). The action of CI is necessary to retain the cellular NAD⁺ pool and the NAD⁺/NADH ratio required to support the action of MDH2, oxidoreductase-dependent NAD⁺/NADH ratio and aspartate generation. Consequently, inhibition of CI affects the equilibrium of NAD⁺/NADH, causing a reduction in electron acceptors. This in turn limits aspartate synthesis, which is a precursor of the synthesis of purine and pyrimidine required for cell proliferation for the biosynthesis of nucleic acids and macromolecules (Birsoy et al., 2015; Sullivan et al., 2015). In addition, inhibition of CI, which is required for the maintenance of the NAD⁺/NADH ratio for the induction of hypoxia adaptive mechanisms through HIF-1 α , results in the accumulation of NADH, which in turn causes the inhibition of α -ketoglutarate (α -KG) dehydrogenase, thereby increasing the α -ketoglutarate/succinate (α KG/Suc) ratio, which favors the activity of the prolyl-hydroxylases in charge of the degradation of HIF-1 α , resulting in tumor growth arrest (Gasparre et al., 2013; Selak et al., 2005; Calabrese et al., 2013). Targeting CI influences tumorigenesis and cancer progression via various pathways. Modulating CI activity affects the development of ROS, the rate of oxygen intake, the levels and use of NADH, the generation of ATP, the use of metabolic pathways and the quantity of signalling metabolites, as explained in the review by Vatrient et al., 2015. Several small molecule CI inhibitors are now being used as anti-cancer strategies, such as carboxyamidotriazole (CAI) BAY 87-2243, fenofibrate, metformin, phenofornin, caulerpin, canagliflozin, and AG311 compounds. The mechanism of action of these inhibitors is triggered by ATP depletion, an increase in the development of ROS that inhibits the signalling of AMP-activated protein kinase (AMPK), angiogenesis and also by HIF-1 α destabilisation (Ju et al., 2016; Agani et al., 2002; Liu et al., 2009; Cheong et al., 2011; Villani et al., 2016; Bastian et al., 2017). This is also in agreement with the study by Iommarini et al., 2014, where the

authors showed that CI-defective cancer cells display an increase cellular AMP/ATP ratio and AMPK activation under metabolic stress conditions (Iommarini et al., 2014). Furthermore, in low nutrient conditions, CI dysfunction was found to increase cellular AMP/ATP ratio, eventually leading to activation of AMPK, by slowing down biosynthetic reactions (Faubert et al., 2013). Thus, CI enzyme can be used as a target for the development of new anticancer therapies, considering its important role in regulating metabolism, hypoxic adaptation and cell proliferation.

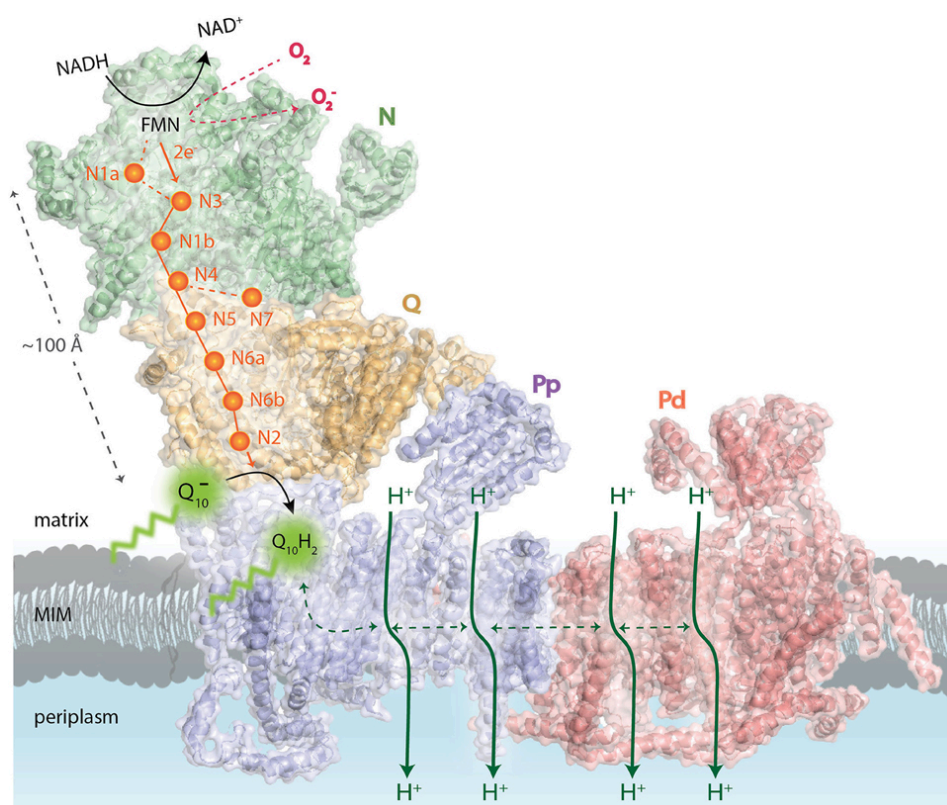


Fig. 1.7 Overview of the CI modules. In it pictured are the N-module (colored in green), iron–sulfur (Fe-S) clusters (orange spheres), Q module (in gold), Pp-proximal in violet and Pd-distal in salmon. (Giachin et al., 2016).

1.3 METABOLIC CROSS TALK BETWEEN CANCER CELLS AND THEIR TUMOR MICROENVIRONMENT

Recent years have seen an outburst of reports revealing that tumor metabolism highly depends on the relationship between malignant cells and the cell populations of TME. As a consequence of metabolite shortage in TME, a series of metabolic relationships are developed between cancer

cells and their neighboring non-malignant cell populations, which apart from available nutrient competition may incorporate mutually beneficial interactions or parasitosis-like phenomena.

1.3.1 METABOLIC COMPETITION AND COOPERATION

Apart from nutrients and waste, poor tissue coverage and irregular tumor vasculature limit the exchange of gases and create hypoxic areas. The hypoxic reaction contributes to increased tumor glycolytic activity and excessive deposition of lactate. The lactate build-up acidifies the TME, which affects how the immune system detects and manages a neoplastic lesion. In addition, nutrient restriction in the TME provides a framework for immune, stromal, and cancer cells where they are in constant competition for nutrients essential for biosynthesis, bioenergetic, and effector activities (Fig. 1.8). Immune cells tend to be less suited to nutritional rivalry, and this is a crucial anti-tumor immunity control mechanism. For example, cancer cells deplete vital nutrients, such as glucose from the TME and thereby avoid cytotoxic T cell activation. (Chang et al., 2015). As the amino acid serine is an important metabolite for the expansion of effector T-cells, local serine depletion by cancer cells is also likely to inhibit penetration and activation of immune cells (Ma et al., 2017). Although immune cells are vying for nutrients with cancer cells, CAFs demonstrate a symbiotic relationship with cancers. When in contact with pancreatic cancer cells, pancreatic CAFs, originated from activated pancreatic stellate cells (PSCs), excrete alanine. Pancreatic cancer cells then capture this alanine and use it to drive macromolecular biosynthesis. In addition, alanine secretion from PSCs requires autophagy activation, which is induced by cancer cells. Collectively, these findings reveal a metabolic crosstalk pathway between PSCs and cancer cells, where pancreatic cancer cells transmit signals to trigger autophagy in PSCs, which promotes access to alanine in the pancreatic TME to promote tumor growth (Sousa et al., 2016).

1.3.2 METABOLIC BY-PRODUCTS AS SIGNALLING MOLECULES IN TME

To create a hostile metabolic environment for immune cells, cancer cells tend to secrete excess metabolites. Metabolites also act as signalling molecules, in addition to their role in biosynthesis, through autonomous and non-autonomous mechanisms. In the latter case, in neighboring cells, metabolite shared within the TME regulates signal transduction and gene expression. In this context, lactate has been acknowledged as a bioenergetics substrate rather than a metabolic waste (Garcia et al., 2016). The most well-known effect of lactate and acidosis on TME regards its promotion of angiogenesis, either by directly acting on endothelial cells (Vegran et al., 2011) or indirectly by instigating the secretion of VEGF (Fukumura et al.,

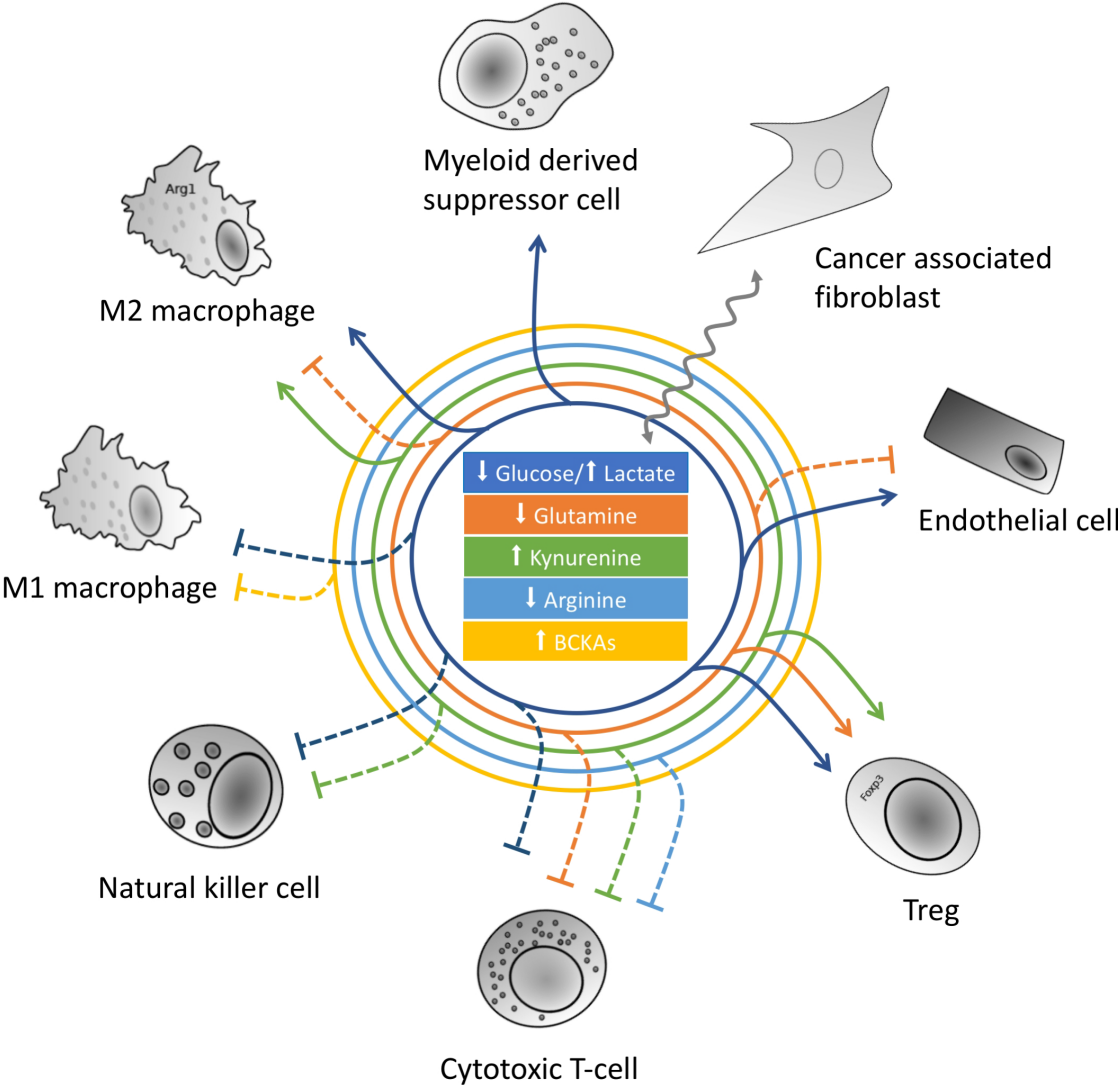


Fig. 1.8 The consequences of cancer cell metabolic reprogramming on the non-malignant populations of TME. Full and dashed lines indicate respectively stimulation and inhibition. Wavy line represents metabolite exchange between cancer associated fibroblasts and cancer cells.

2001) from tumor cells and TAMs (Colegio et al., 2014). Apart from its role in promoting angiogenesis, lactate was also associated with suppression of the anti tumor immune response by inducing an increase in the numbers of myeloid-derived suppressor cells (MDSCs) and therefore inhibiting function of natural Killer (NK) cells. Moreover, lactate also perturbs the metabolism of the T cells and protects the tumor cells from the cytotoxic T-cell targeting (Husain et al., 2013; Brand et al., 2016; Fischer et al., 2007). Similarly, lactate also facilitates the induction of M2 macrophage phenotype (Mu et al., 2018; Chen, 2017; Colegio et al., 2014) (Fig. 1.8). More recently, cancer-secreted succinate, in addition to stabilizing HIF-1 α expression, induced macrophage polarization and increased macrophage migration and cancer metastasis (Wu et al., 2020). The other ways by which the metabolic activity of cancer cell alters the tumor microenvironment and promotes them to support tumor development is by the release of kynurenine (Kyn), another metabolic waste, eventually blunting the immune cell function. IDO and Kyn, the byproduct of tryptophan degradation, can induce FoxP3 expression and the generation of Treg cells and can blunt the generation of TH17 helper cells in cancer cells (Romani, 2008; Sharma et al., 2009). These studies provide further evidence that tumor metabolism and immunity are tightly interconnected.

1.3.3 TARGETING MITOCHONDRIAL COMPLEX I (CI) AND ITS CONSEQUENCES ON TME

Despite the involvement of all components of immunity in a host, it is a daunting clinical task to establish how components of TME, tumor metabolism and immune checkpoints all play a part in the effective survival and dissemination of tumors. However, non-specific toxicity poses a significant challenge in the use of metabolic inhibitors for anti-cancer therapy, as all host cells that also contain TME use the same survival metabolic pathways. In this regard, the use of metabolic drug can also cause unintentional adverse effects on the TME (Table 1). For example, it has been shown that mTOR inhibitors have pleiotropic effects on multiple immune cells and endothelial cells. An active area of research is the role of mTOR in controlling the differentiation and function of CD8 + T cells, as well as the effect of inhibition on these cells. While some studies indicate that mTOR inhibition can promote the function of memory T, other results indicate that T cells lacking mTOR differentiate into Tregs (Conciatori et al., 2018). CI inhibition by BAY87-2243 on H460 lung cancer xenografts in nude mice caused HIF-1 α deactivation and reduced HIF-1 mediated gene expression (Ellinghaus et al., 2013). Metformin and Phenformin targeted both breast cancer cells and white adipose tissue endothelial progenitor cells *in vivo* and *in vitro*, resulting in profound effects on angiogenesis of breast cancer and their metastatic development, possibly due to additive effects on both tumor and TME cells

(Orecchioni et al., 2015). Metformin also reduced production of angiogenesis related proteins like VEGF, Angiogenin, MMP-9 in Human MDA-MB-436 breast cancer (Wang et al., 2015). In addition, AG311 CI inhibitor destabilized HIF-1 α in hypoxia and reduced expression of HIF-1 target genes in breast cancers (Bastein et al., 2017). Metformin treatment also increased T-cell infiltration into murine melanoma tumors *in vivo* (Pereira et al., 2018). Of note, although a growing body of epidemiological and clinical studies report metformin as a viable anti-cancer drug, the subject is still controversial. Although there is a bulk of literature reporting the effect of metformin on the TME, there is a lack of evidence regarding the effects of other anti-metabolic drugs on TME, pressing the importance of considering this parameter for future studies.

Table 1.1 A list of studies reporting TME-related effects of metformin and/or complex inhibition (Kurelac et al., 2019).

	TME model	Experimental setting	Effect of metformin (or other complex I inhibitors)
Endothelial cells	<i>in vivo</i> vessels (muscle)	C57BL/6	increased capillary density, upregulated VEGF and promoted angiogenesis in Ischemic Tissue <i>in vivo</i>
	C2C12	<i>in vitro</i>	increased VEGF mRNA expression in C2C12 myotubes
	indirect effect	MDA-MB-435 (expresses melanocytic markers) xenografts in nude mice	increased VEGFA production <i>in vitro</i> and <i>in vivo</i> , increased microvascular density (reduced Ki-67)
	indirect effect	A374, Mel-HO, MDA-MB-435 melanoma xenografts	increased VEGFA production in cancer cells
	indirect effect	H460 lung cancer xenografts in nude mice	BAY 87-2243 complex I inhibitor caused HIF-1 α deactivation and reduced in HIF1-mediated gene expression
	indirect effect	HCT116p53-/-	reduced HIF1, VEGF and CAIX <i>in vitro</i> and <i>in vivo</i> in xenografts

	indirect effect	Human MDA-MB-436 breast cancer <i>in vitro</i>	metformin and phenphormin reduced production of angiogenesis-related proteins (IGFBP-2, PDGFAA, VEGF, Angiogenin, MMP-9 and endostatin)
	<i>in vivo</i> vessels	FVB mice injected with murine MMTV-ErbB2 BC cells	reduced microvascular density and endothelial cell component in the tumors
	<i>in vivo</i> vessels	matrigel sponge assay in C57Bl6 mice	reduced angiogenesis
	HUVEC	<i>in vitro</i>	reduced endothelial cell proliferation, migration and network formation
	indirect effect	HepG2, Huh7 hepatocellular carcinoma cell lines	HIF1, CAIX and Glut1 downregulation <i>in vitro</i> and <i>in vivo</i> in xenografts
	HUVEC	co-culture with 4T1 or MDA-MB-453 breast cancer cells	reduced proangiogenic capacity of metformin pre-treated cancer cells
	<i>in vivo</i> vessels (tumor)	4T1 tumors in Balb/c mice	reduced vessel leakiness and smaller vessel size/diameter in tumors
	<i>in vitro</i>	MDA-MB-435 and MDA-MB-231 <i>in vitro</i>	AG311 CI inhibitor destabilized HIF-1 α in hypoxia and reduced expression of HIF1-target genes
	indirect effect	GBC-SD xenograft model	HIF1 and VEGF downregulation in GBC cells
	indirect effect	143B (osteosarcoma) and HCT116p53 ^{-/-} (colorectal cancer) xenografts in nude mice	genetic knock-out of CI in cancer cells prevented HIF-1 α stabilization, reduced vessel size and number of pericyte-positive vessels
Fibroblasts	hTERT-BJ1 (Human immortalized fibroblasts)	co-culture with MDA-MB-231 breast cancer cell lines	overexpression of mitochondrial uncoupling proteins induced high-energy nutrient production in fibroblasts, which may support cancer cell survival in a paracrine fashion
	MRC5 fibroblast cell line	organotypic co-culture with SKOV3	metformin reduced CAF-mediated support of cancer cell progression

	MRC5 fibroblast cell line	co-injection of MRC5 and SKOV3 in NOD/SCID mice	tumors in which MRC5 were primed with metformin increased sensitivity to cisplatin
	patient-derived CAFs	ovarian cancer	reduced IL-6 secretion
	<i>in vivo</i> CAFs	pancreatic adenocarcinoma 6606PDA orthotopic in C57BL/6	no effect on collagen I deposition by activated stromal cells
	gastric cancer patient derived CAFs	co-culture with SGC-7901, BGC823, GES-1 and MGT-803 gastric cancer cell lines	suppressed proclonogenic CAF effect on cancer cells
	<i>in vivo</i> CAFs	143B (osteosarcoma) and HCT116p53-/- (colorectal cancer) xenografts in nude mice	genetic knock-out of CI in cancer cells associated with stromal component abundance in tumors
Macrophages	RAW.264.7	<i>in vitro</i> LPS stimulation	inhibited NF-KB pathway (translocation of RALA into the nucleus)
	RAW.264.7, <i>ex vivo</i> peritoneal macrophages (C57/BL6)	<i>in vitro</i> LPS stimulation	suppressed TNF- α and IL-6 expression
	<i>ex vivo</i> PBMCs from healthy human donors	<i>in vitro</i> LPS stimulation, co-culture with BxPC-3 pancreatic cancer	decreased number of CD68+ cells, decreased LPS-induced cytokine secretion (IL-6, IL-8, IL-1b, TNF- α and IL-10)
	RAW.264.7	<i>in vitro</i>	induced expression of M2 markers (Arg1, IL-4 and IL-10) and downregulated IL-1b and IL-6
	RAW.264.7	co-culture with HepG2 hepatocellular carcinoma cells	upregulated proinflammatory factors (IL-6, IL-1b, TNF- α , MCP-1)

<i>in vivo</i> TAMs	pancreatic cancer: PAN02 (in C57BL/6) and AK4.4 (in FVB)	decreased number of TAMs, decreased Arg1 and IL-10 mRNA, decreased IL-1b and CXCL1 protein
<i>ex vivo</i> BMDM (C57/BL6)	<i>in vitro</i> LPS stimulation	metformin and rotenone decreased IL-1b, TNF- α and increased IL-10 expression
THP-1	<i>in vitro</i> PMA stimulation	reduced CD206 receptor expression, and MRC1 and dectin mRNA
RAW.264.7	<i>in vitro</i> IL-13 stimulation	reduced M2 signature (Mrc1, Ppar γ , Ccl24, Ccr2, Mgl2, Retnla, and Arg1)
<i>in vivo</i> TAMs	Lewis lung carcinoma (in C57BL/6)	no difference in TAM numbers, but reduced CD206 receptor expression
THP-1	<i>in vitro</i> PMA stimulation	reduced monocyte to macrophage differentiation (reduced TNF- α , IL-1b, MCP-1)
serum cytokine levels	Apo-/- mice (unknown background)	reduced TNF- α , MCP-1 and increased IL-10 in serum
THP-1/RAW.264.7	co-culture with LNCap/RM1 prostate cancer	inhibited cancer cell-mediated macrophage migration
<i>in vivo</i> TAMs	adenocarcinoma of the mouse prostate/metformin treated human prostate tumors	reduced macrophage abundance in tumor tissue
<i>ex vivo</i> BMDM (C57BL/6)	calvaria model of osteolysis	increased CD206 expression, decreased TNF- α and IL-6, increased IL-10
<i>in vivo</i> adipose tissue macrophages	obese C57BL/6 mice	decreased serum levels of the proinflammatory cytokines IL-6 and TNF- α , lowered the expression of the M1 macrophage markers CD11c and MCP-1 in adipose tissue
RAW.264.7	<i>in vitro</i> palmitate stimulation	reduced the secretion of IL-6 and TNF- α
<i>ex vivo</i> BMDM (C57BL/6)	<i>in vitro</i> palmitate stimulation	decreased the ratio of M1/M2 macrophages (increased CD206 expression)
<i>in vivo</i> TAMs	4T1 breast cancer in BALB/c	increased CD68+ in tumors, higher iNOS, lower Arg1 expression

	RAW.264.7	<i>in vitro</i> IL-13 stimulation	reduced Arg1 expression, no effect on iNOS
	<i>in vivo</i> TAMs	143B (osteosarcoma) and HCT116p53 ^{-/-} (colorectal cancer) xenografts in nude mice	higher number of F4/80, higher number of Ly6C ⁻ monocytes, no difference in CD206 expression
	<i>in vivo</i> TAMs		genetic knock-out of CI in cancer cells induced higher TAM abundance, higher number of Ly6C ⁻ monocytes, no difference in CD206 expression and reduction of Arg1 expression
T-cells	<i>in vivo</i> TILs	RLmale1 tumors in Balb/c mice	increased of total number of TILs
	<i>ex vivo</i> TILs from RLmale1 tumors	<i>in vitro</i> PMA/ionomycin stimulation	metformin promotes multifunctionality (triple cytokine secretion:IL-2, IFN γ , TNF- α)
	<i>in vivo</i> TILs	murine melanoma cells (B16F10) in C57BL/6	metformin increases T cells infiltration into tumor
	<i>ex vivo</i> CD4 ⁺ cells from murine melanoma tumors (B16F10)	<i>in vitro</i> PMA/ionomycin stimulation	CD4 ⁺ Foxp3 ⁺ IL10 ⁺ T cells (IL10 negatively regulates Th17 inflammation in the tumor microenvironment)
	indirect effect	B16-F10 (melanoma) and MC38 (colon adenocarcinoma) in C57BL/6	repression of tumor cell OCR and an increase in T cell OCR; tumor infiltrating T cells have an increase in the number of the activated T cells;
	<i>in vivo</i> CTL	4T1 breast cancer in BALB/c	metformin decreases PD-L1 levels in cancer cells, increased of the CD8 ⁺ CTL population;
	<i>in vivo</i> T cell subsets	Hepa1-6 orthotopic in C57BL/6 (HCC model)	lower levels of IL22 in the tumors by decreasing the numbers of both Th1 cells and Th17 cell

<i>in vivo</i> TILs	fibrosarcoma methA, RLmale1, B6 fibrosarcoma MCA and B16 melanoma M05 in BALB/c	metformin decreases in the Treg/CD4+ T cell ratio in tumors
---------------------	---	---

1.3.4 TARGETING MITOCHONDRIAL COMPLEX I (CI) AND ITS CONSEQUENCES ON MACROPHAGES

In the tumour microenvironment of solid tumours, macrophages are one of the most abundant immune cells and their existence coincides with decreased survival in most cancers (Noy and Pollard, 2014). At all stages of tumour development, macrophages are present and promote angiogenesis, tumour cell invasion, and intravasation at the primary site. In this context, the consequence of TAMs in metabolic therapy has been explained. In obese / diabetic persons with pancreatic cancer, metformin alleviates the fibro-inflammatory microenvironment by reprogramming pancreatic stellate cells and TAMs, which coincides with decreased development of the disease (Incio et al., 2015). Although not in tumor settings, metformin atherosclerosis therapy inhibits monocyte-to-macrophage differentiation through inhibition of STAT3 activation mediated by AMPK (Vasamsetti et al., 2015). Metformin prevented the development of prostate cancer in transgenic adenocarcinoma of the mouse prostate (TRAMP) by targeting TAM infiltration (Liu et al., 2018). *in vitro* studies using TAMs-conditioned medium and a multi-cancer co-culture system demonstrated an inhibitory effect of metformin by encouraging M2-polarized RAW264.7 macrophages on endothelial sprouting and tumor cell proliferation (Wang et al., 2018). The findings of our group regarding the effect of CI deficiency showed contribution of TAM infiltrations as an adaptive mechanism acquired by the CI deficient osteosarcomas and colorectal cancers (Kurelac et al., 2019). This instigated us to dissect the mechanism of TAM recruitment in these metabolically constrained models of CI deficient tumors, which is the focus of this thesis.

Chapter 2

AIMS

Disruption of the mitochondrial CI by genetic or pharmacological targeting has been envisaged as plausible anti-cancer therapy. The metabolic disruption following CI disassembly prompts HIF-1 α destabilization that has been attributed as one of the primary mechanisms triggered in these tumors. However, it has never been demonstrated whether HIF-1 inactivation is the cause of lower tumorigenic potential of CI deficient tumors.

(1a) Thus, the first aim was to prove that the lack of HIF-1 α stabilization and subsequent inability to adapt to hypoxic environment contributes to the anti-tumorigenic effect of CI deficiency.

(1b) To prove that this phenomenon is generalized in murine setting and that it also occurs in an orthotopic cancer model that closely mimic human condition.

It is important to note that even though maintaining low-proliferative phenotype, CI-deficient tumors still persist when left to grow overtime. Most recent data imply that the progression of CI-deficient tumors seems to be supported by components of TME, in particular TAMs.

(2) Thus, the second aim was to determine the factors leading to macrophage abundance in CI deficient tumors, with the overall goal to identify a specific druggable target that could inhibit protumorigenic macrophage activity and optimize CI anti-cancer effects.

Chapter 3

EXPERIMENTAL PROCEDURES

3.1 CELL LINES MAINTENANCE

Osteosarcoma 143B Tk- cells, HCT116 cells and B16F10 murine melanoma cells were cultivated in Dulbecco's modified Eagle medium (DMEM) High Glucose (Euroclone), supplemented with 10 % fetal bovine serum (Euroclone), L-glutamine (2mM, Euroclone), penicillin / streptomycin (Euroclone) and uridine (50 μ g / ml, Sigma-Aldrich), in a humidified atmospheric incubator at 5% CO₂ and 37 ° C , respectively. On 15 passages, cells were replaced by a fresh batch (approximately every two months) and mycoplasma testing was performed before disposal and after each thawing. Hypoxia experiments with 1% of O₂ concentration, were carried out within the Invivo2 300 (Baker Ruskinn) chamber, set up at 5% CO₂ and 37 ° C.

3.2 GENERATION OF TM-HIF-1 α

The HIF-1 α cDNA wild-type sequence was cloned in the pGEM (Promega # A1360) vector and mutagenesis was performed using the Quickchange Site-Guided Mutagenesis Kit (Agilent # 200518) to induce mutations at the PHD hydroxylation sites following previously mentioned indications as directed by the manufacturer (Tal et al., 2008). The HIF-TM ensures constitutive activation of the protein, even in normoxia. In specific, three mutations were introduced in the HIF-1 α sequence, to replace the prolyl hydroxylase (PHD)-targeted prolines and Factor Inhibiting HIF (FIH)-targeted asparagine with residues that can not be hydroxylated (P402A, P564 G, and N803A) (Fig. 3.1). The triple mutant HIF-1 α was then transferred into the retroviral vector of pMSCV-Puro (Clontech # PT3303-5). Following the phxA transduction protocol mentioned above, the empty vector and the vector comprising TM-HIF-1 α were then used to transduce 143B and HCT116 cells. Cells carrying the vectors were picked with

puromycin $2 \mu\text{g mL}^{-1}$ (Sigma # P8833) and grown in medium supplemented with puromycin $1 \mu\text{g mL}^{-1}$. To classify the clones with the highest levels of TM-HIF-1 α protein in normoxia, clonal selection was performed and a pool of 20 clones was made.

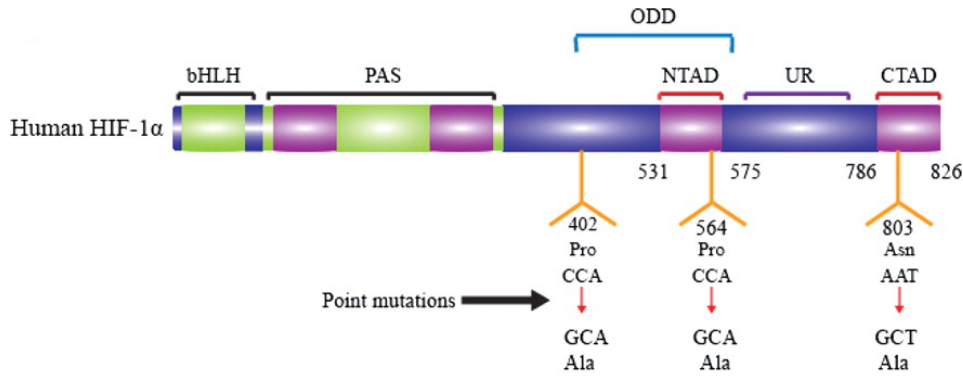


Fig. 3.1 Representation of the three point mutations of the HIF-1 α ensuring a non degradable and constitutive activation of the protein, even in normoxia.

3.3 GENOME EDITING FOR GENERATION OF NDUFS3 KNOCK-OUT

The generation of the NDUFS3 KO using zing finger nucleases for the 143B osteosarcomas and HCT colorectals was carried out as described previously (Kurelac et al., 2019). CRISPR/Cas9 system was used to introduce a frameshift mutation in *Ndufs3* gene for the murine melanoma B16F10 cell lines. In detail, Cas9 protein (Invitrogen#A36497) was transfected by following manufacturers instructions using Lipofectamine™ CRISPRMAX™ Cas9 Transfection Reagent (Invitrogen #CMA00015) together with synthetic RNA guides designed by Deskgen and purchased from Synthego. Exon 1 targeting guide ACATGGCGGCGGCTGCAGCC with PAM sequence AGG was used to create clone E6(1) and Exon 3 targeting guide TTGTGGGTCA-CATCACTCCG with PAM sequence GGG was used to create G4(2). Cells were split and harvested 48 hours after transfection and DNA was extracted using Mammalian Genomic DNA Miniprep Kit (Sigma-Aldrich #G1N350). Non-homologous repair efficiency was evaluated by Sanger Sequencing using KAPA2G Taq polymerase (Kapa Biosystems #KK5601) and Big Dye protocol (Life Technologies #4337451). In particular, for Exon 1 58°C annealing temperature was used for the PCR reaction, with primers forward TGCGTCTTCTTCTTCTCGGC and reverse CAACGAAAGGCCCCAGCTAA. For Exon 3 61°C annealing temperature was used for the PCR reaction, with primers forward CTGTAACTCCAGTCTCAGGGA and reverse

CACACTGCAGGGATCACTTG. Manual clonal selection was performed in order to identify the cells with frameshift Ndufs3 mutations. DNA extraction from 96-well plates was performed using 8 μ l of Lysis Solution (Sigma-Aldrich #L3289) and 80 μ l of Neutralization Buffer (Sigma-Aldrich #N9784) per sample, following manufacturer's instructions.

3.4 MITOCHONDRIA ISOLATION

Membrane fractions enriched with mitochondrial proteins (mitoplasts) were extracted using digitonin (final 50 μ g / mL concentration) from cell pellets (10×10^6 cells). Digitonin, which destabilizes and solubilizes the cell membranes, binds to membrane cholesterol. Unlike the outer membrane, the inner membrane is almost devoid of cholesterol, so digitonin solubilizes the cell membranes, with the exception of the inner membrane, which can be separated while remaining intact. In short, cells were centrifuged and pellets suspended with cold PBS at a concentration of 10×10^6 cells / mL, and incubated on ice for 1 minute after the addition of digitonin. Cold Phosphate-buffered saline (PBS) was then applied to dilute the suspension volume to 2.5-fold, thus disrupting cell permeabilization. Treatment with digitonin was repeated until at least 90% of the cells were permeabilized, as detected by Trypan blue cell permeabilization under the microscope. At 13000 rpm for 15 minutes at 4 ° C, the cells were then centrifuged and the pellet was stored at -80 ° C. Proteins were then quantified using the Bradford assay.

3.5 CN-PAGE

Complex I was separated by Clear Native PAGE (CN-PAGE)(Wittig et al., 2006). Cells were resuspended in PBS at 10^7 cells / ml, permeabilized with digitonin at 50 μ g / ml, centrifuged for 10 minutes at 13000 rpm and the mitochondrial pellet was stored at -80 ° C. The next day, the mitochondrial buffer (750 mM 6-aminocaproic acid, ACA; 50 mM BisTris, pH 7.0) was used to resuspend the pellet, the proteins were quantified and DDM (n-Dodecyl β -D-maltoside) added 2.5 times the amount of protein. Subsequently samples were incubated for 10 minutes in ice and then centrifuged for 15 minutes at 4 ° C at 13000 rpm. We then retrieved the supernatant containing the mitochondrial proteins and quantified the proteins. In the CN-Sample Buffer (0.1% Red Ponceaux and 50 percent Glycerol), the supernatant collected was diluted. 50 μ g of mitochondrial protein samples were loaded onto a native gel made of a polyacrylamide gradient of 4% to 12%, made with gradient construction machinery and a Delta-Pump (Peristaltic Pump). Running gels were prepared to add 25 mM Imidazole, 0.5 M ACA, pH 7, 0.02 percent APS and 0.02 percent TEMED to the existing acrylamide concentrations; 10 percent glycerol was

applied to the higher concentration gradient. There was 4 percent acrylamide in the stacking gel. For CN-PAGE (50 mM Tricine, 7.5 mM Imidazole, 0.02 percent DDM, 0.05 percent NaDOC pH 7), the anode buffer and cathode buffer were used. At 80V, electrophoresis was performed. Gels were immersed in a solution containing 2 mM Tris-HCl, 0.5 percent 3-(4,5-dimethylthiazol-2-yl)-2,5-diphenyltetrazolium bromide (MTT) and 0.02 percent NADH for 15 minutes after electrophoresis at room temperature, in the dark. Because of the reduction of MTT to tetrazolium salts by NADH oxidation by CI, the CI emerged as a black band.

3.6 SDS-PAGE AND WESTERN BLOT ANALYSIS

In RIPA buffer [TrisHCl pH7.4 (50mM), NaCl (150mM), SDS (1%), Triton (1%), EDTA pH7.6 (1mM)] supplemented with protease inhibitors (Roche) and quantified by Lowry protein assay (Biorad), whole lysates of cultured cells and freshly snapped frozen xenograft samples were prepared. Samples were isolated by SDS-PAGE and moved to the nitrocellulose membrane using the Turbopack method (Biorad) The membranes were blocked at 37 °C for 30 minutes and incubated with primary antibodies using the following dilutions / conditions: anti-NDUFS3 (AbCam #177471) 1:1000/1-h at room temperature (RT); anti-HIF-1 α (GeneTex #GTX127309) 1:2000/1-h at RT; anti-Vinculin (Sigma-Aldrich #V9131) 1:10,000/1-h at RT; anti-MIF (AbCam #175189) 1:5000/1-h at RT; anti-ACTB (Santa Cruz #SC-1615) 1:500/1-h at RT; anti-p53 (Santa Cruz #SC-126) 1:1000/1-h at RT. TBS-Tween [0.1 percent Tween 20 (Sigma-Aldrich # P9416) in Tris Buffered Saline] was washed for 4 \times 5 minutes and secondary antibody incubation (Jackson ImmunoResearch Labs # 111035144 and # 111035146), diluted 1:20,000 in TBS-Tween, was conducted at RT for 30 minutes. The membrane development was carried out with Clarification Western ECL Substrate (Bio-Rad # 1705061) and ChemiDoc XRS+ (Bio-Rad) exposure. The Western Breeze method (Life Technology # WB7106) was used for anti-NDUFS3 antibodies for secondary antibodies and developing solutions, following the manufacturer's instructions.

3.7 CELL VIABILITY

The Sulforhodamine B (SRB) assay (Sigma-Aldrich) and cell counting after staining with trypan Blue (Sigma-Aldrich) measured cell viability. Cells were seeded in a complete medium onto 24-well plates (7.5 \times 10³cells / well for B16F10). For additional conditions, cells were washed twice in PBS 24 hours after seeding and incubated in the specified media i.e., either low glucose (5mM), galactose (5mM) or high glucose (25mM). Briefly, cells were fixed with 50 percent trichloroacetic acid for 1 hour at 4 ° C at the end of incubation time, washed 5 times

with H₂O and finally dried at room temperature for 1 hour. Cells were then stained at room temperature with SRB 0.4% diluted in 1% acetic acid for 1 hour, washed 4 times with 1% acetic acid, and disrupted at pH 9.8 with 10 mM Tris-HCl. SRB absorbance was detected at a wavelength of 560 nm by the Tecan plate reader.

3.8 RNA EXTRACTIONS, qRT-PCR

The expression of quantitative real-time PCR gene was evaluated based on minimal knowledge for the publication of guidance for quantitative real-time PCR (qRT-PCR) experiments (Bustin et al., 2009). In particular, RNA was extracted for cell lines using Trizol (Life Technologies # 15596018) and for snap-frozen xenograft samples using the Mammalian Genomic DNA Miniprep Kit (Sigma-Aldrich # RTN70). Applied Biosystems # 4368814 (High Capacity cDNA Reverse Transcription Kit) was used to prepare cDNA with random hexamers beginning from 300 ng of RNA. Using Primer3 program (Skaletsky and Rozen, 2000), Primer sequences were designed. Using IDT OligoAnalyze tool (<http://eu.idtdna.com/analyzer/Applications/OligoAnalyzer/>), the presence of 3' intra/inter primer homology was ruled out. Primer sequences used for SLC2A1, VEGF, LDHA and TBP were previously designed and sequences mentioned in publication from Calabrese et al. for (Calabrese et al., 2013). MIF primers: F: AGAAC-CGCTCCTACAGCAAG, R: GAGTTGTTCCAGCCCACATT. P21 primers: F: GGCA-GACCAGCATGGACAGATT, R: GCGGATTAGGGCTTCCTCCT. GoTaq qPCR Master Mix (Promega # A6002) was used to execute the PCR reaction and operate the 7500 Fast Real-Time PCR Method (Applied Biosystems), under the following conditions: 95 ° C for 5 minutes; 95 ° C for 45 intervals for 15 seconds and 60 ° C for 45 seconds. The measurements were carried out using the [ct(control)-ct(experiment)] 2- $\Delta\Delta$ CT calculus, where the control was determined as the average ct value obtained from control samples. The normalization was done using TBP. Using the Δ ct values [ct(gene of interest)-ct(reference gene)] for each biological replication in a population and applying student T-test, the statistical significance was determined (Yuan et al., 2006).

3.9 P53 TRANSFECTION

For the P53 experiments (Fig. 3.2), X-tremeGENE™ HP DNA Transfection Reagent (XTGHP-RO Roche) was used to transfect P53 Wild type (WT) or P54 Mutated (Mut) plasmid according to the manufacturer's instructions for time period of 24 hours. The cell lines were then subjected to hypoxia incubation in 1% O₂ hypoxic chamber or in 21% O₂ conditions in an incubator. The

RNA was extracted using Trizol (Life Technologies #15596018) for cell lines. qRT-PCR was used to evaluate the expression of P53, P53-responsive genes, HIF-1 α and MIF.

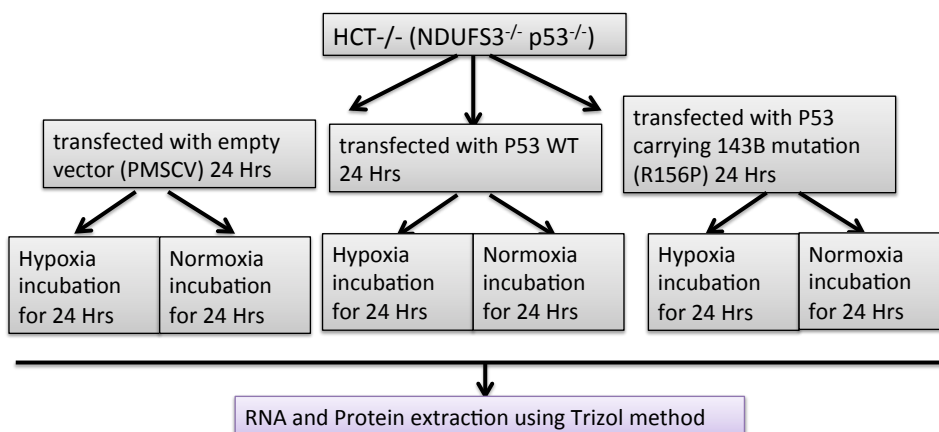


Fig. 3.2 Graphical representation of P53 transfection method in the HCT-/- cells.

3.10 *IN VIVO* TUMOR GROWTH

Nu / nu mice (CD-1 @ Nude Mouse Crl: CD1- Foxn1n) were purchased from Charles River Laboratories for *in vivo* tests. Animal testing and analysis has been complied with all applicable ethical legislation. The animals were treated at the university of Bologna in compliance with institutional standards and regulations. The Italian Ministry of Health (authorization code 437/2018-PR) authorised the ethical report. Female mice aged five to six weeks were subcutaneously injected with a 100 μ L suspension of 5×10^6 cells in serum-free medium and matrigel (Corning # 356234) on the right flank of the animal. Using a sliding caliper, the xenograft scale was calculated twice a week according to the formula: volume = width * height * length/2 and the tumor growth was followed accordingly. Mice were either sacrificed concurrently when 10% of animal weight was achieved by the first xenograft, or consecutively when each animal achieved xenograft volume corresponding to 10% of animal weight or met the requirements for termination.

3.11 ESTABLISHING PSEUDO-ORTHOTOPIC OSTEOSARCOMAS

The pseudoorthotopic model was established by Ander Abberateghi from The Francis Crick Institute, London, UK. Briefly, in sterile conditions, all pre-surgical operations have been

carried out. Gelfoam gelatin sponges (2 cm × 6 cm × 7 mm) (Pfizer, Kalamazoo, MI, USA) were cut into 24 parts, washed in sterile PBS with 70% ethanol, rehydrated and put in a 24-well plate. HMSC cells (5×10^5 in 50 μ l) were injected with a syringe (29 G) and left in a 37 C incubator for 4 hours for attachment. Cultural media was introduced and for 7 days the cells were left to expand. Cells of osteosarcoma (10^5 in 30 μ l) were inserted into the scaffold on day 8 and left to attach before adding new culture media. A 15 mL tube and 8 μ l of Bone Morphogenic Protein 2 (BMP-2) (Noricum, Tres Cantos, Spain) were assigned to each scaffold. Then 30 μ l of human plasma thrombin (Sigma, Dorset, UK) (reconstituted by 2% CaCl_2 at 20 U / mL) and 20 μ l of human plasma fibrinogen (Sigma) (reconstituted by 4 mg/100 mL PBS) were incorporated. In cell culture conditions, solidification was permitted for 30 minutes before progressing to *in vivo* implantation. In aseptic conditions, surgery was performed. At The Francis Crick Institute Biological Research Facility (London, UK), five to six-week old female *Rag1*^{-/-} FVB / n mice were used. For each implantation of the scaffold, a 0.5 cm vertical incision was made on each side of the animal 1 cm away from the spine. A pocket under the skin in the incision, down the side of the animal, was made with forceps. A scaffold was inserted to ensure that it was positioned deep within the bag, and then incisions were dried and glued (Fig. 3.3).

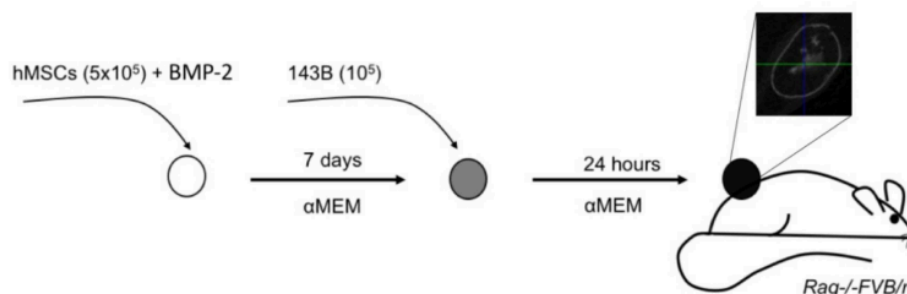


Fig. 3.3 Schematic diagram representing the generation of the pseudo-orthotopic osteosarcomas in *Rag1*^{-/-} FVB/n mice.

3.12 CYTOKINE ARRAY

Xenograft-derived cell cultures were generated by a 10-day cultivation of liberase-digested tissue in basal conditions. Supernatant (0.5 mL) was taken 2 days after medium renewal and analyzed with human Proteome Profiler Array kit (R&D Systems, ARY005B) following manufacturer's instructions.

3.13 IMMUNOFLUORESCENT (IF) AND IMMUNOHISTOCHEMICAL (IHC) STAINING

3.13.1 IHC

Following standard protocols, the samples were fixed in formalin for 24 hours before transferring them into 70% ethanol. The tissue was then fixed in paraffin and cut using the microtome. Tissue parts (4 μm) in xylene were deparaffinized, rehydrated in absolute ethanol, followed by heat-induced buffer epitope retrieval (TE-T with 10 mM Tris pH 8.0, 1 mM EDTA, 0.05 percent Tween 20 or trypsin-based antigen retrieval with 0.05% trypsin in 0.1 mM Calcium chloride solution, pH 7.8) for 40 min at 95 ° C and 20 min at RT. Sections are then washed with phosphate-buffered saline containing 0.5 percent Tween 20 (PBS-T pH 7.4). Primary antibodies were dissolved in antibody diluent with background reducing components (Dako # S3022) and incubated for 30 min or 1 hour at RT. Blocking, secondary staining and development of antibodies with DAB substrate were conducted using the Envision Detection System (Dako # K4007 and # K4011) as directed by the manufacturer. Hematoxylin was used as a counter stain. The following primary antibodies were used: rabbit monoclonal anti-NDUFS3 (1:200, Abcam #177471); rabbit polyclonal anti-HIF-1 α (1:350, Sigma-Aldrich #HPA001275) and rat monoclonal F4/80 (1:100, eBiosciences #14-4801). Neutrophil marker 2b10 antibody was developed in house at The Francis Crick Institute.

3.13.2 IF

Following standard protocols, the samples were fixed in formalin for 24 hours before transferring them into 70% ethanol. The tissue was then fixed in paraffin and cut using the microtome. Tissue parts (4 μm) in xylene were deparaffinized, rehydrated in absolute ethanol, followed by citrate antigen retrieval (10mM sodium citrate, pH 6) at 95 ° C for 15 min and at RT for 20 min. Blocking with goat serum (Abcam # 156046) for 10 min at RT and incubation with secondary antibodies to Alexa Fluor (488-goat anti-mouse diluted 1:500 and 555-goat anti-rat diluted 1:350) for 40 min at RT was carried out. Rat anti-Endomucin (1:200, Santa Cruz # SC-65495) and mouse anti-SMA (1:750, Dako # M0851) were the following primary antibodies used. Vectashield Antifade Mounting Medium with DAPI (Vector Labs, # H-1200) was used to mount slides. The size of the vessel was measured by calculating 30 endomucin positive cells per tumor longer in diameter and avoiding fibroblast infiltrated areas. At 20X magnification per tumor, fibroblasts (SMA+Endo-) and immature vessels (Endo+SMA-) were counted in five fields of view. Pictures were taken with the Zeiss Axio Scope Z1 scanner using the software ZEN (Carl Zeiss Microscopy GmbH, Germany). Trypsin-based antigen retrieval

(0.05 percent trypsin in 0.1mM calcium chloride solution, pH 7.8) was conducted for 30 min at 37 ° C for macrophage staining with anti-F4/80 and biotinylated goat secondary anti-rat antibody (Sigma-Aldrich # A9037) was used along with VECTASTAIN ABC-HRP Kit (Vector Laboratories # PK-4005). Macrophage was counted at five fields of view per tumor (F4/80 +) at 20X magnification.

3.14 FLOW CYTOMETRY ANALYSIS

The cytometry data were obtained by Ivana Kurelac at the The Francis Crick Institute, London, UK. Briefly, immediately after the mice sacrifice, xenograft samples (50 mm³) were digested in HBSS for 40 min at 37 ° C with Liberase TL (Sigma # 5401020001), Liberase TM (Sigma # 5401135001) and DNaseI (Sigma # DN25) and passed through a 100 μm strainer. Red Blood Cell Lysis Buffer (Sigma # 11814389001) hypotonic lysis was carried out and the residual cells were washed with MACS buffer (2 mM EDTA, 0.5 percent BSA in PBS), blocked with FcR Blocking Reagent (Miltenyi # 130-092-575) and incubated with pre-labeled antibody panels. In parallel, for fluorescence minus one (FMO) reading, spleen, lung and a control tumor tissue were digested together and stained, which was considered when setting the gating strategy. The panel used was: anti-F4/80-APC780 (clone BM8, eBioscience #47-4801-80), anti-CD45-PE (clone 30-F11, eBioscience #12-0451-82), anti-Ly6G-APC (clone 1A8, BD Bioscience #560599), anti-CD11b-ef450 (clone M1/70, eBioscience #48-0112-82), anti-CD11c-PeCy7 (clone N418, Biolegend #117317), and anti-CD49b-FITC (clone 30-F11, Biolegend #108905) at 1:100 dilutions while anti-CD45 was used at 1:300 dilution. Dead cells were stained with DAPI. The samples were run on LSRFortessa Cell Analyzer (BD Biosciences). BD FACSDIVA Software (BD Bioscience) and Flow Jo (Tree Star Inc.) software were used for the analysis of the results.

3.15 METABOLOMICS

The metabolomics analysis was carried out in University of Cambridge in Dr Christian Frezza's lab (MRC cancer unit). The conditioned media for the LC-MS were extracted according to the protocol from Frezza's lab. The *ex vivo* cultures were seeded in 6 well plates and left to attach for 24 hours after which the media was replaced by a fresh media. After a period of 24 hours, the conditioned media was collected and processed (Fig. 3.4). 5uM d8-Valine was used as the internal standard. LC-MS analysis was performed using a Q Exactive mass spectrometer (Thermo Fisher Scientific) joined to a U3000 UHPLC system Dionex. The LC system was fitted with a Sequant ZIC-PHILIC column (150 mm × 2.1 mm) and guard column (20 mm

× 2.1 mm) from Merck Millipore (Germany). The mobile phase was composed of 20 mM ammonium carbonate and 0.1% ammonium hydroxide in water (solvent A), and acetonitrile (solvent B). The mass spectrometer was operated in full MS and polarity switching mode. The acquired spectra (an ion chromatograms) were analyzed using XCalibur Quan Browser software. To generate the heatmap, the pathway analysis using KEGG metabolic pathways as the backend knowledge base and the metabolite set enrichment analysis, metaboanlyst was used (<https://www.metaboanalyst.ca/MetaboAnalyst/faces/home.xhtml>)

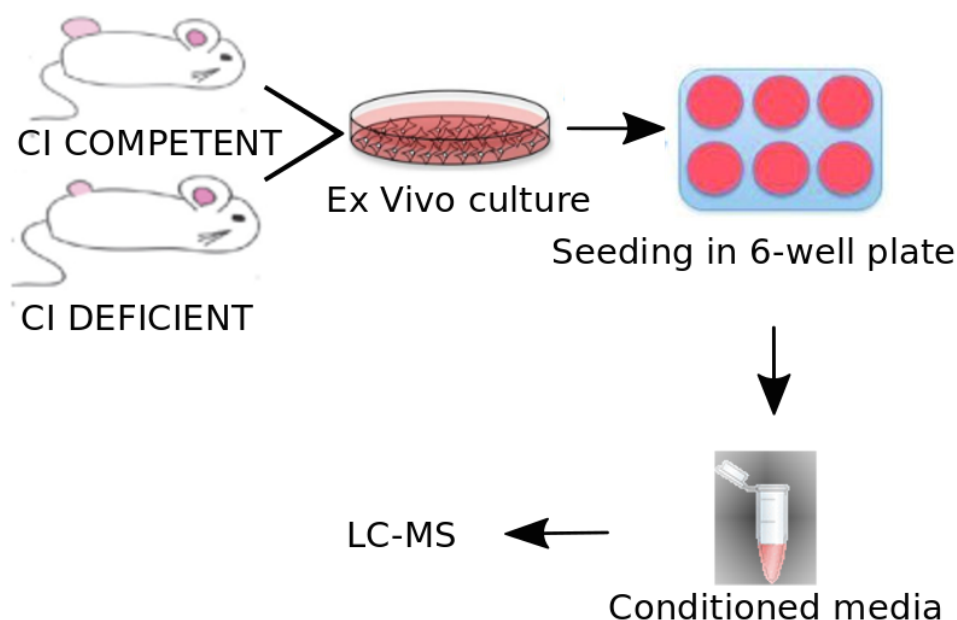


Fig. 3.4 Experimental setting of the extraction of the conditioned media from the *ex vivo* cultures for LC-MS analysis.

3.16 PROTEOMICS

The proteomics was carried out in Max Planck Institute for Molecular Genetics in the lab of Prof David Meierhofer. The *ex vivo* cultures were seeded at concentration of 1×10^6 cells in triplicates on a 10cm dish and were left to attach overnight. The next day, cells were washed stringently and gently, twice with Hanks balanced salt solution with calcium and magnesium. 6ml of media without FCS and phenol red was added. The media was collected after 24 hours in a low protein binding tube and centrifuged for 10 min at $2000 \times g$ at 4°C .

5.5ml of the media was then transferred into a new low protein binding tube and 750ul of TCA (final concentration 12%) and precipitated on ice for 2 hours. After 2 hours, the sample were centrifuged at 3500x g for 10 min at 4°C. The supernatant was discarded and 2 ml of pre-cooled tetrahydrofurane (THF) was added. The pellet was vortexed until it was dislodged from bottom of tube and dissolved completely. The wash with THF was repeated again and the samples were collected and processed by nanoflow reverse phase liquid chromatography (Dionex Ultimate 3000, Thermo Scientific, Waltham, MA) coupled online to a Q-Exactive HF Orbitrap mass spectrometer (Thermo Scientific, Waltham, MA) as previously described (Kürschner et al., 2017).

3.17 STATISTICAL ANALYSIS

GraphPad Prism version 6 (GraphPad Software Inc., San Diego, CA, USA) was used to perform statistical tests and create bar plots and graphs. Unless stated otherwise, a two-tailed unpaired Student's t-test assuming equal variance was performed to compare averages. For each experiment, at least three biological replicates were analyzed. *In vitro* analyses were repeated by at least two independent experiments. Where indicated, standard error of the mean (SEM) measuring how far the sample mean of data is likely to be from true population mean, is represented by the error bars.

Chapter 4

RESULTS

4.1 HIF-1 α IS ACCOUNTABLE FOR LOW TUMORIGENIC POTENTIAL OF CI DEFICIENT CANCER CELLS

Our group has already reported that in the presence of homoplasmic disruptive mtDNA mutations, as seen in oncocytic tumors, cancer cells present with a severe mitochondrial CI damage and lower tumorigenic potential than CI competent tumors (Kurelac et al., 2013). To mimic the effects of disruptive mtDNA mutations in order to better understand their anti-tumorigenic effects, 143B osteosarcoma, HCT116 colorectal human cancer cell lines and B16F10 murine melanoma cell lines were genetically targeted for CI by knocking out its NDUFS3 subunit. We hypothesized that these CI deficient tumors were associated with HIF-1 α destabilization even in hypoxia. The HIF-1 α destabilization, as observed in CI deficient 143B and HCT tumors by our group (Kurelac et al., 2019), could be attributed to high intracellular oxygen concentrations and/or NADH accumulation which then consequently leads to an increased α KG/succinate ratio in them (Calabrese et al., 2013). This data was also consistent with wide range of studies that target OXPHOS pharmacologically in cancers resulting in decreased HIF-1 α stability (Selak et al., 2005; Bastein et al., 2017; Wang et al., 2015).

4.1.1 INTRODUCING THE HIF-TM IN CI DEFICIENT CELLS RESCUES THEIR TUMORIGENIC POTENTIAL AND VESSEL MATURATION

With the aim to prove that CI deficiency reduces tumor progression due to lack of HIF-1 α stabilization and subsequent inability to adapt to hypoxic environment, a constitutively and non-degradable human form of HIF-1 α , named HIF-TM was introduced into both 143B CI

deficient (143B^{-/-}) and HCT CI deficient (HCT^{-/-}) human models. In parallel, a mock with empty vector was introduced as a control. In order to evaluate the presence of a stable and constitutively expressed HIF-1 α in the HIF-TM cells, immunofluorescent staining was carried out, which confirmed the translocation of HIF-TM into the nucleus in normoxia (Fig. 4.1A). Western blot analysis further confirmed a higher expression of HIF-1 α in the HIF-TM cells compared to the mock, irrespective of oxygen concentration (Fig. 4.1B).

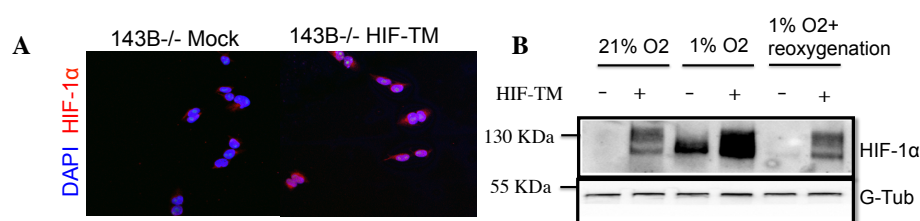


Fig. 4.1 HIF-TM introduction ensures a stable, non-degradable HIF-1 α protein and its translocation to the nucleus (A)- Immunofluorescence of 143B^{-/-} cells cultured *in vitro* and carrying empty vector (Mock) or HIF-TM. Magnification 200x. (B) HIF-1 α protein SDS-PAGE and Western Blot analysis of 143B^{-/-} cells carrying empty vector (mock) and HIF-TM, cultured in 1% O₂ and 21% O₂. Gamma tubulin was used as loading control.

Although *in vitro* models have been utilized as an important tool in cancer research, they do not reflect the essential features of *in vivo* tumor-microenvironment, particularly important when studying phenomena like hypoxia. Thus, to fully comprehend the inherent intricacy of tumors, it is a pre-requisite to replicate them *in vivo*. Taking this into account, 143B^{-/-} and HCT^{-/-} HIF-TM and Mock tumors were injected into nude mice to assess the effects of introduction of the HIF-1 α in the CI deficient cells on their tumorigenic potential.

In both osteosarcoma and colorectal cancer models of CI deficiency, the presence of HIF-TM, which was confirmed by the western blot analysis (Fig. 4.2B), the xenografts grew significantly larger than their controls (Fig. 4.2A), suggesting that inserting HIF-1 α in CI deficient cells was partially responsible for the rescue of their tumor growth. HIF-1 transactivates a wide array of genes including those promoting angiogenesis and anaerobic metabolism. Accordingly, RT-PCR analysis confirmed a higher expression of HIF-1 target genes SLC2A1, LDHA and VEGF in the HIF-TM than in the Mock xenografts (Fig. 4.2C), corroborating that xenografts expressing HIF-TM activated the HIF-1 regulated hypoxic signalling pathways. Moreover, to exclude possibilities of an epistatic effect of the transcription factor *in vivo*, HIF-TM was also introduced into 143B^{+/+} cells, which were then inoculated into the nude mice. However, no significant effect on tumorigenic potential was observed upon HIF-TM induction in CI competent model (Fig. 4.3), providing additional proof that lack of HIF-1 α transcription factor impaired tumorigenic potential of CI deficient cells.

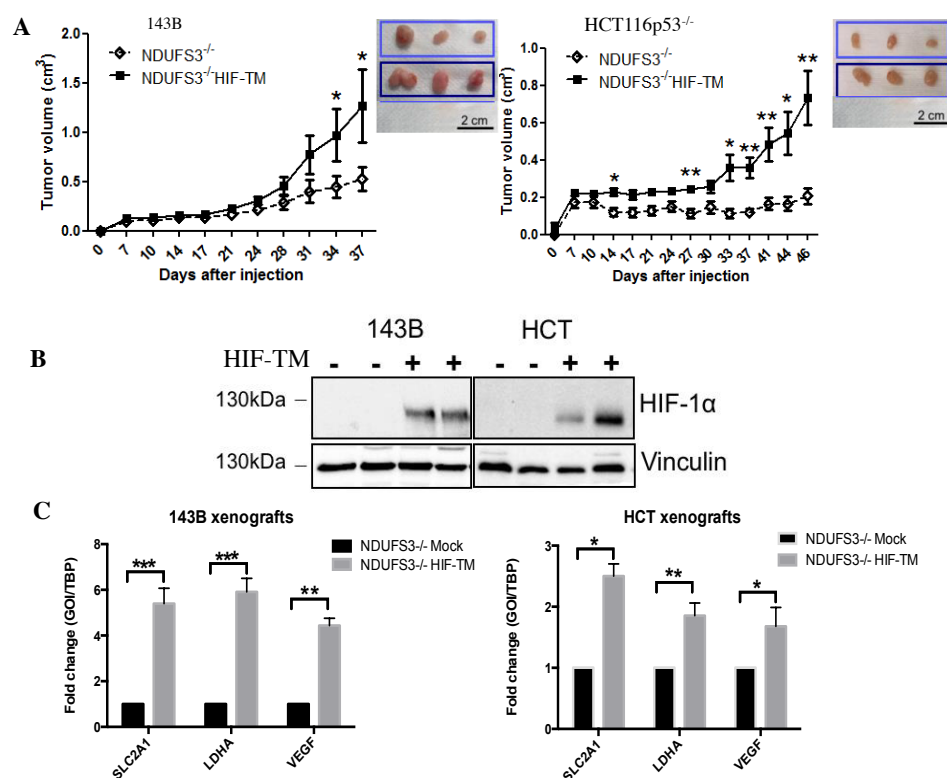


Fig. 4.2 Introducing HIF-TM in CI deficient cells rescues their tumorigenic potential (A) Tumor growth curves of 143B^{-/-} and HCT116^{-/-} after injection into nude mice (for each cell line: N=8, EXP=2). Data represent average tumor mass + SEM (*p<0.05, **p<0.01). Representative images of tumor masses are shown. Bars=2cm. (B) SDS-PAGE and western blot analysis of HIF-1 α protein levels. Vinculin was used as a loading control. (C) qRT-PCR analyses of xenografts for HIF-1 responsive genes SLC2A1, LDHA and VEGF. Data display mean+SEM; N=3 (*p<0.05, **p<0.01, ***p<0.001).

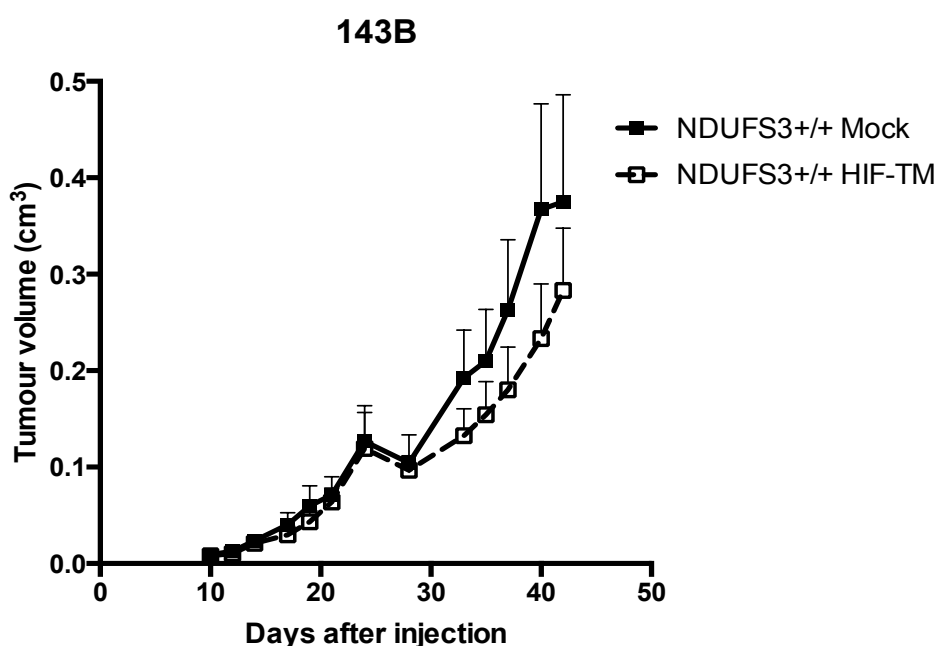


Fig. 4.3 HIF-TM does not induce increase in the tumorigenic potential of 143B^{+/+} tumors - Tumor growth curve of the 143B^{+/+} Mock and 143B^{+/+} HIF-TM xenografts after subcutaneous injection into nude mice. Data display mean+SEM. N=6, EXP=1.

Owing to their high metabolic demand, tumors rapidly exhaust the oxygen supply and nutrients from the normal vasculature, and become hypoxic, which in turn drives the production of angiogenic factors from the hypoxic tumor sites, triggering the vascularization of the tumor mass. From this perspective, angiogenesis was investigated in the CI competent and CI deficient models. The latter revealed several small, smooth muscle actin (SMA) negative and poorly developed vessels, while CI competent tumors displayed SMA positive vessels, indicative of mature vasculature (Kurelac et al., 2019). To understand whether HIF-1 activity is sufficient to mediate tumor angiogenesis, vasculature was investigated also in CI deficient tumors harbouring HIF-TM (Fig. 4.4). Immunohistochemical analysis of the CI deficient 143B and HCT HIF-TM xenografts displayed a fully developed mature vasculature positive for the pericyte marker SMA, while the Mock controls showed SMA negative, lumen free immature vessels (Fig. 4.4). The fact that re-expression of constitutively active HIF-1 α rescues the mature phenotype of the vessels in CI deficient models, suggests that HIF-1 α inactivation impairs tumor vasculature in CI-deficient tumors.

Altogether, these data suggest that the antitumorigenic effect of CI deficiency tumors, at least to a certain extent, is attributed to their inability to promote appropriate angiogenesis on account of HIF-1 α destabilization.

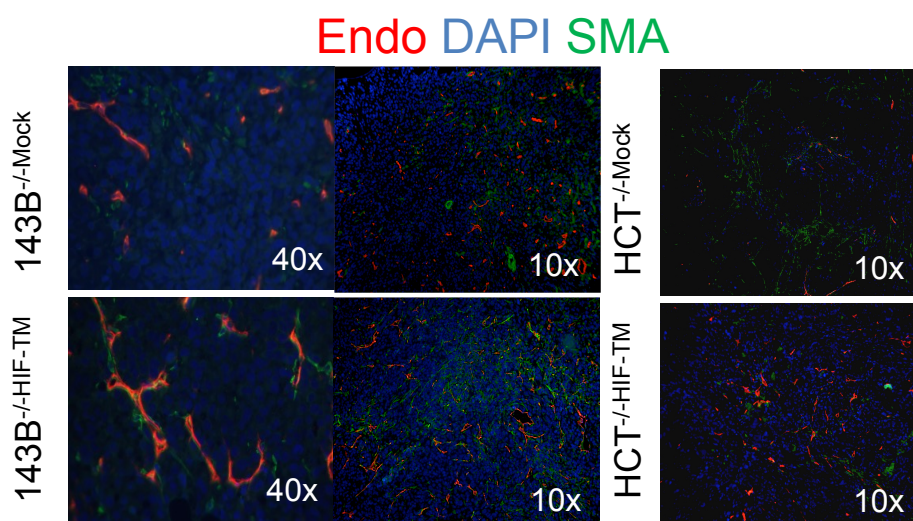


Fig. 4.4 HIF-TM xenografts present with mature vessels positive for pericytes. Immunofluorescent staining analyzing vessel morphology of 143B^{-/-} Mock and 143B^{-/-} HIF-TM xenografts. SMA (green) is fibroblasts marker, Endomucin (Endo-red) is vessels marker and DAPI (blue) is nuclei marker.

4.1.2 INDUCING NDUFS3 KO IN B16F10 MURINE MELANOMA MODEL LEADS TO CI INACTIVATION, INABILITY TO PERFORM OXIDATIVE PHOSPHORYLATION AND PREVENTS HIF-1 α STABILIZATION IN HYPOXIA

To investigate whether the lack of HIF-1 α in CI deficient cells is generalized to other mammalian species and to eventually comprehend the effects of CI deficiency on its TME in an immunocompetent model, by taking into consideration the adaptive immune system, Crispr/Cas9 technology was used to obtain the knock-out (KO) of NDUFS3 gene in B16F10 murine melanoma tumors. From the 451 cells seeded for clonal selection, 117 clones grew and were expanded, and their NDUFS3 sequence was genotyped using Sanger sequencing (Fig. 4.5).

Out of 117 clones, 51 presented with a frameshift insertion or deletion, 11 of which were homozygous mutants and 40 were heterozygous mutants. The following genotypes were found among the homozygous mutants: *c.289₂91insA*, *c.32₃4insA*, *c.30C > A*, 16 base deletion at *c.325*, *c.329₃32delTC* and *c.330₃31insC*. The latter clone harbored also a homozygous *c.328A > G* mutation (Fig. 4.5). To take into consideration potential Crispr/Cas9 off-target effects, 51 wildtype (WT) clones (NDUFS3 +/+) following the same selection procedure were analyzed to identify appropriate controls. The western blot identified 10 clones in which the absence of NDUFS3 (B16^{-/-}) protein expression was confirmed (Fig. 4.6A). 13 of the

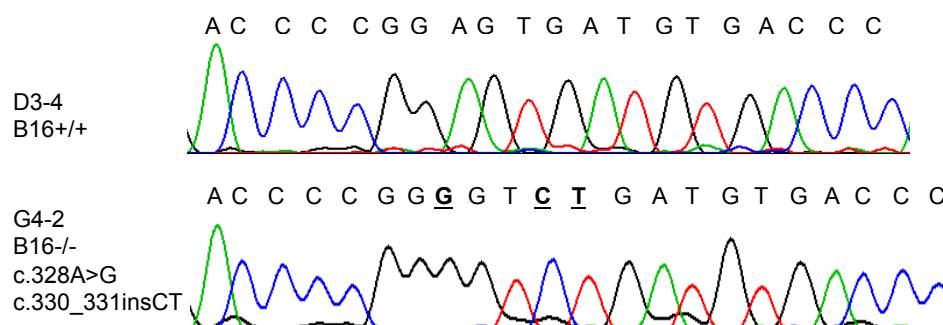


Fig. 4.5 Sanger sequence identifying the *NDUFS3* KO clones. Electropherograms compare the wild type sequence D3-4 clone B16+/+ to one of the G4-2 B16-/- clone carrying homozygous *c.330₃₃₁insC* frameshift mutation. Moreover, the same clone also harbors a *c.328A > G* point mutation. The mutated nucleotides are underlined and indicated in bold black.

NDUFS3^{+/+} clones (B16+/+) were checked for *NDUFS3* and showed to express it and could, thus, be used as controls.

The complete disruption of the CI in 143B and HCT *NDUFS3*^{-/-} cells was shown to impair the cell capacity to use OXPHOS and grow in galactose only media (which forces cells to rely on OXPHOS for energy requirements), as well as compromise their growth in low glucose conditions (Kurelac et al, 2019). Thus, with the aim to identify B16 clones in which the *NDUFS3* knock-out is associated with OXPHOS defects indicating CI-deficiency, cell proliferation in conditions of low glucose (5mM) and galactose were evaluated in 10 B16-/- clones and compared with the growth of eight control B16+/+ clones. Five B16-/- clones presented with growth decrease when incubated in galactose only condition, four of which presented also with growth decrease in low glucose media (Fig. 4.6B). In general, when compared to B16+/+ controls, the B16-/- clones had lower net proliferation in stress conditions, suggesting a reduced OXPHOS efficiency. The five clones positive for OXPHOS defect were selected for further experiments.

To verify whether the lack of *NDUFS3* had an impact on CI assembly and function, In-gel NADH dehydrogenase CI activity was measured on two B16+/+ and five B16-/- clones to examine the activity of CI. Out of the five B16-/- clones analyzed, two clones E6-1 and G4-2 displayed a significant decline of CI activity in comparison to the B16+/+ clones G4-5 and D3-4 (Fig. 4.7A). Furthermore, western blot analysis on the isolated crude mitochondria from the five B16-/- clones confirmed the absence of *NDUFS3* protein expression in only two B16-/- clones E6-1 and G4-2 (Fig. 4.7B).

Finally, to check our hypothesis that CI deficit is associated with lack of HIF-1 impairment, HIF-1 α protein levels were evaluated in the two B16-/- clones that lacked CI activity and two B16+/+ clones after incubation in normoxia (21% O₂) and hypoxia (1% O₂). We found

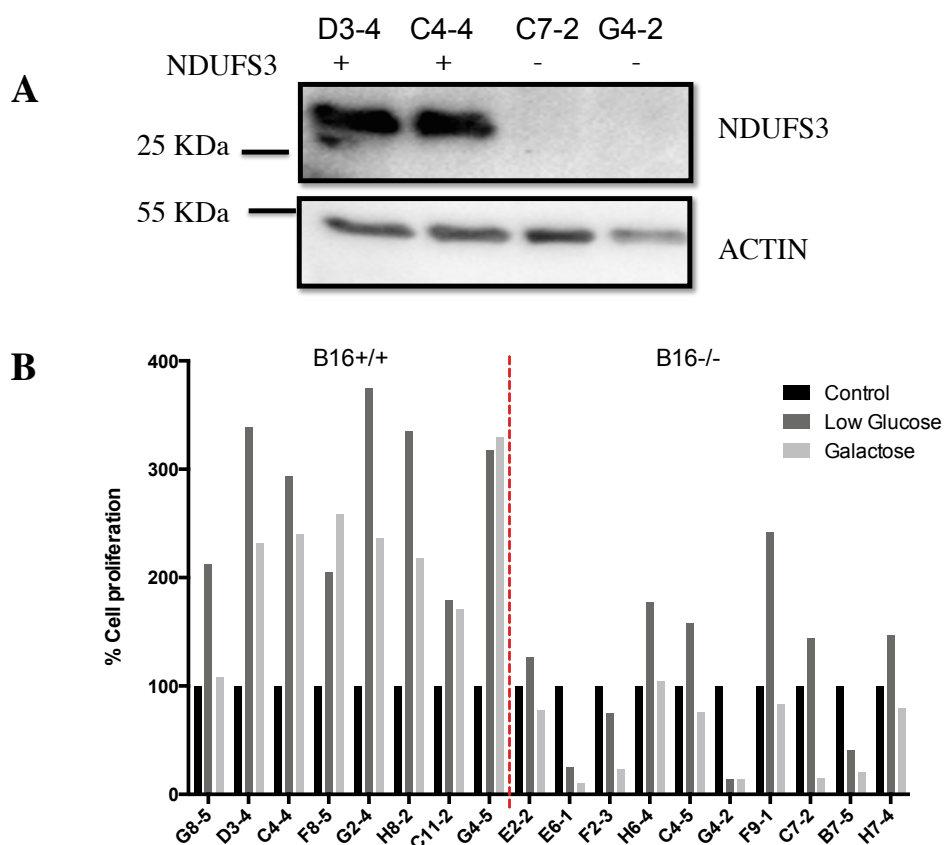


Fig. 4.6 The identified B16^{-/-} cells from the NDUF53 western blot cannot sustain proliferation when cultivated in low glucose or compelled to depend on OXPHOS for energy production in galactose media. (A) SDS-PAGE analysis followed by western blot identifies clones with absence of NDUF53 protein in this representative image. Actin is used as a loading control. (B) B16^{-/-} cells cannot sustain proliferation when cultivated in low glucose or compelled to depend on OXPHOS for energy production in galactose media. Sulforhodamine B (SRB) assay was performed *in vitro* on B16F10 clones incubated for 48 hours in low glucose (5mM) or galactose (5mM). Data represent the percentage of cell proliferation (y axis) of each clone (x axis) in the stress condition normalized to time zero. The dashed red line separates the B16^{+/+} and B16^{-/-} clones. N=3, Exp=1.

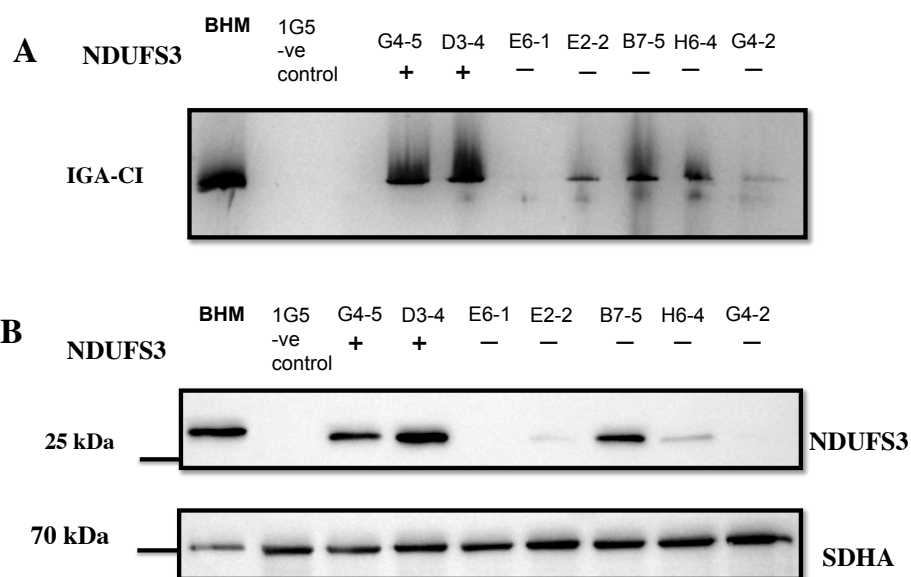


Fig. 4.7 The effect of NDUFS3 knock-out on CI assembly and function in selected B16^{-/-} clones. (A) CI-in gel NADH dehydrogenase activity following clear native page in the B16^{+/+} and B16^{-/-} clones. Bovine heart mitochondria (BHM) were used as a positive control and 143B^{-/-} clone 1G5 was used as a negative control (B) Representative SDS-PAGE and Western Blot of the mitochondrial lysates isolated from the clones analyzed in (B). Succinate dehydrogenase subunit A (SDHA) was used as loading control.

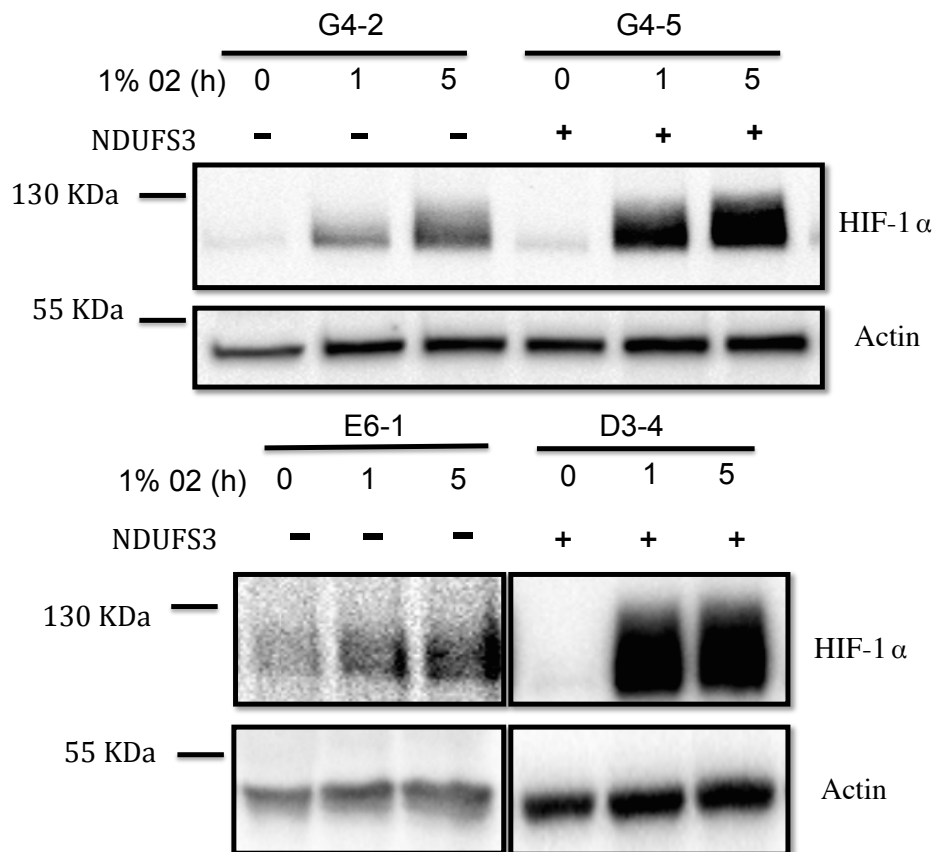


Fig. 4.8 B16^{-/-} clones cannot stabilize HIF-1 α expression. SDS-PAGE and Western Blot analysis of HIF-1 α expression in B16^{-/-} E6-1 and G4-2 clones and B16^{+/+} G4-5 and D3-4 clones in normoxia (N) and 1 hour and 5 hours of hypoxic conditions (h). Actin is used as a loading control.

that both E6-1 and G4-2 B16^{-/-} clones failed to show a stable HIF-1 α expression even when exposed to hypoxia (Fig. 4.8). Taken together, these data suggest that HIF-1 α destabilization is a general mechanism adopted by tumor cells with CI deficiency.

4.2 MACROPHAGE ABUNDANCE IN CI DEFICIENT OSTEOSARCOMAS IS ASSOCIATED WITH DOWNREGULATION OF HIF-1-MIF AXIS

Although the CI deficient models display anti-tumorigenic potential, if allowed to grow they progress to malignancy similar to their CI competent counterparts (Kurelac et al., 2019). It is important to note that a severe respiration impairment, which is a characteristic feature of CI deficient tumors, promotes metabolic reprogramming by switching from OXPHOS to glycolysis that alters not only the cancer cells but also their TME. The interactions between the cancer cells and the populations of their microenvironment immensely influence the fate of the tumor. In particular, there is accumulating evidence supporting the involvement of TME to sustain tumor progression and survival (Sousa et al., 2016; Quian et al, 2011; Orimo et al 2016). In this context, with the aim of understanding the alternative mechanisms that the CI-deficient tumors activate to progress despite the lack of a proper hypoxic response, their innate immune cells and CAFs were analyzed.

4.2.1 MACROPHAGE ABUNDANCE IS ASSOCIATED WITH CI DEFICIENCY IN 143B XENOGRAFTS

Flow cytometry analysis of innate immune system namely, macrophages, neutrophils, dendritic cells and natural killer cells were analyzed in 143B^{-/-} and 143B^{+/+} xenografts at day 30 post injection (Fig. 4.9). The significant upregulation of neutrophil could be attributed to lot of necrosis observed in 143B^{+/+} tumors as demonstrated by the histological staining (Fig. 4.10). There were no significant differences in the dendritic and natural killer cell contribution. However, a significant and consistent increase in tumor associated macrophages (TAM) was observed in 143B^{-/-} tumors (Fig. 4.9). This finding was further corroborated by significant increase in F4/80 (M2 macrophage marker) TAM infiltrations observed by immunofluorescence on sections from the 143B^{-/-} cancer masses (Fig. 4.11).

Overall, these data suggest that the macrophage abundance is a hallmark of CI deficient tumors and is a possible effect of the HIF-1 α inactivation in the 143B^{-/-} tumors. In addition, our data are also in agreement with previous reports that frequently associate high M2 macrophage

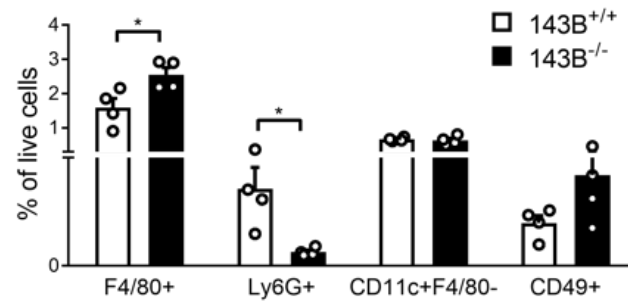


Fig. 4.9 Macrophage infiltration is a phenotype of 143B^{-/-} tumors. Flow cytometry analysis of innate immune system populations in 143B. The contribution of macrophages (F4/80+), neutrophils (Lys6G+), dendritic cells (CD11c+F4/80-) and natural killer cells (CD49b+) is shown at day 30 post injection in ICRF nude mice. Data are mean+SEM. N= 4; (* P<0.05). (Kurelac et al., 2019)

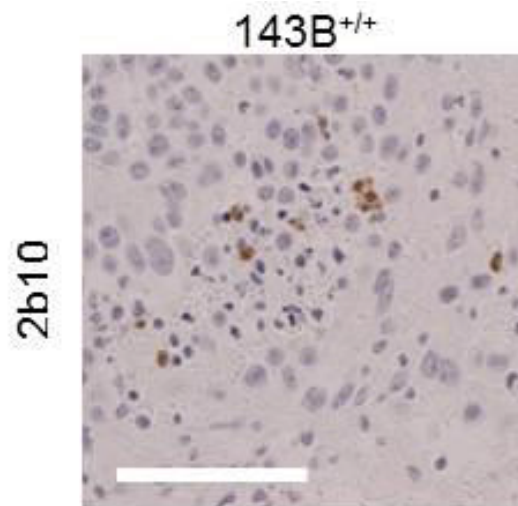


Fig. 4.10 143B^{+/+} tumors present with necrosis. Immunohistochemistry in 143B^{+/+} xenograft for neutrophil marker 2b10. Scale bar: 100 μ m.

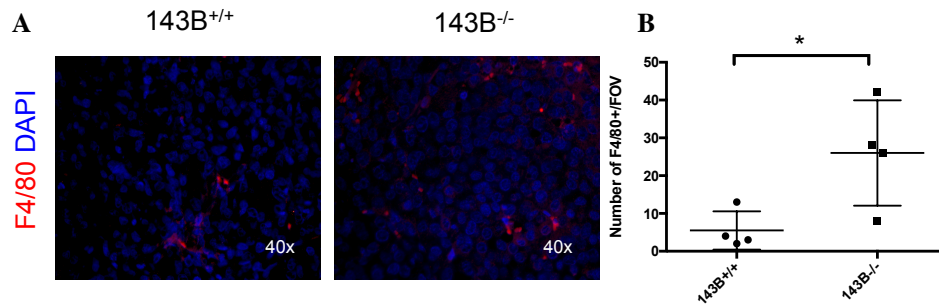


Fig. 4.11 143B^{-/-} xenografts present with higher macrophage abundance. (A) Immunofluorescence staining of 143B xenografts for macrophage marker F4/80. (B) Representative graph of the macrophage count of the 143B xenografts per field of view (FOV). Data displayed are mean \pm SEM N= 4; (* P<0.05).

numbers with increased vascular density and anomalies as seen in the CI deficient tumors (Clear et al., 2010).

4.2.2 HIF-1-MIF AXIS CONTRIBUTES TO MACROPHAGE ABUNDANCE IN 143B CI DEFICIENT TUMORS

After establishing that macrophage infiltration is one of the adaptive mechanisms triggered by the CI deficient tumors to maintain their growth, we aimed to investigate the various mechanisms and factors responsible for its abundance. The activation of the TAMs towards a pro-angiogenic phenotype is modulated by the stimuli in their surrounding TME and also by the cytokine milieu to which they are exposed (Arango and Descoteaux, 2014). The local cytokine microenvironment plays a significant role in tumorigenesis, tumor progression and resistance to oncotherapy. The development of cytokines in tumor disease is studied for three key purposes: first to understand and disclose tumorigenesis and immune escape mechanisms, second, to classify biomarkers for cancer detection, prognosis and clinical follow-up, and finally to assess them as potential cancer treatment immunotherapy targets (Kelso, 1998). Therefore, human cytokine array was used to detect the relative expression levels of 36 human cytokines in our 143B^{-/-} and 143B^{+/+} xenograft derived supernatants (Fig. 4.12B). The array showed a significant upregulation in the expression levels of IL-8 (CXCL8) and CXCL1, while MIF, CXCL12, SERPIN-E1 and G-CSF levels were downregulated in the 143B^{-/-} xenograft derived supernatant (Fig. 4.12A).

Among the above cytokines, macrophage migration inhibitory factor (MIF), which although exhibits pleiotropic functions, was of interest to us since hypoxia-induced HIF-1 α activation is implicated to stimulate its expression and it is also responsible for the inhibition of macrophage

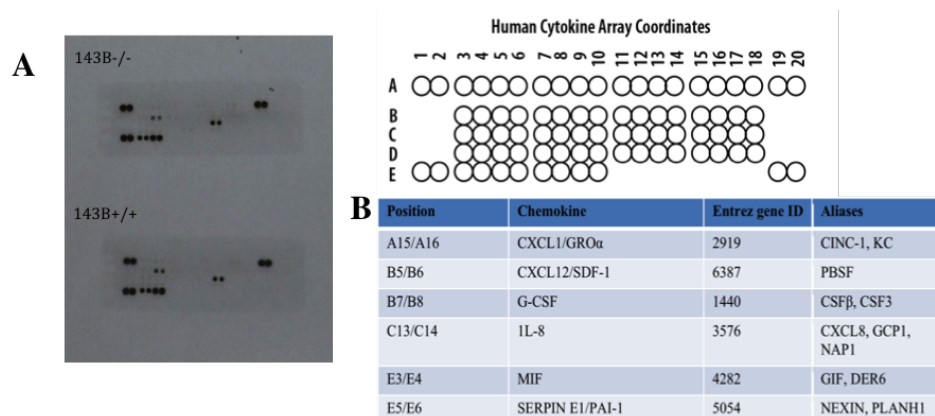


Fig. 4.12 MIF is one of the downregulated cytokine in HCT^{-/-} tumors. (A) Blotting of supernatants from 143B and HCT xenograft-derived cancer cells against the human cytokine array (B) Table representing the coordinates of the cytokine in the kit and the representative graph of the cytokine array analysis.

migration. Its expression level is directly associated with degrees of disease pathogenesis. In addition, MIF is also associated in the regulation of hypoxia-induced angiogenesis. (Castro et al., 2017; Abdul et al., 2018; Fu et al., 2010). Since MIF is also known for its endocrine and enzymatic functions, the correlation between its intracellular protein levels and mRNA was investigated next. To check for the difference in MIF gene expression and intracellular protein levels, qRT-PCR and western blot analyses were carried out respectively.

MIF expression was also checked in the *in vitro* cultures grown in hypoxia since it is one of a HIF-1 α target gene. Expression of the MIF was down regulated in the 143B^{-/-} with respect to the 143B^{+/+} tumors in xenografts after 30 days post inoculation (Fig. 4.13A) and even in hypoxia *in vitro* (Fig. 4.13B) indicating that the MIF downregulation could be a consequence of impaired response to hypoxia in 143B^{-/-} tumors. This was further corroborated by WB analysis where 143B^{-/-} showed MIF down regulation as presented by the lower band intensity (Fig. 4.13C).

Furthermore, 143B^{-/-} complemented with HIF-TM were analysed to confirm if HIF-1 is responsible for MIF regulation in these models. Indeed, in 143B^{-/-} HIF-TM xenografts, there was an up regulation of MIF expression in comparison to the Mocks and was evidenced by both qRT-PCR in xenografts (Fig. 4.14A) and *in vitro* (Fig. 4.14B) and also with WB analysis, providing further evidence that MIF followed HIF-1 regulation in these cells (Fig. 4.14C). Among other, TAMs are known to guide angiogenesis in tumors (Zhu et al., 2017), which generated hypothesis that increased TAM infiltration could be a compensatory mechanism to survive the inactivation of HIF-1 α mediated angiogenesis in 143B^{-/-} tumors. Thus, the contribution of the TAMs in 143B^{-/-} xenografts were checked after re-introducing the HIF-TM.

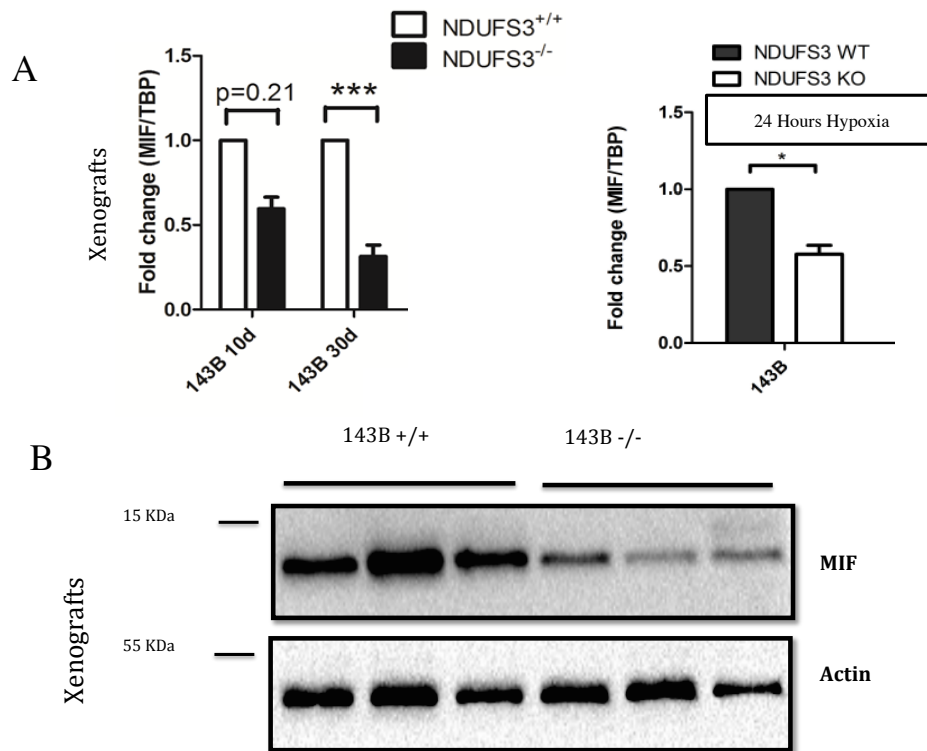


Fig. 4.13 143B^{-/-} tumors demonstrate a higher MIF expression compared to 143B^{+/+}. (A) qRT-PCR analysis of MIF expression in xenografts and (B) *in vitro* after 24H incubation in hypoxia (C) SDS-PAGE and Western Blot analysis of MIF expression in xenografts. Actin was used as a loading control. Data display mean \pm SEM. N = 3; (* P<0.05; ** P<0.01; ***P<0.001).

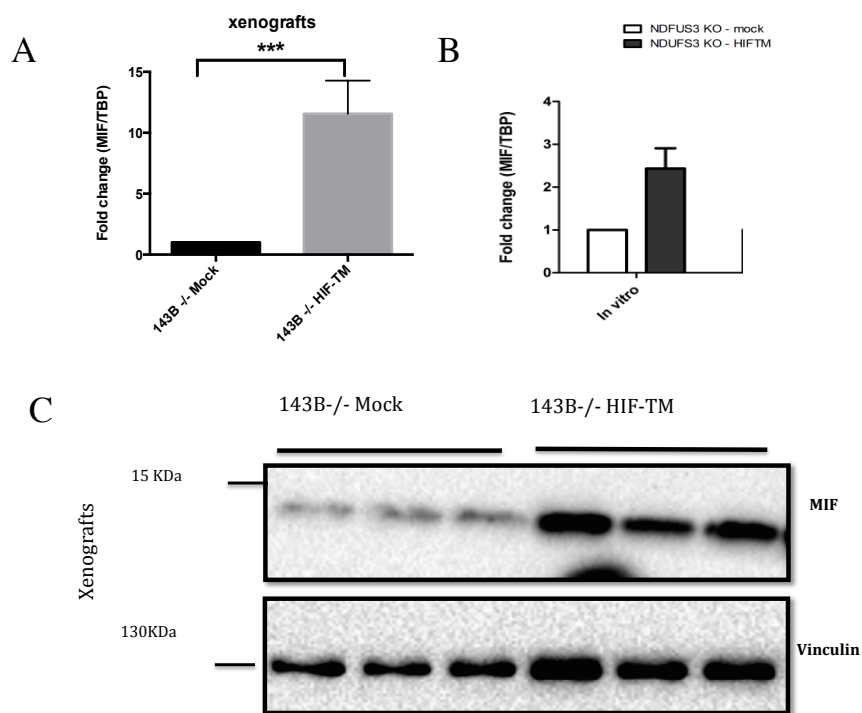


Fig. 4.14 143B^{-/-} HIF-TM tumors exhibits a higher MIF expression compared to 143B^{-/-} Mocks due to presence of stable HIF-1 α . (A) qRT-PCR analysis of MIF expression in xenografts and (B) *in vitro* (C) SDS-PAGE and Western Blot analysis of MIF expression in xenografts. Vinculin was used as a loading control. Data display mean \pm SEM. N = 3; (* P<0.05; ** P<0.01; ***P<0.001).

Indeed, the 143B^{-/-} HIF-TM masses showed a reduced F4/80 macrophage numbers compared to their 143B^{-/-} Mock controls (Fig. 4.15A and Fig. 4.15B), suggesting that HIF-1 α inactivity is partly responsible for TAM recruitment in 143B^{-/-} tumors.

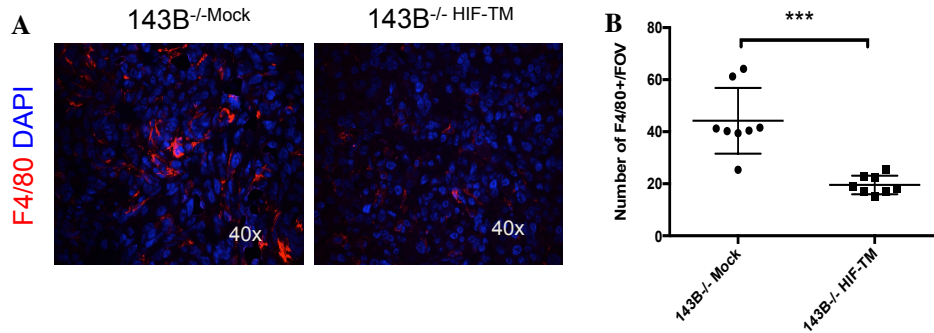


Fig. 4.15 143B^{-/-} HIF-TM xenografts arrest macrophage infiltration. (A) Immunofluorescence staining of 143B^{-/-} Mock and 143B^{-/-} HIF-TM xenografts for macrophage marker F480 represented in red and DAPI nuclei marker represented in blue. Magnification 40X. (B) Quantification of the macrophage count of 143B^{-/-} Mock and 143B^{-/-} HIF-TM xenografts per field of view (FOV) are represented by the graphs. Data displayed are mean \pm SEM N= 8; (***)P<0.001).

In conclusion MIF-HIF-1 axis disruption is one of the factors accountable for macrophage abundance in 143B^{-/-} tumors.

4.2.3 MACROPHAGE ABUNDANCE IS ASSOCIATED WITH CI DEFICIENCY AND HIF-1-MIF DOWNREGULATION IN THE ORTHOTOPIC OSTEOSARCOMA MODEL

The translatability of animal models is one of the biggest difficulties researchers face in preclinical oncology studies. It is a daunting challenge to accurately replicate human diseases to study the effects of novel therapeutics. Models are required in which the cancer cells interact with the complex microenvironment to recapitulate each form of cancer more faithfully. Only in the organ where the tumor has first developed can this relevant microenvironment be established. Due to the establishment of an organ-specific tumor microenvironment, which may vary in each type of cancer, orthotopic tumor models are clinically more important than their subcutaneous equivalents. Thus, a humanized bone-forming ectopic xenotransplantation model, recapitulating the bone like microenvironment was applied as a pseudo-orthotopic approach to grow osteosarcoma cells. In particular, already established 143^{+/+} and 143B^{-/-} models were used to corroborate the findings obtained in subcutaneous xenografts. The histology of these mesenchymal cell populations in the humanized bone xenografts was analyzed to study

the TME specific to osteosarcoma progression, which identified 143B^{-/-} to have more TAM contribution (Fig. 4.16), which was consistent with our previous findings that presented the same phenomenon in the 143B^{-/-} and HCT^{-/-} nude mice xenografts (Kurelac et al., 2019).

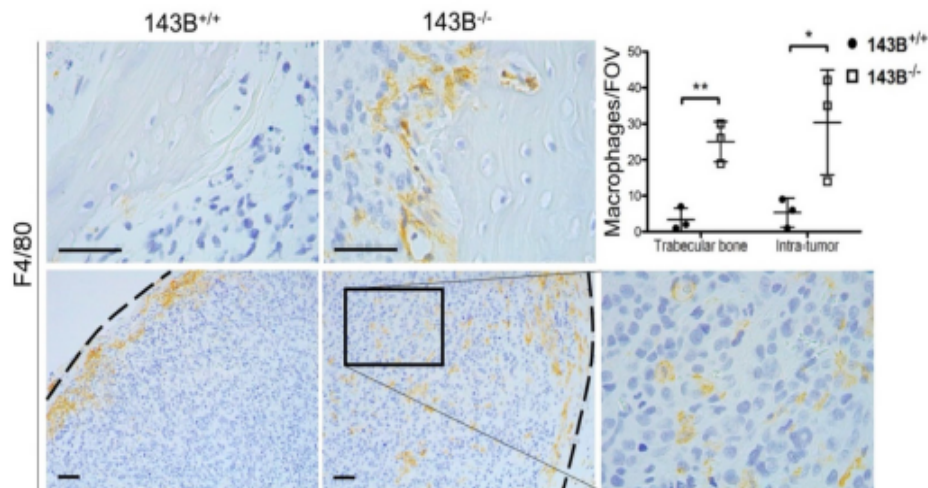


Fig. 4.16 143B^{-/-} tumors had higher macrophage infiltration. Representative images of immunohistochemistry analysis for macrophage marker F4/80 in 143B xenografts at day 30 in trabecular bone (upper images) and infiltrating the tissue (lower images). Scale bars: 50 μ m. Data displayed are mean \pm SEM; (* P<0.05; ** P<0.01).

Moreover, to check if these orthotopic 143B^{-/-} tumors were also characterized by lack of HIF-1 α stabilization like our 143B^{-/-} and HCT^{-/-} tumors, the expression of HIF-1 α and also their vasculature were checked at day 30 and day 60 post inoculation. Indeed orthotopic 143B^{-/-} displayed no HIF-1 α stabilization and small, lumen-free and SMA-negative vessels, while their 143B^{+/+} controls showed a HIF-1 α mediated mature, SMA positive vascularization as evidenced by the IHC analysis. Although, CI-deficient tumors associated with a higher number of vessels due to lack of HIF-1 α , they were relatively smaller in size compared to the control. Moreover they also lacked pericyte marker SMA (Fig. 4.17A and Fig. 4.17B).

Additionally, to identify the factors responsible for TAM recruitment in the 143B^{-/-} xenografts ,its supernatants were blotted on a human cytokine array and indeed MIF was found to be downregulated in the 143B^{-/-} tumors with respect to 143B^{+/+} tumors (Fig. 4.18).

In addition, it is interesting to note that morphological analysis revealed that 143B^{+/+} controls were characterized by loss of osteocytes with empty osteocytic lacunae in the mineralized bone matrix and by intensive necrosis, while the 143B^{-/-} tumors presented with no necrosis and higher osteocytes and osteoblasts in the trabecular bone confirming that the 143B^{-/-} pseudo-orthotopic xenografts preserved osteocytes and osteoblasts. This provided evidence of a humanized bone microenvironment (Fig. 4.19).

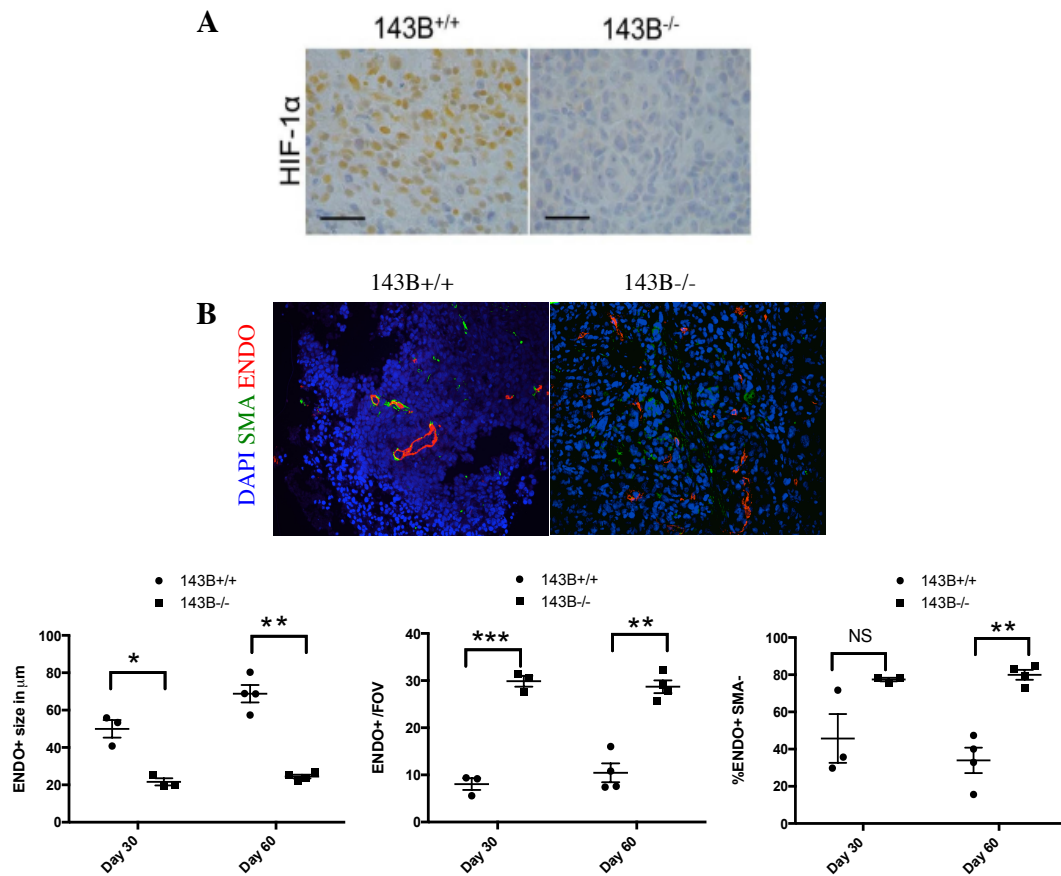


Fig. 4.17 143B^{-/-} xenografts are associated with HIF-1 α destabilization and demonstrate higher immature vessels count, negative for pericytes. (A) Immunohistochemistry analysis of the HIF-1 α in 143B^{+/+} and 143B^{-/-} osteosarcomas xenografts. Scale bars: 50 μm . (B) Immunofluorescent staining analyzing vessel morphology in CI-deficient and competent osteosarcoma xenografts. SMA (green) is fibroblasts marker, Endomucin (red) is vessels marker and DAPI (blue) is nuclei marker. Quantification of the total number of vessels per field of view (FOV), percentage of pericyte negative vessels (%Endo+SMA-) and the average vessel size in 143B^{+/+} and 143B^{-/-} tumors are represented by the graphs. Data displayed are mean \pm SEM. N=4; (* P<0.05; ** P<0.01; ***P<0.001; NS= Not significant). N=4.

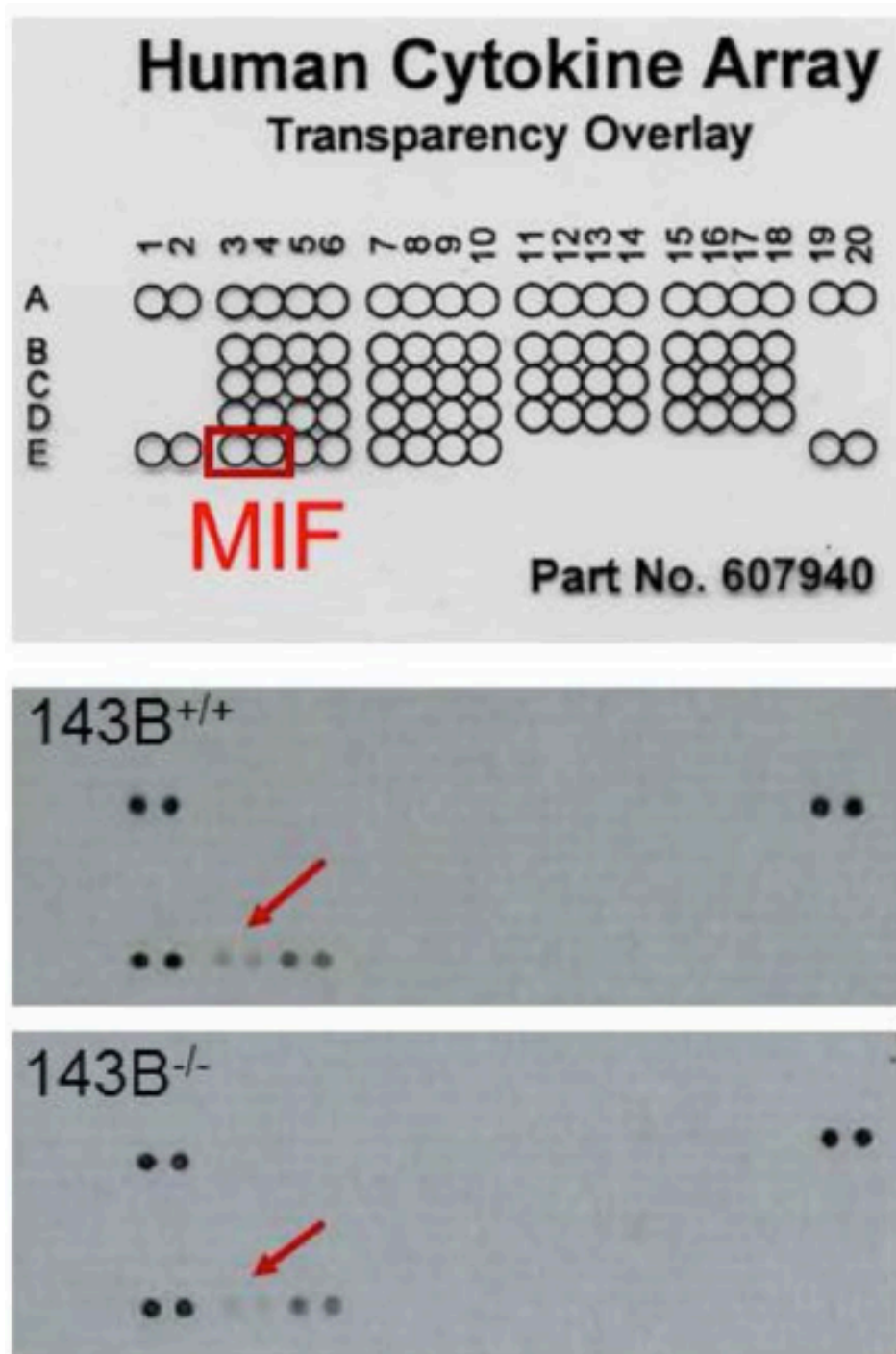


Fig. 4.18 143B^{-/-} xenograft derived supernatant is associated with MIF downregulation. In xenograft-derived cell culture supernatants, the results of cytokine screening. The arrows show the dot blots of the cytokine array for MIF.

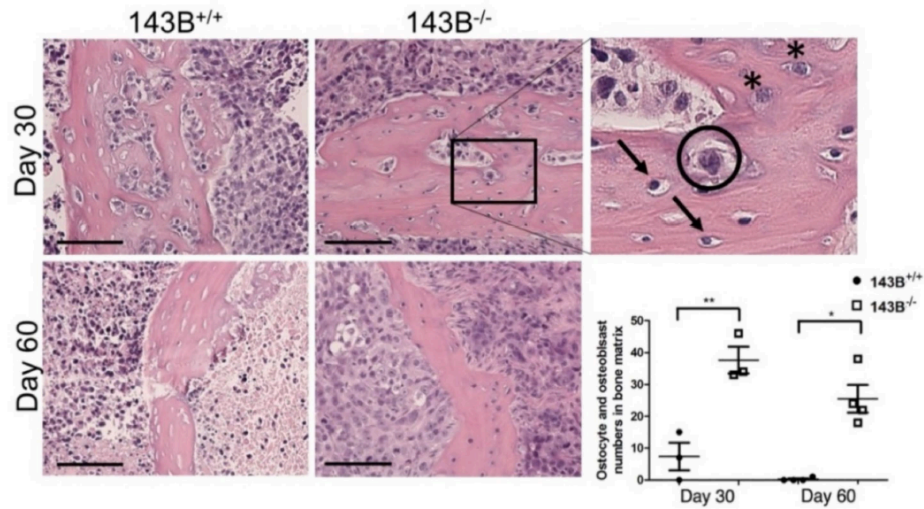


Fig. 4.19 143B^{-/-} pseudo-orthotopic xenografts preserved bone microenvironment. Hematoxylin and eosin staining of the trabecular bone in the 143B xenografts at day 30 and day 60 post implantation.; osteoblasts are indicated by the asterisks, osteocytes by arrows and the neoplastic cells are circled. Scale bars: 100 μ m. Quantification of osteocytes and osteoblasts in the osteosarcoma xenografts are represented by the graphs. Data displayed are mean \pm SEM; (* $p < 0.05$, ** $p < 0.01$).

Orthotopic tumor models are more clinically suited than subcutaneous models, on account of the formation of an organ-explicit TME, which can vary in each malignant growth type. The penetrating immune cells from subcutaneous mouse tumors can vary from those in orthotopic tumors from a similar model. Altogether, these data provide us with additional evidence that macrophages recruitment is one of the prominent phenotype associated with 143B^{-/-} tumors and is most likely a consequence of HIF-1-MIF axis disruption.

4.3 MACROPHAGE ABUNDANCE IN COLORECTAL CI DEFICIENT TUMORS IS NOT ASSOCIATED WITH Deregulation of HIF-1-MIF AXIS, REGARDLESS OF P53 STATUS

To understand if macrophage abundance is a generalizable phenomenon in CI deficient tumors, the TME of HCT tumors were investigated. Flow cytometry analysis of innate immune system namely macrophages, dendritic cells, neutrophils and natural killer cells were analyzed also in HCT^{-/-} and HCT^{+/+} xenografts at day 30 post injection. There were no significant differences in the neutrophils, dendritic and natural killer cells contribution. However, a significant increase

in TAM was observed in HCT^{-/-} tumors as well (Fig. 4.20). Thus, it may be concluded that macrophage infiltration was a common adaptive mechanism activated by CI deficient tumors.

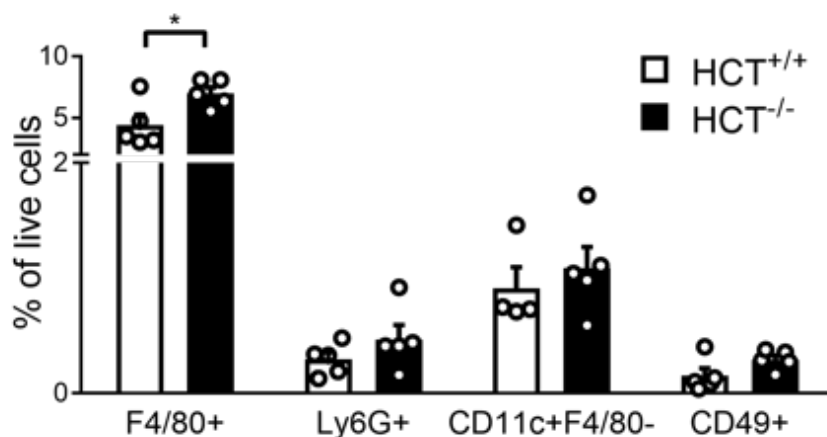


Fig. 4.20 Macrophage infiltration is a phenotype of HCT^{-/-} tumors. Flow cytometry analysis of innate immune system populations in HCT tumors. The contribution of macrophages (F4/80 +), neutrophils (Lys6G +), dendritic cells (CD11c + F4/80-) and natural killer cells (CD49b +) is shown at day 30 post injection in ICRF nude mice. Data are mean + SEM. (* P<0.05).

4.3.1 MIF IS NOT DOWNREGULATED IN HCT CI DEFICIENT TUMORS, DESPITE LACKING HIF-1 ACTIVITY

Since we found that the downregulation of MIF cytokine was involved in 143B masses, we wanted to understand whether the same mechanism could be associated with macrophage abundance in HCT models as well. qRT-PCR was done to analyze the MIF mRNA levels in HCT xenografts. Although there was a significant downregulation of MIF after 10 days in the HCT^{-/-}, there was no difference in MIF expression after 30 days *in vivo* (Fig. 4.21A). MIF expression was also checked in controlled conditions *in vitro* in hypoxia to understand better the differences we see *in vivo*. There was no difference in MIF expression *in vitro* (Fig. 4.21B) suggesting that after initial decrease, MIF levels are recovered in the HCT^{-/-} tumors eventually. The incongruous expression between mRNAs and intracellular proteins highlights the significance of posttranscriptional regulatory mechanisms that can be revealed only by integrated studies of both intracellular proteins and mRNAs in cell growth or disruption. Thus, the MIF intracellular protein expression was checked in HCT tumors. However, there were no changes in the MIF intracellular protein expression of the HCT^{-/-} and HCT^{+/+} masses analyzed by WB at 30 days post injection, which showed similar band intensities (Fig. 4.21C). This gives us further evidence that intracellular MIF is not regulated by HIF-1 in HCT tumors.

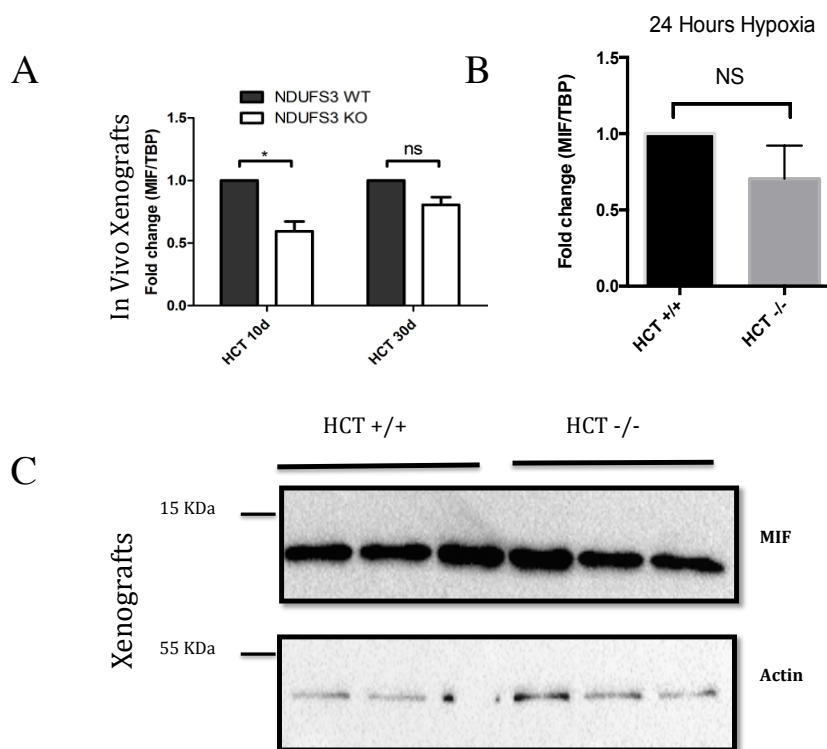


Fig. 4.21 HCT+/+ tumors demonstrate no significant changes in MIF expression compared to HCT-/- counterpart. (A) qRT-PCR analysis of MIF expression in xenografts and (B) *in vitro* after 24H incubation in hypoxia (C) SDS-PAGE and Western Blot analysis of MIF expression in xenografts. Actin was used as a loading control. Data display mean \pm SEM. N = 3; (NS= not significant).

4.3.2 HIF-1 IS NOT ACCOUNTABLE FOR MACROPHAGE ABUNDANCE IN HCT CI DEFICIENT TUMORS

As mentioned previously, MIF is a HIF-1 target and since we did not see any difference in MIF status in HCT model we hypothesized that mechanism other than HIF-1 could be involved in macrophage abundance in colorectal cancer setting. To corroborate this, we next tested whether the macrophage abundance depends on HIF-1 activity in HCT^{-/-} tumors. The macrophage count was analyzed in the HCT^{-/-} HIF-TM and HCT^{-/-} Mock xenografts. There were no differences in the macrophage count between the HCT^{-/-} HIF-TM and Mock samples, demonstrating that the mechanisms involved in the macrophage abundance in the HCT^{-/-} tumors is infact independent of HIF-1 activation (Fig. 4.22).

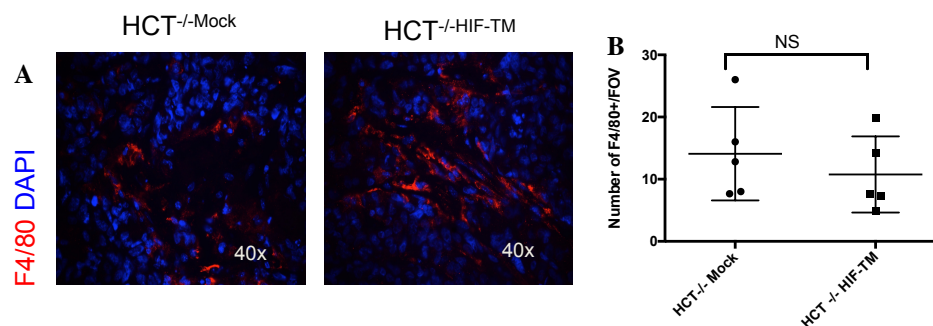


Fig. 4.22 HCT^{-/-} HIF-TM xenografts has no significant changes in macrophage count compared to HCT^{-/-} mocks. (A) Immunofluorescence staining of HCT xenografts for macrophage marker F480 represented in red and DAPI nuclei marker represented in blue. Magnification 40X. (B) Quantification of the macrophage count of the HCT^{-/-} Mock and HCT^{-/-} HIF-TM xenografts per field of view (FOV) are represented by the graphs. Data displayed are mean ± SEM. N = 4; (NS= Not significant).

Moreover, the incorporation of HIF-TM did not result in any significant changes in MIF expression in the HCT^{-/-} HIF-TM and Mock as evaluated by both transcriptional *in vivo* (Fig. 4.23A), *in vitro* (Fig. 4.23B) and translational regulation (Fig. 4.23C), indicating that mechanisms other than downregulation of HIF-1-MIF axis are involved in TAM abundance in HCT tumors.

Collectively, the data indicate that the difference in MIF expression is tissue specific and that the macrophage abundance may be a consequence of HIF-1 α /MIF axis disruption in 143B^{-/-} but not in HCT^{-/-} background.

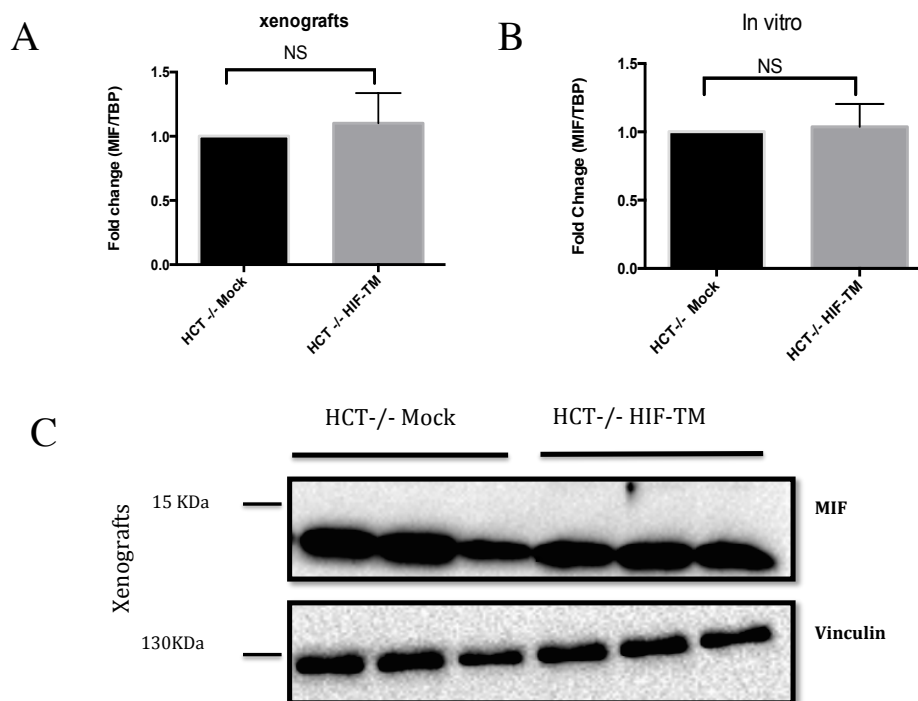


Fig. 4.23 HCT-/- HIF-TM tumors show similar MIF expression compared to HCT-/- Mock irrespective of presence of HIF-1 α . (A) qRT-PCR analysis of MIF expression in xenografts and (B) *in vitro* (C) SDS-PAGE and Western Blot analysis of MIF expression in xenografts. Vinculin was used as a loading control. Data display mean \pm SEM. N = 3; (NS= not significant).

4.3.3 LACK OF MIF DOWNREGULATION IN CI DEFICIENT TUMORS DOES NOT DEPEND ON p53

We have demonstrated that MIF is not regulated by HIF-1 in the HCT models as compared to 143B models. It is important to note that our 143B models have TP53 with R156P mutation, while our HCT models lack p53, disrupted through homologous recombination (Bunz et al., 1999). p53 is a well-known ‘guardian of genome’ and tumor suppressor frequently mutated in cancer. MIF was first reported as a negative regulator of p53 by Hudson et al., 1999. Since then, several studies have validated MIF as a significant endogenous regulator of the expression and function of p53 in a variety of biological processes (Kleemann et al., 2000; Mitchell et al., 2002). There is compelling proof that overlapping pathways mediate the effects of MIF on cell survival and tumorigenesis, in which MIF and p53 functionally antagonize each other in the cell (Fingerle-Rowson, Petrenko, 2007). Therefore, we hypothesized that the lack of MIF downregulation in HCT^{-/-} model, as seen in 143B^{-/-}, could be due to lack of p53 in the HCTs. Thus, to eventually comprehend the mechanism behind the TAM infiltration in the HCT CI deficient models, the relation between HIF-1 α , MIF and P53 was investigated next. HCT NDUFS3^{-/-} p53^{-/-} cell lines were transfected with wildtype p53, R156P mutated p53 or mock empty vector control (PMSCV) and were subjected to hypoxia or normoxia for 24 hours. To verify the transfection of p53 to make sure there were no technical issues, WB analysis was carried out, which confirmed the expression of the WT and Mut p53 in HCT^{-/-} cell lines, both in normoxia and hypoxia (Fig. 4.24B). Moreover, the appropriate activation of p53 was confirmed by qRT-PCR analysis of p53 responsive genes P21 whose expression was upregulated in WT and Mut p53 transfected cells as compared to the PMSCV control (Fig. 4.24C). By comparing the MIF expression against HCT^{-/-} PMSCV mock controls we observed that HCT^{-/-} showed no difference in MIF expression between hypoxia and normoxia when they lacked p53, however they displayed a substantially higher MIF expression in hypoxia compared to normoxia after the p53 transfection with WT or Mut as indicated by the qRT-PCR (Fig. 4.24A), which was antithesis of what we had predicted. In particular, an increased MIF levels in hypoxia was detected in the presence of wild type p53 (Fig. 4.24A). However, intracellular MIF showed no difference in its protein expression in HCT^{-/-} cells, regardless of p53 status or oxygen concentrations (Fig. 4.24B).

Based on our studies, we can conclude that the HCT^{-/-} cells showed a p53 dependent MIF upregulation. Unexpectedly, incubation in hypoxia significantly increased HCT^{-/-} MIF expression further despite their inability to activate HIF-1, indicating, p53 upregulated MIF in hypoxia, independent of HIF-1 α stability. Therefore, p53 does not downregulate the MIF expression in HCT^{-/-} cells as hypothesized.

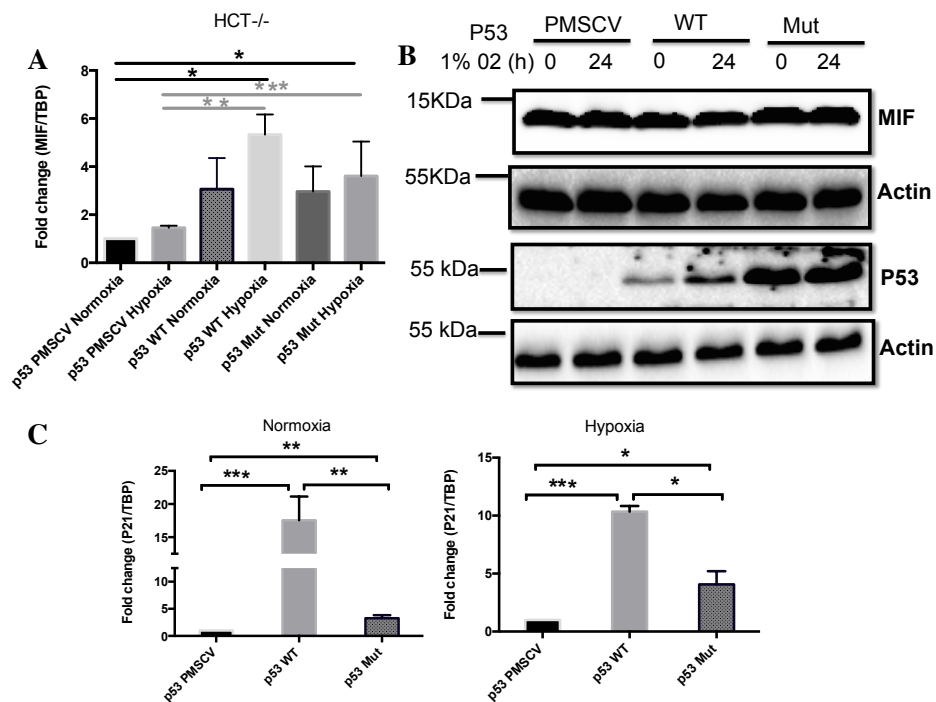


Fig. 4.24 MIF upregulation is P53-dependent and is significant in hypoxia but not normoxia in presence of a defective CI. (A) RT-PCR analysis of MIF expression in HCT^{-/-} with PMSCV mock or WT P53 or Mut P53 transfected cells after a total RNA extraction, incubated 24h in normoxia or hypoxia. HCT^{-/-} p53 PMSCV cell cultured in normoxia used as a control (B) SDS-PAGE and Western Blot analysis for MIF and p53 expression of the same cultured in normoxia or incubated in hypoxia for 24h. Actin was used as a loading control. (C) qRT-PCR analysis of P21 in HCT^{-/-} cells with either PMSCV control, WT or Mut P53 genotype incubated in normoxia (21% O₂) or hypoxia (1% O₂) for 24 hours. Data are mean \pm SEM. N = 3; (* P<0.05; ** P<0.01; ***P<0.001).

4.4 NINE METABOLITES IDENTIFIED AS POSSIBLE FACTORS DRIVING MACROPHAGE ABUNDANCE IN CI DEFICIENT TUMORS

Although we suggest disruption of HIF-1-MIF axis as a possible mechanism of macrophage attraction in 143B^{-/-} tumors, we were not able to identify any factors linking the CI deficiency to macrophage abundance in HCT tumors. Moreover, pharmacological targeting of MIF downregulation to prevent TAM abundance in CI deficient tumors is difficult to achieve. Thus, we next searched for further factors involved in TAM abundance in CI deficient tumors. Medical science has been revolutionized by high-throughput technologies, such as proteomics and metabolomics, which are now integrated into biological researchers' regular methodology to identify essential networks and signalling pathways that can play an important role in cancer metabolic control. In line with this, to identify the specific molecular/metabolic targets that could contribute to the recruitment of the TAMs in the CI deficient tumors, to eventually target them to improve the anti-cancer effects of CI inhibition, proteomics and metabolomics analyses were carried out on the 143B and HCT secretome (*post vivo* conditioned media).

4.4.1 PROTEOMICS DOES NOT IDENTIFY COMMON SECRETED PROTEINS BETWEEN CI-DEFICIENT 143B AND HCT CELLS

Small proteins such as cytokines help to regulate nearly all-immune processes and enables immune cells to communicate; they are secreted through interaction with a pathogen- or damage-related molecular pattern or an antigen from immune cells. To identify the potential common factors involved in TAM recruitment by the CI-deficient cancer cells, proteomics was performed on the conditioned media of osteosarcoma and colorectal cancer, to expand the cytokine array analysis to the whole secreted proteome.

In both 143B and HCT model, the principal component analysis (PCA) analysis showed two distinct clusters for the two different groups being compared (Fig. 4.25A), meaning that there was no variation within each compared groups. The volcano plots with threshold $-\text{Log}_p=1$ were obtained to visualize significantly upregulated or downregulated proteins from the proteomics data (Fig. 4.25B). Eight proteins and 32 proteins were identified as upregulated in the 143B and HCT CI-deficient xenografts, respectively. On the other hand, eight proteins in 143B and 53 proteins in HCT were downregulated in the CI-deficient xenografts. For example, the upregulated secreted proteins in the 143B deficient included LOXL2, TIM and MSMP, whereas HCT deficient cells secreted GPI, FABP5, NCL and FEN1. However, after analyzing data with VENNY 2.1 software, we could not identify any factors secreted by both of the cancer

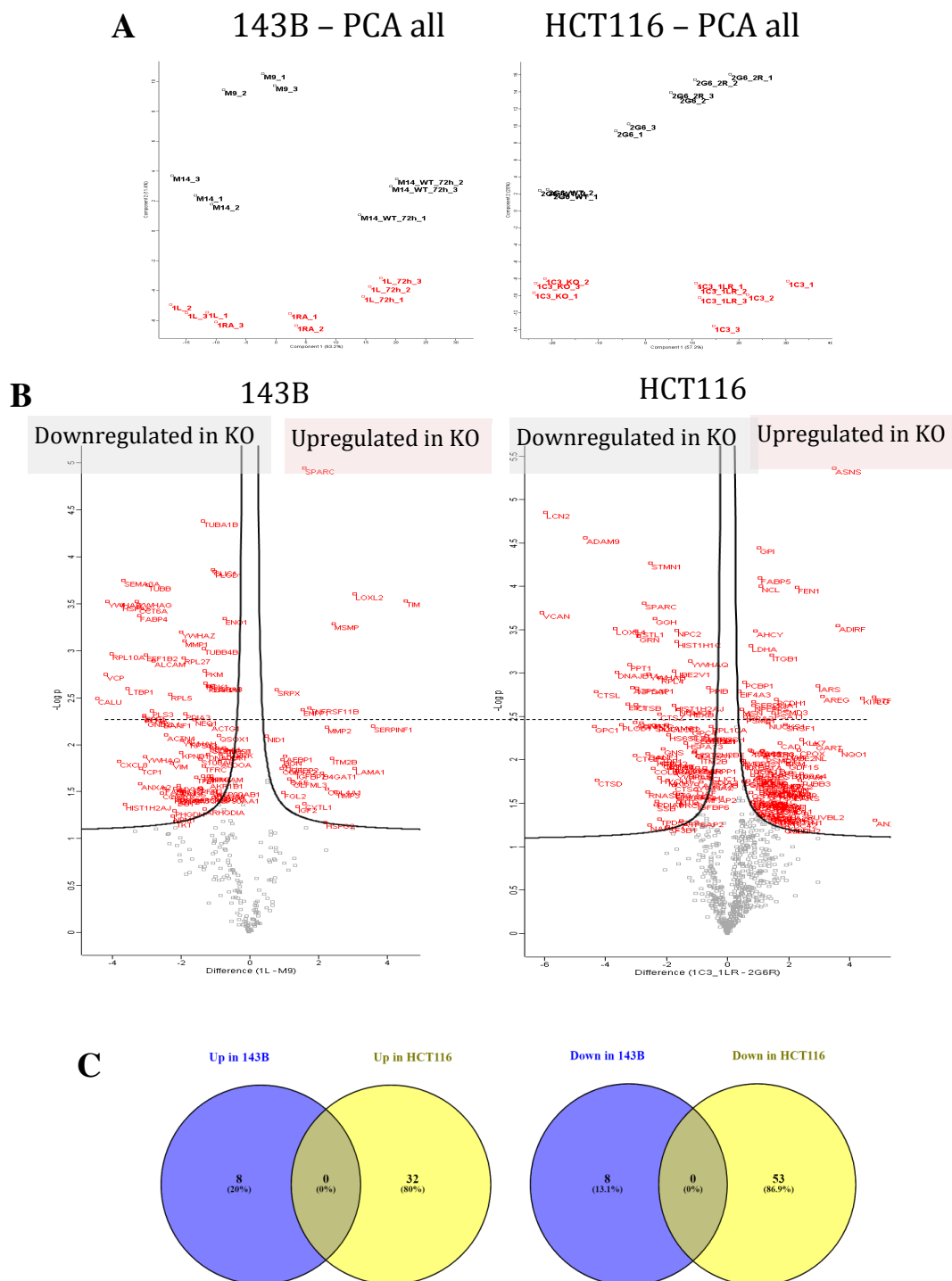
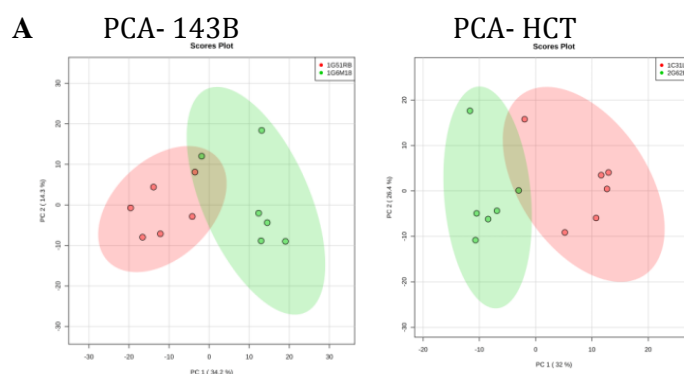


Fig. 4.25 No common secreted proteins between 143B and HCT. (A) Principal component analysis (PCA) of the proteomics data of 143B and HCT CI-deficient and CI-competent models (B) Volcano plots presenting the proteomics summary of the post *ex vivo* conditioned media of osteosarcomas 143B and colorectal HCT cancers (B) Venn diagrams using the VENNY 2.1 software showing overlap of the proteomics data of 143B and HCT secretome.

cells (Fig. 4.25C), suggesting that there was no common secreted proteins upregulated or downregulated between 143B and HCT.

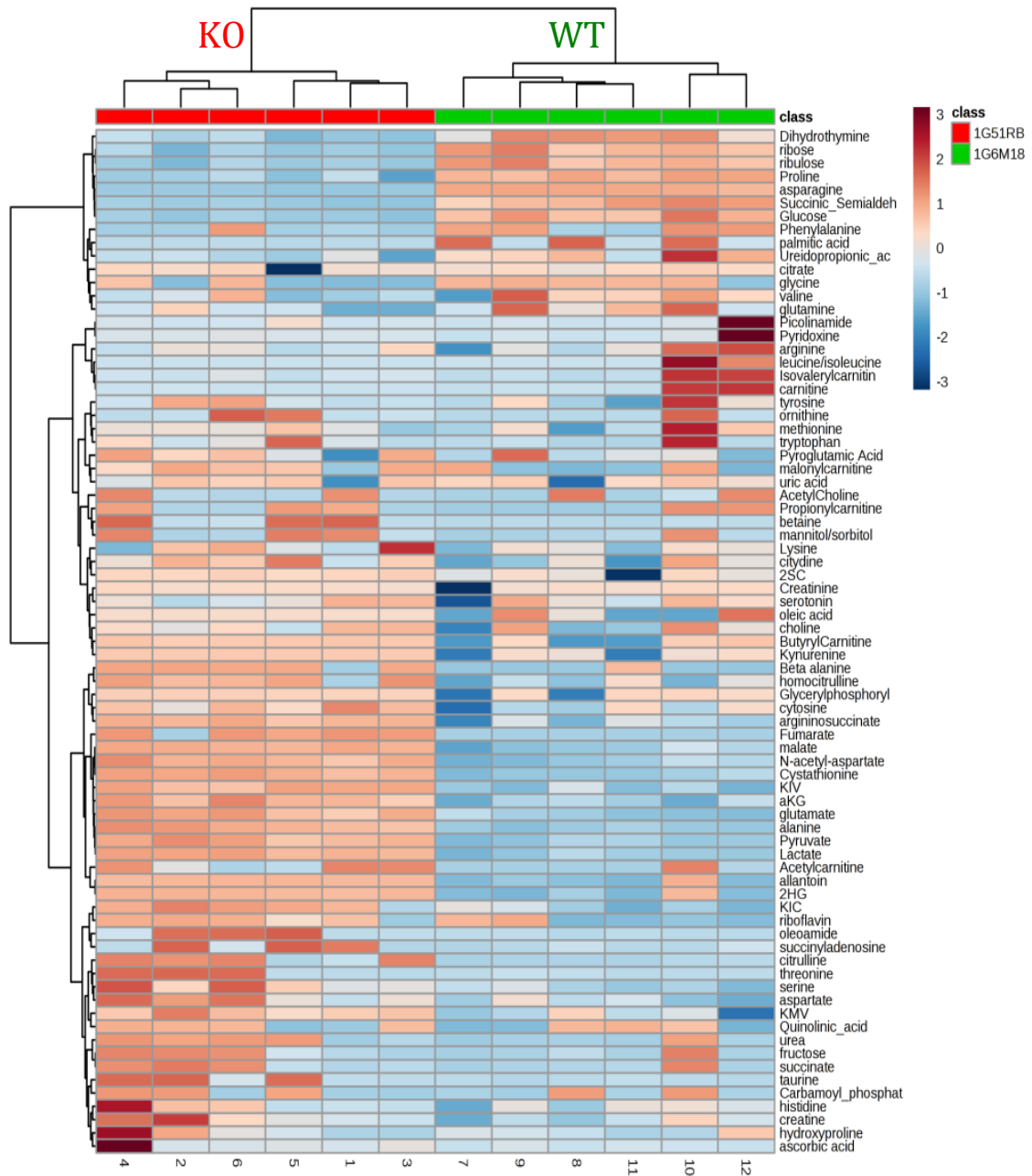
4.4.2 METABOLOMICS ANALYSIS IDENTIFIES NINE METABOLITES SPECIFICALLY SECRETED BY CI-DEFICIENT MODELS

There is a new emerging concept indicating that metabolites may regulate cytokine like effects, by modulating the activity of specific enzymes, proteins or transcription factors as described in detail in the review by Zaslona and O'Neill (2020). Thus, metabolomics analysis was carried out on the secretome of the CI deficient and CI competent *ex vivo* cultures, to identify the small molecule types like fatty acids, carbohydrates, amino acids and other metabolites that could be involved in modifying TME of CI deficient cancers. In both 143B and HCT, the PCA analysis showed two distinct clusters for the two different groups being compared (Fig. 4.25A), confirming there was no variation within each compared groups. The homogeneous distribution of metabolites within WT versus KO secretomes is furthermore evident from hierarchical clustering (Fig. 4.25B). Eight upregulated metabolites that included ribose, ribulose, proline, asparagine etc were found in 143B+/+ secretome, and 21 downregulated metabolites including citrulline, serine, aspartate among others were identified in 143B-/- secretome. 15 upregulated metabolites that included cytidine, proline, taurine, glycine etc were recognized in HCT+/+ secretome and 18 downregulated metabolites including aconitate, adenosine, beta alanine among others were identified in HCT-/- secretome. Out of the total 21 downregulated metabolites in 143B-/- and 18 downregulated metabolites in HCT-/- analyzed, the VENNY 2.1 software overlapping the metabolomics data revealed nine metabolites secreted by CI deficient cells common to both the cancers (Fig. 4.25C). These include lactate, 2HG, Fumarate, Malate, α -KG, Glutamate, Alanine, KIC (a-ketoisocaproate) and KMV (a-keto methylvalerate) (Table 1).

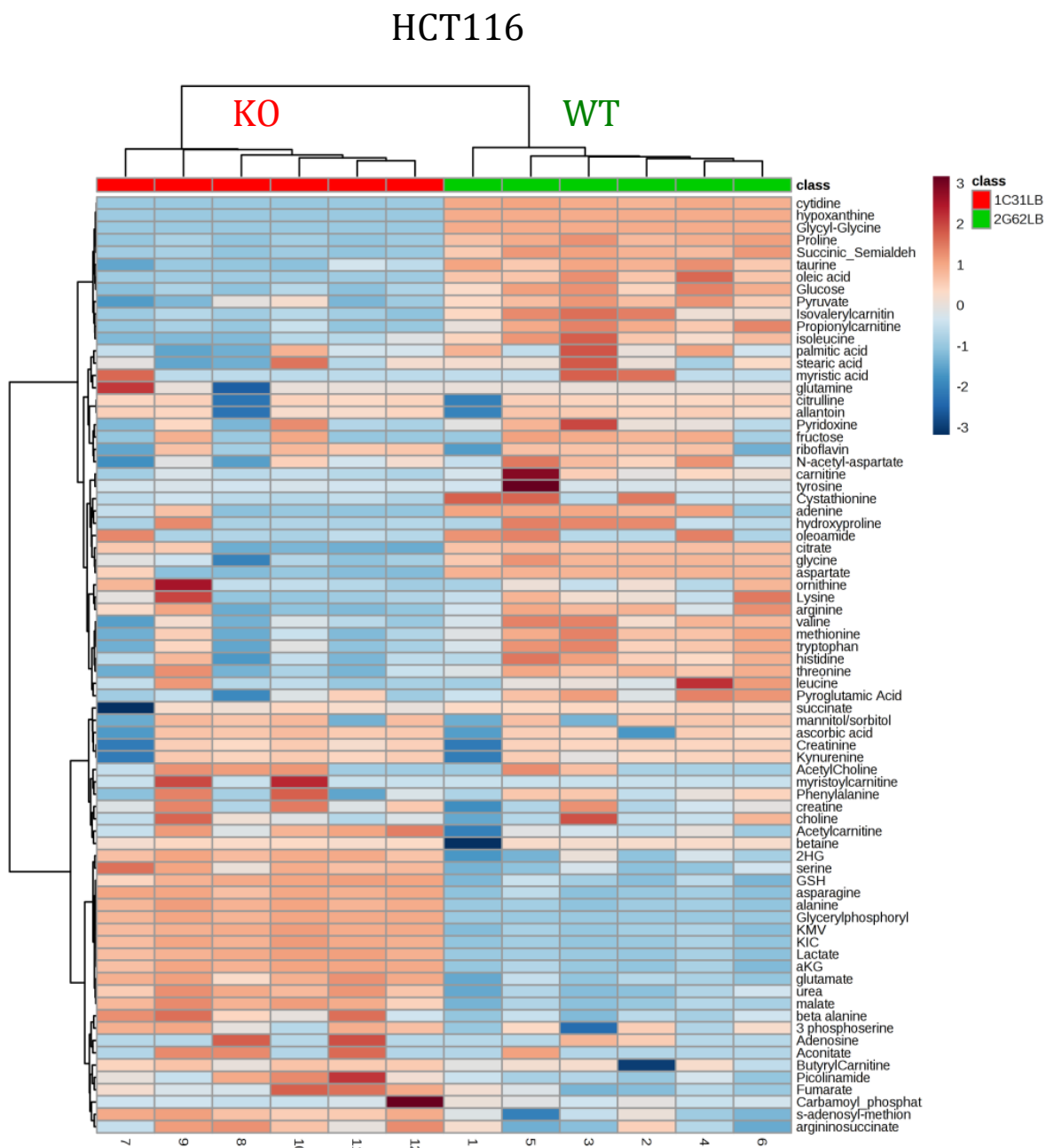


B

143B



4.4 NINE METABOLITES IDENTIFIED AS POSSIBLE FACTORS DRIVING MACROPHAGE ABUNDANCE IN CI DEFICIENT TUMORS



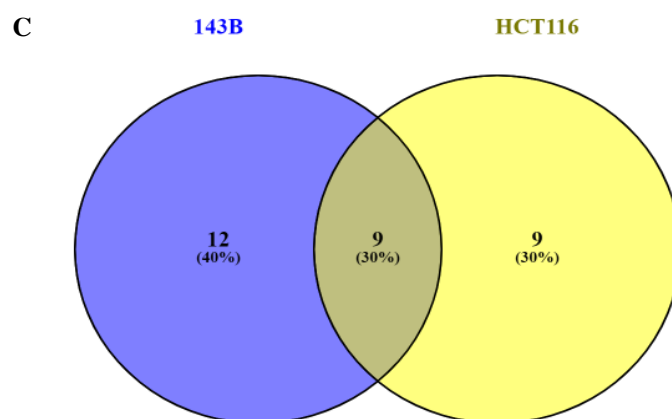


Fig. 4.25 LC-MS analysis reveals nine common metabolites between 143B and HCT conditioned media. (A) Principal component analysis (PCA) of the metabolomics data of 143B and HCT CI-deficient and CI-competent models. The CI-deficient 143B and HCT is represented in green and the CI-competent 143B and HCT tumors are represented in red (B) HeatMap analysis of the metabolites after post *ex vivo* conditioned media based LC-MS analysis in 143B+/+ & 143B-/-osteosarcomas and HCT+/+ & HCT-/-colorectals. Data was mean normalized, log transformed and paretoscaled. The color scale indicates the relative expression levels of the metabolites across all samples(C) Venn diagrams using the VENNY 2.1 software showing overlap of the metabolomics data of 143B and HCT revealed nine secreted metabolites common to both.

There are already indications in the literature that metabolites may exert immunomodulatory effects. For example, KIC and KMC are the branched chain keto acids (BCKAs) that have been reported to modulate the tumor-associated macrophages, contributing to their role in tumor immunosuppression in glioblastoma (Silva et al., 2017) In addition, high α KG/succinate ratio, as seen in our CI deficient tumors, resulted in the alternative M2 activation of macrophages, including engagement of fatty acid oxidation (FAO) and Jmjd3-dependent epigenetic reprogramming of M2 genes (Liu et al., 2017).

Metabolites	CI competent (WT)	CI competent (KO)
Lactate	↓Release	↑Release
2HG	↓Release	↑Release
Fumarate	↓Release	↑Release
Malate	↓Release	↑Release
α KG	↓Release	↑Release
Glutamate	↓Release	↑Release
Alanine	↓Release	↑Release
KIC (a-ketoisocaproate)	↓Release	↑Release
KMV (a-keto methylvalerate)	↓Release	↑Release

Fig. 4.26 Metabolites significant in both osteosarcomas 143B and colorectal HCT cancer

Next, the obtained significantly upregulated or downregulated secreted metabolites were subjected to pathway and enrichment analysis based on Metaboanalyst 4.0 to identify and interpret patterns of metabolite changes in a biologically relevant way. The associated metabolic pathways are shown in (Fig. 4.27). As a possible target pathway, the pathway impact value determined from pathway topology analysis of > 0.1 was filtered out. Glutamine and glutamate, pyruvate biosynthesis, alanine, aspartate and glutamate metabolism were the most important metabolic pathways affected by 143B $^{-/-}$ and HCT $^{-/-}$ tumors compared to the 143B $^{+/+}$ and HCT $^{+/+}$ tumors respectively (Fig. 4.27A). The three important metabolic pathways were all related with amino acid metabolism, suggesting that the latter might play a major role in assisting the adaptive mechanism of CI deficient cells to grow. In addition, the metabolite set enrichment analysis indicated that glycolysis, selenocompound metabolism, glutamine and glutamate metabolism, and pyruvate metabolism, valine, leucine, and isoleucine degradation, and alanine metabolism are the top common metabolite concentrated sets being altered in CI deficiency tumors compared to the CI competent tumors (Fig. 4.27B). All metabolite sets were directly associated with amino acid metabolism. Furthermore, there were pathways known to relate to the suppression of cancer, one of the significant pathways being selenocompound metabolism. The potential for the anticancer effects of the micronutrient element selenium was

demonstrated previously (Bartolini et al., 2017). All together, the metabolite set enrichment analysis provides further evidence that amino acid metabolism, glycolysis, glutaminolysis could be a key common mechanisms differentially regulated in the CI deficient cells for the maintenance of their growth.

4.4 NINE METABOLITES IDENTIFIED AS POSSIBLE FACTORS DRIVING MACROPHAGE ABUNDANCE IN CI DEFICIENT TUMORS

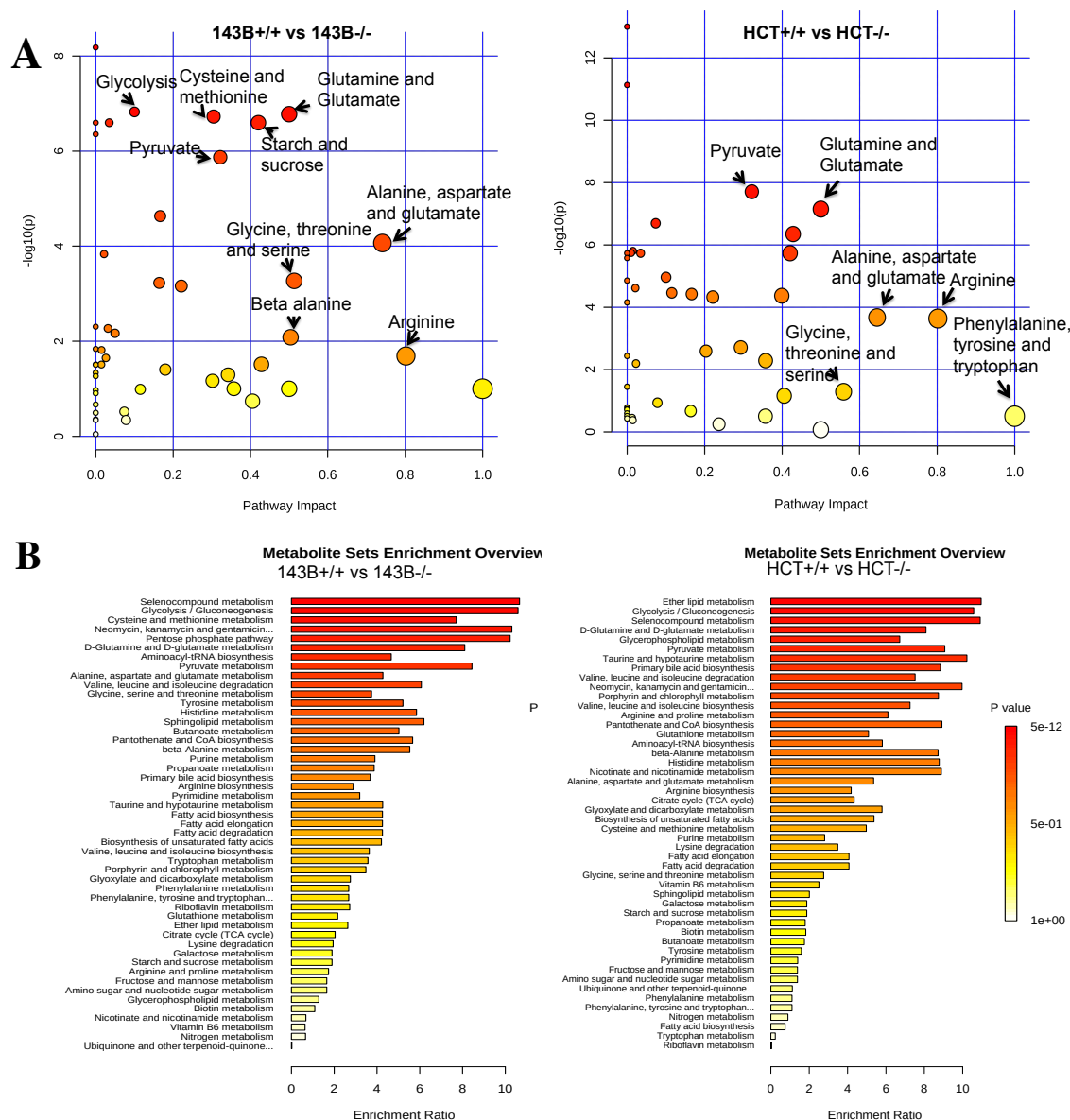


Fig. 4.27 Summary of pathway analysis of the 143B and HCT xenograft derived supernatants showing glycolysis and selenocompound metabolism that was the most disrupted pathways. (A) The matched paths are all seen as circles. The color of each circle is dependent on p-values (in the subsequent pathway, darker colors reflect more important changes in metabolites), while the size of the circle corresponds to the impact score of the pathway. The most influenced pathways with high scores of statistical importance are annotated. The x-axis represents the pathway impact value computed from pathway topological analysis and $-\log$ of the P-value obtained from pathway enrichment analysis is represented as the y-axis. (B) Overview of the metabolite set enrichment analysis in 143B and HCT post *ex vivo* conditioned media. The intensity of the color is correlated with the degree of statistical importance of each pathway (highly significant - red, not significant - white), while the length of each bar reflects the fold enrichment of each pathway.

Chapter 5

DISCUSSION

In the last decade, 70 years after Warburg identified aerobic glycolysis as a characteristic of cancer cells, cancer metabolism has undergone resurgence. The vast variations between tissues, tumor types and intratumor heterogeneity have been elucidated by a wide variety of techniques. Despite a broad knowledge of metabolic regulation based on nearly a century of biochemistry studies, our knowledge of how pathways are regulated to promote cell proliferation remains incomplete. Further knowledge of precisely how cells control nutrient flux into pathways needed for biosynthesis in particular genetic contexts would result in success in targeting cancer metabolism. Understanding the metabolism of tumor cells involves the use of techniques to test metabolite flux and pathway modulation that are not often used in the development of cancer drugs. However, provided that all cancer cells rely on metabolic changes to sustain their growth, targeting the metabolism has the potential to impact cancers arising from many different tissues.

Targeting mitochondrial CI is considered a promising anti-cancer therapeutic strategy in recent years (Akatsuka et al., 2016; Bastein et al., 2017). Particularly, CI inhibitor metformin has given encouraging results in experimental and clinical settings for the treatment of solid cancers (Wheaton et al., 2014; Gong et al., 2016; Higurashi et al., 2016). Severe CI deficiency has been shown in low-proliferative, indolent oncogenic tumors where HIF-1 α stabilization is prevented by metabolic rearrangements following CI disassembly (Porcelli et al., 2010) leading to the inability of cancer cells to respond to hypoxia. The reduction of stabilized HIF-1 α is accounted by the accumulation of α -KG and O₂ (Tennant et al., 2009; Hagen et al., 2003; Kurelac et al., 2019). This results in pseudonormoxic feature preventing the tumor from developing a warburg phenotype and progressing to malignancy. In addition, genetically targeting CI in various cancer types to prompt their conversion to oncocytomas, lead to a lack of HIF-1 α while accumulating defective mitochondria and showed impaired metabolic flexibility in hypoxia (Calabrese et al., 2013; Gasparre et al., 2011). Extending this

idea, using Crispr/Cas9 technology, *Ndufs3* was targeted to abolish CI activity in B16F10 murine melanoma cells to check if HIF-1 α destabilization was a generalized phenomenon in mammalian species other than humans. Indeed, two clones, which represented the phenotype of our already established CI deficient 143B and HCT cells (Kurelac et al., 2019) that lacked CI activity demonstrated that they could not stabilize HIF-1 α expression even in hypoxia *in vitro*. Of note, the absence of an adaptive immune system in immunodeficient mice such as the nude mice used in the previous studies prevents the investigation of anti-tumor metabolic or immune response treatments. Therefore the B16^{-/-} clones will be eventually used to understand the complete effects of CI deficiency on its TME and to corroborate our findings in this study in an immunocompetent model by taking into consideration the adaptive immune system. There has been conflicting evidence on the effects of CI targeting on its TME. Recently it was observed that tumor associated macrophages might be involved in compensatory mechanisms triggered by targeting CI in several solid cancers (Kurelac et al., 2019). On a similar note, it has recently been suggested that mitochondrial function needs to be maintained in order to respond to immunotherapy (Harel et al., 2019). In addition, by knocking out CI using experimental small interfering RNA, reduced 1L-2 and 1L-4 secretion were demonstrated by the activated T cells. By blocking 1L-4, known to be associated with differentiation of helper CD4⁺ T cells into Th2 cells through CI inhibition promoted the pro tumorigenic T regs (Kaminski et al., 2010). Conversely, others have shown that inhibiting CI in cancer cells reduces myeloid derived suppressor cell activity (Uehara et al 2019) and actually improves T-cell cytotoxicity (Eikawa et al., 2015). Moreover, CI blockade, however, also has tumor-promoting effects, leading to increased lactate content and expression of VEGF in cancer cells, promoting tumor growth in mice (Chaube et al., 2015). These opposing observations prompt for a more detailed investigation of the effects of CI inhibition on individual TME cell populations. It is rational to suggest that the loss of HIF-1 α threatens the progression of CI-deficient masses due to the large number of pro-survival mechanisms triggered by HIF-1 α . In this present study, we have provided evidence for such hypothesis by complementing CI-deficient cells with a non-degradable and stable HIF-TM. Introducing the HIF-TM into the 143B^{-/-}-HIF-TM and HCT^{-/-}-HIF-TM cells rescued their tumorigenic potential *in vivo* in addition to upregulation of HIF-1 target genes *SLC2A1*, *LDHA* and *VEGF* as compared to the mock controls. But this is not surprising in itself; because it has been extensively shown by other groups that knockdown of HIF slows down the tumor progression. Indeed loss of HIF-1 reduced tumor progression in several cancer models (Schwab et al., 2012; Gillespie et al, 2007) and also by authoritative groups such as Semenza's (Lee et al., 2009) and Simon's group (Shay et al., 2014). By decreasing oxygen intake and increasing its supply, HIF-1 controls the expression of several genes that assist cells to respond to hypoxic conditions. This typically

entails transferring the energy metabolism to the less oxygen consuming glycolytic pathway and activating the angiogenic genes to increase vascular supply to the hypoxic areas. Indeed we see that degradation of HIF-1 α impairs tumor vasculature in CI-deficient osteosarcoma and colorectal tumors (Kurelac et al., 2019). Moreover, through suppression of the HIF-1 α /VEGF signalling pathway, aloe-emodin, an antiangiogenic agent, diminished hypoxia-induced retinal angiogenesis (Wu et al., 2016). Similarly, inhibition of HIF-1 α decreased retinal neovascularization in hypoxic condition (Iwase et al., 2013). In line with this, both 143B^{-/-}-HIF-TM and HCT^{-/-}-HIF-TM tumors rescued the vessel maturation demonstrating that stimulation of vasculogenesis by HIF-1 contributed to the rescue of their tumorigenic potential. However, the CI deficient tumors still persist and present with vascularization, which raised the question of what other mechanisms could be guiding their angiogenesis in the absence of HIF-1. Signals produced within the TME not only mobilize myeloid cells from the bone marrow (or their precursors), but also recruit them into tumors from the bloodstream and then activate their pro-angiogenic functions (De Palma et al., 2017). In this respect, our observation of a different histological architecture in CI-deficient masses compared to the CI competent masses revealed that difference in their TME composition could be responsible for the alternative, HIF-1 independent vascularization in CI deficient tumors. Indeed the 143B^{-/-} and HCT^{-/-} xenografts presented with a higher infiltration of TAM with respect to their CI competent masses.

Interestingly, 143B^{+/+} tumors additionally presented with an upregulated neutrophil expression, which is in line with the fact that CI competent masses are enriched with necrotic sites, to which neutrophils are attracted. (Patricia et al., 2020). Furthermore, the accumulation of neutrophils is a process that is tightly controlled by cytokines. The increased cytokine levels of G-CSF and CXCL12 in 143B^{+/+} tumors, which are known regulators of neutrophil release and modulates their retention at inflammatory sites respectively, provides additional explanation for the elevated neutrophil levels (Semerad et al., 2002; Isles et al., 2019).

Multiple immature vessels like that found in our CI deficient tumors are associated with TAMs proangiogenic activity, which may aggravate the tumor progression. It is worth noting that myeloid cells, especially macrophages, play an important role in the abnormalization of blood vessels and restrict the transmission of chemotherapeutic agents into tumors (Chen et al., 2013). For example, studies by Rolny et al speculate that by expressing elevated levels or various types of angiogenic stimuli, M2-polarized TAMs make vessels irregular and immature as seen in our CI deficient models. Upregulation of angiogenic M2-cytokines (IL-10, CCL22, IL-1 β , TNF α) or downregulation of angiostatic M1-cytokines (IFN- β , CXCL10, IL-12) can also lead to abnormalization of vessels (Rolny et al., 2011; Chen et al., 2013; Murdoch et al., 2013). Because their vasculature has been correlated with the TME of CI-deficient tumors, we

believe that TAMs could be involved in compensatory processes activated to bypass the inability of CI-deficient tumors to enable angiogenesis induced by HIF-1 α . This is further confirmed by the fact that introducing HIF-TM decreased the macrophage count in the 143B-/-HIF-TM tumors as compared to the 143B-/-Mock controls, meaning that HIF-1 α destabilization was one of the factors contributing to TAM recruitment.

In immune evasion, the hypoxic tumor microenvironment plays a fundamental function. In fact, tumor hypoxia is thought to play a pivotal role in TAM phenotypic regulation, as hypoxic TAMs release variables that assist in tumor development, immunosuppression of cancer, and angiogenesis (Casazza et al., 2013; Du et al., 2008). The accumulation of macrophages in hypoxic / necrotic regions could account for two possible mechanisms as explained by Henze and Mazzone in their review, the attraction of macrophages by a cytokine gradient and the impaired mobility of macrophages within these areas (Henze and Mazzone, 2016). This is in contradiction to the macrophage infiltrations we observe in our non-necrotic, hypoxia lacking CI deficient models.

In addition, CI deficient osteosarcoma tumors presented with MIF downregulation, a mechanism recently associated with macrophage-mediated vascularization triggered as a compensatory reaction to anti-VEGF therapy (Castro et al., 2017) which is in line with the hypothesis that lack of HIF-1-guided angiogenesis triggers TAM abundance. This is also further evidenced by the decrease in MIF expression after introducing the HIF-TM into the 143B-/-HIF-TM tumors. As mentioned before, MIF is a known HIF-1-responsive gene. It was also shown that MIF promoted Warburg effect by upregulating HIF-1 α and the promotional influence of MIF on the Warburg effect was effectively eliminated by the knockdown of HIF-1 α (Li et al., 2018). MIF, among other functions, is also known to inhibit the migration of macrophages. However, it must be acknowledged that the role of MIF in macrophage inhibition is still controversial. In addition, a humanized niche model of the osteosarcoma graft that provided us with additional information on the osteosarcoma development in the context of CI targeting and establishes a more disease-relevant environment for tumor growth measurement, also presented with an increased macrophage infiltrations and downregulation of the HIF1-MIF axis in the 143B-/-tumors. Taken together, the abnormal vessels indicative of myeloid-driven vasculogenesis, the invasion of macrophages found in CI-deficient tumors and the reduction of their number when HIF-1 activity was complemented by TM-HIF-1 α and a similar phenomenon of higher macrophages and decreased HIF1-MIF axis presented in the orthotopic 143B-/- tumors, all together suggest that macrophage abundance is an implication of HIF-1 α destabilization in 143B-/- tumors.

On the other hand, analysis of HCT-/-HIF-TM and HCT-/-Mock revealed that the macrophage count was unchanged in them. Furthermore, although qRT-PCR displayed a decrease in the

MIF expression in HCT^{-/-} xenografts at day 10, its gene expression 30 days *in vivo* and also *in vitro* in hypoxia and intracellular protein expression of xenografts showed no difference in MIF expression between the HCT^{-/-} and HCT^{+/+} tumors. Moreover, HCT^{-/-}-HIF-TM and HCT^{-/-}-Mock masses also showed no difference in the MIF expression both *in vitro* and *in vivo* indicating that the MIF-HIF1 axis was not responsible for macrophage attraction in these models. Furthermore we hypothesized that MIF down regulation could depend on p53 since HCT models lacked their expression. A strong correlation between inflammation and tumorigenesis is demonstrated by MIF. As well as its proven function in inflammation, by inhibiting p53 aggregation, MIF directly promotes tumorigenesis (Vogelstein et al., 2000; Lu et al., 2007). p53 is a classic tumour suppressor gene that can stimulate cell cycle arrest and apoptosis in response to DNA damage. This essential checkpoint for preserving genetic stability interferes with the absence or downregulation of p53 and enables cell survival and proliferation despite possible mutation accumulation. Functional screens conducted by Hudson et al. identified MIF as one of the cDNAs capable of negatively regulating p53 (Hudson et al., 1999). Additionally, it is also shown that in a p53-dependent manner, MIF controls HIF-1 activity (Oda et al., 2008). Therefore, we hypothesized that MIF regulation could depend on p53 since HCT models lacked the expression of this tumor suppressor. It must be acknowledged that when it comes to p53, there is a massive amount of accumulated literature and the list of proteins that interact with p53 is broad. Furthermore, p53 and MIF display multifaceted functions and it is therefore difficult to rationalize in our models with just mRNA and intracellular MIF and p53 expressions, what is their exact link. However, in the context of the data we have, we can suggest that the addition of WT p53 or Mut p53 upregulates MIF expression in HCT^{-/-} tumors in hypoxia when compared to the HCT^{-/-} p53 null tumors. In conclusion the lack of downregulation of MIF in HCT^{-/-} cells does not depend on p53 expression.

For the preparation and export of proteins to the extracellular environment, the protein secretory pathway is essential, effective and precise molecular machinery (Feizi et al., 2017). We reasoned that tissue-specific expression of secretome could put different post-translational modifications processing pressure on secretory pathway subsystems, which could possibly explain the contradictory results of MIF expression between 143B and HCT models. In this context, we can suggest that although the macrophage data revealed a more generic redistribution of TME in CI-deficient tumors, the mechanism behind their recruitment maybe exclusive and tissue specific. This result further emphasizes the fact that the sensitivity of tissues to particular oncogenic events varies greatly and that barriers to tumour development are highly tissue-specific. Unraveling processes that control their tissue-specific manifestations are crucial to our knowledge of the etiologies of diseases and may lead efforts to establish treatments. The heterogeneous populations in a tumor including the TME secrete multiple

signals that, individually and collectively, can promote or impede any or all of the hallmarks of cancer necessary for tumor growth, development, and progression. In this context, the other cytokines analyzed by the cytokine array, are suggested to have a paradoxical pro-tumorigenic and anti-tumorigenic effect on cancer cells. IL-8 secreted by the macrophages of TME promoted tumor migration and survival (Fu et al., 2015). CXCL1 secreted by TAMs promoted breast cancer metastasis via NF- κ B/SOX4 activation (Wang et al., 2018). Interestingly, both these cytokines promoted EMT process. Therefore the upregulation of the IL-8 and CXCL1 could possibly be attributed to the higher macrophage abundance and in turn their secretion in our 143B^{-/-} tumors. Cytokines CXCL12, SERPIN-E1 and G-CSF are known to be induced in hypoxia by HIF-1 α (Ceradini et al., 2004; D'Alessandro et al., 2019; Chafe et al., 2015) and are also inhibited by metformin treatment (Dirat et al., 2015; Kita et al., 2012; Kim et al., 2017) which could possibly explain their downregulation in 143B^{-/-} tumors since they rarely acquire hypoxic phenotype due to unstable HIF-1 α . Therefore, future research should explore the effects of these cytokines on our models to gain further experimental evidence. In addition, it would also be interesting to check if the above cytokines were tumor or TME derived. Apart from the possibility of tissue-specific TAM attraction, another hypothesis may be that MIF downregulation is merely a consequence of HIF-1 inactivation, and that TAM abundance in CI deficient tumors is guided by another factor, possibly common to both HCT and 143B models. With the aim of understanding whether such a common factor exists, proteomics and metabolomics has been performed on the secretome of the CI deficient and CI competent xenografts. However, proteomics did not identify any common factors between 143B and HCT, and some of them showed to have opposite expression levels in the two models. Among the proteins identified, secreted protein acidic and rich in cysteine (SPARC), that binds calcium in the bone, was found to be upregulated in the 143B^{-/-} but downregulated in the HCT^{-/-}. The multifaceted effects of SPARC is due to its involvement in numerous biological functions like, modulation of cell-extracellular matrix (ECM) interaction, angiogenesis and tissue remodeling (Kzhyshkowska et al., 2006; Gilles et al., 1998). Interestingly it is one of the factors that drive macrophage-mediated tumor invasion (Sangaletti et al., 2008). On the other, SPARC derived from M2 macrophage phenotype attenuated its proliferative effects in gastric cancer (Hu et al., 2020). The complexity of SPARC effects emanates from the cell origin and the interplay between its production by tumor and TME, which explains the contradictory results in 143B and HCT CI deficient tumors. In order to completely interpret and understand the proteomics data, its needs to be further analyzed using GO- term enrichment analysis. Metabolomics plays a vital role in dissecting the possible biochemical rearrangements in cancer cells. As mentioned before, intratumoral mechanisms of metabolite communication function symbiotically to promote repair, and development of tumors, or competitively to

inhibit immunity to antitumors. For example, succinate induces intracellular calcium in DCs, facilitating migratory responses and working synergistically inducing pro-inflammatory production of cytokines with Toll-like receptor ligands. Succinate effectively enhanced antigen specific activation of T cells via SUCNR1 (Rubic et al., 2008). Similarly, itaconate a redirected derivative from the TCA cycle was recently discovered to have a compelling immune-regulated function. In LPS-treated murine bone marrow-derived macrophages (BMDMs) under dimethyl itaconate (DI) administration activity of M1 macrophages has been reported to be partially inhibited *in vitro* along with reduction of proinflammatory mediators like IL-1 β and IL-6 (Lampropoulou et al., 2016). IL-2-driven differentiation of CD4 + and CD8 + T cells has been shown to be promoted by α -KG. H3K27me3 and DNA methylation states were decreased by α -KG, establishing its function as a cofactor for DNA and histone demethylases in T cells (Chisolm et al., 2017). In line with this, we identified 9 secreted metabolites namely lactate, 2HG, Fumarate, Malate, α -KG, Glutamate, Alanine, KIC and KMV that were accumulated, significantly more in CI deficient conditioned media of HCT and 143B tumors. Previously identified with bioenergetics or biosynthesis, metabolites have arisen as molecules of immune effectors with specific function of immune system regulation. They act as signalling molecules linked to transcription factors, can alter the structure and function of proteins, and can change the mechanisms of molecular and cellular signalling (Zaslona and O'Neill, 2020). Interestingly most of the above mentioned metabolites have an effect on macrophage polarization, proliferation or differentiation, which makes them a promising target. Indeed, by inhibiting KDM5 histone demethylases fumarate incorporates immune and metabolic circuits to cause macrophage epigenetic reprogramming (Arts et al., 2016). Likewise, intracellular glutamate elevation and mGluR5 expression may induce metabolic rearrangement in macrophages that may lead to the production of an immunosuppressive phenotype (Shanshiashvili et al., 2017). Of note, since the release of extracellular glutamate has been shown to allow tumor expansion and providing growth advantage in OXPHOS competent tumors (Takano et al., 2001), its accumulation in CI deficient cells was unexpected.

Future studies are necessary to explore the role of each of these metabolites on macrophage proliferation, migration, phagocytic activity, differentiation and polarization, for example in co-culture experiments.

Finally, following the metabolomics, pathway analysis and metabolite set enrichment analysis was carried out, which could be proposed as a future research avenue. It is well known that cancer cells often use other amino acids as "alternative fuels" to compete with different cells in the tumor stroma for energy and to maximize the use of nutrients during tumor evolution either by metabolic competition or through the process of macropinocytosis (Keenan et al., 2015). The majority of carbon in cancer cells originates from amino acids, which, in the

case of certain non-essential amino acids, are either taken up directly from the environment or synthesized de novo. For example, the study by Nilsson and co showed that when produced in the mitochondria, glutamate is metabolized but excreted when produced in abundance in the cytosol (Nilsson et al., 2020). Our metabolite enrichment and pathway analysis suggests the amino acid metabolism in addition to glycolysis was differentially regulated in our CI deficient and CI competent models and thus lead us to speculate that metabolic changes induced in cancer cells upon CI deficiency could triggers them to utilize the amino acid released by the tumor stroma for their survival as described in a review by Vettore et al., 2020. Moreover, the deregulated uptake of amino acids is another frequently found metabolic perturbation in cancer cells (Yang et al., 2017). However, this needs to be validated with metabolic tracing experiments. In conclusion, further insight into metabolic dependencies can be provided by fully understanding the metabolic flexibility and diversity of the use of amino acids in cancer cells. The additional degree of sophistication provided to and altered by TME populations in response to metabolic therapy draws attention to the fact that even the most general treatment may involve customized adjuvant therapies targeting TME. Therefore, in order to guide such therapeutic choices, a comprehensive pre-evaluation of the immunophenotype and stromal proportion of a tumor should be considered.

Chapter 6

CONCLUSIONS

Despite a broad knowledge of metabolic regulation based on nearly a century of biochemistry studies, our knowledge of how pathways are regulated to promote cell proliferation remains incomplete. In a hypoxic tumor microenvironment, tumor cells also have the potential to adjust their metabolism and prefer metabolic pathways that are less oxygen dependent to satisfy their demand for energy. Keeping in mind the importance of the hypoxic adaptation in cancer cells, our study proves that CI deficient 143B and HCT tumors display a reduced HIF-1 α stabilization phenotype that accounts for their anti-tumorigenic potential in various *in vitro* and *in vivo* settings. By activating non-cell-autonomous pathways, independent of HIF-1 α , CI-deficient tumors guarantee nutritional availability and indeed, we show decreased tumor growth accompanied by downregulation of MIF (only in the case of osteosarcomas) and excess of TAM in CI deficient models, indicating that it may be one of the adaptive mechanisms enabled to maintain survival after CI targeting. In addition it is well known that hypoxia-mediated tumour-secreted proteins play a multi-directional role within TME, which probed us to identify a common HIF-1 α independent mechanism of macrophage attraction among the two cell types within the altered secretion profile of CI deficient tumors for a more specific inhibition using the omics approach. Our results on the metabolomics analysis of the CI deficient secretome identified accumulation of lactate, fumarate, malate, 2-HG, BCKA's (KIC, KMV), glutamate, α KG and alanine that could possibly explain the TAM accumulation phenotype in these tumors. This was not surprising since in ETC impairment conditions, NADH accumulates and inhibits all regulatory enzymes in the TCA cycle, resulting in the shutdown of the TCA cycle and accumulation of its intermediates. However, the effects and molecular mechanism of action of these intermediates in immunoregulation, more specifically in the context of mitochondrial respiration deficiency and macrophages has yet to be investigated. In conclusion, our results provide a novel insight into the alternative survival mechanisms adapted by the slow growing but persistent CI deficient tumors and identifies potential mode of mechanisms of the TAM

recruitment in them. High expression of immune control point proteins in TME promotes metabolic reprogramming in the microenvironment of the tumor, further creating a positive feedback loop to sustain or worsen their growth. Combinational therapy targeting metabolism and immunity may be helpful in this aspect. In line with this, our results also highlights the importance of considering tumor type and their environmental context for determining the potential efficacy of any adjuvant therapies targeting cancer metabolism and TME.

Chapter 7

REFERENCES

Abdul-Aziz AM, Shafat MS, Sun Y, et al. HIF1 α drives chemokine factor pro-tumoral signaling pathways in acute myeloid leukemia. *Oncogene*. 2018;37(20):2676-2686. doi:10.1038/s41388-018-0151-1

Agani FH, Pichiule P, Carlos Chavez J, LaManna JC. Inhibitors of mitochondrial complex I attenuate the accumulation of hypoxia-inducible factor-1 during hypoxia in Hep3B cells. *Comp Biochem Physiol A Mol Integr Physiol*. 2002;132(1):107-109. doi:10.1016/s1095-6433(01)00535-9

Akatsuka A, Kojima N, Okamura M, Dan S, Yamori T. A novel thiophene-3-carboxamide analog of annonaceous acetogenin exhibits antitumor activity via inhibition of mitochondrial complex I. *Pharmacol Res Perspect*. 2016;4(4):e00246. Published 2016 Jul 12. doi:10.1002/prp2.246

Akouchekian M, Houshmand M, Akbari MH, Kamalidehghan B, Dehghan M. Analysis of mitochondrial ND1 gene in human colorectal cancer. *J Res Med Sci*. 2011;16(1):50-55.

Allegra E, Garozzo A, Lombardo N, De Clemente M, Carey TE. Mutations and polymorphisms in mitochondrial DNA in head and neck cancer cell lines. *Acta Otorhinolaryngol Ital*. 2006;26(4):185-190

Allison KE, Coomber BL, Bridle BW. Metabolic reprogramming in the tumour microenvironment: a hallmark shared by cancer cells and T lymphocytes. *Immunology*. 2017;152(2):175-184. doi:10.1111/imm.12777

Arango Duque G, Descoteaux A. Macrophage cytokines: involvement in immunity and infec-

- tious diseases. *Front Immunol.* 2014;5:491. Published 2014 Oct 7. doi:10.3389/fimmu.2014.00491
- Arts RJ, Novakovic B, Ter Horst R, et al. Glutaminolysis and Fumarate Accumulation Integrate Immunometabolic and Epigenetic Programs in Trained Immunity. *Cell Metab.* 2016;24(6):807-819. doi:10.1016/j.cmet.2016.10.008
- Baba Y, Nosho K, Shima K, et al. HIF1A overexpression is associated with poor prognosis in a cohort of 731 colorectal cancers. *Am J Pathol.* 2010;176(5):2292-2301. doi:10.2353/ajpath.2010.090972
- Baghban R, Roshangar L, Jahanban-Esfahlan R, et al. Tumor microenvironment complexity and therapeutic implications at a glance. *Cell Commun Signal.* 2020;18(1):59. Published 2020 Apr 7. doi:10.1186/s12964-020-0530-4
- Bartolini D, Sancineto L, Fabro de Bem A, et al. Selenocompounds in Cancer Therapy: An Overview. *Adv Cancer Res.* 2017;136:259-302. doi:10.1016/bs.acr.2017.07.007
- Bastian A, Matsuzaki S, Humphries KM, et al. AG311, a small molecule inhibitor of complex I and hypoxia-induced HIF-1 α stabilization. *Cancer Lett.* 2017;388:149-157. doi:10.1016/j.canlet.2016.11.040
- Birsoy K, Wang T, Chen WW, Freinkman E, Abu-Remaileh M, Sabatini DM. An Essential Role of the Mitochondrial Electron Transport Chain in Cell Proliferation Is to Enable Aspartate Synthesis. *Cell.* 2015;162(3):540-551. doi:10.1016/j.cell.2015.07.016
- Brand A, Singer K, Koehl GE, et al. LDHA-Associated Lactic Acid Production Blunts Tumor Immunosurveillance by T and NK Cells. *Cell Metab.* 2016;24(5):657-671. doi:10.1016/j.cmet.2016.08.011
- Bunz F, Hwang PM, Torrance C, et al. Disruption of p53 in human cancer cells alters the responses to therapeutic agents. *J Clin Invest.* 1999;104(3):263-269. doi:10.1172/JCI6863
- Busk M, Horsman MR, Kristjansen PE, van der Kogel AJ, Bussink J, Overgaard J. Aerobic glycolysis in cancers: implications for the usability of oxygen-responsive genes and fluorodeoxyglucose-PET as markers of tissue hypoxia. *Int J Cancer.* 2008;122(12):2726-2734. doi:10.1002/ijc.23449
- Bustin SA, Benes V, Garson JA, et al. The MIQE guidelines: minimum information for

publication of quantitative real-time PCR experiments. *Clin Chem.* 2009;55(4):611-622. doi:10.1373/clinchem.2008.112797

Caino MC, Ghosh JC, Chae YC, et al. PI3K therapy reprograms mitochondrial trafficking to fuel tumor cell invasion. *Proc Natl Acad Sci U S A.* 2015;112(28):8638-8643. doi:10.1073/pnas.1500722112

Calabrese C, Iommarini L, Kurelac I, et al. Respiratory complex I is essential to induce a Warburg profile in mitochondria-defective tumor cells. *Cancer Metab.* 2013;1(1):11. Published 2013 Mar 18. doi:10.1186/2049-3002-1-11

Calvo SE, Mootha VK. The mitochondrial proteome and human disease. *Annu Rev Genomics Hum Genet.* 2010;11:25-44. doi:10.1146/annurev-genom-082509-141720

Cardaci S, Ciriolo MR. TCA Cycle Defects and Cancer: When Metabolism Tunes Redox State. *Int J Cell Biol.* 2012;2012:161837. doi:10.1155/2012/161837

Casazza A, Laoui D, Wenes M, et al. Impeding macrophage entry into hypoxic tumor areas by Sema3A/Nrp1 signaling blockade inhibits angiogenesis and restores antitumor immunity. *Cancer Cell.* 2013;24(6):695-709. doi:10.1016/j.ccr.2013.11.007

Castro BA, Flanigan P, Jahangiri A, et al. Macrophage migration inhibitory factor downregulation: a novel mechanism of resistance to anti-angiogenic therapy. *Oncogene.* 2017;36(26):3749-3759. doi:10.1038/onc.2017.1

Ceradini DJ, Kulkarni AR, Callaghan MJ, et al. Progenitor cell trafficking is regulated by hypoxic gradients through HIF-1 induction of SDF-1. *Nat Med.* 2004;10(8):858-864. doi:10.1038/nm1075

Chafe SC, Lou Y, Sceneay J, et al. Carbonic anhydrase IX promotes myeloid-derived suppressor cell mobilization and establishment of a metastatic niche by stimulating G-CSF production. *Cancer Res.* 2015;75(6):996-1008. doi:10.1158/0008-5472.CAN-14-3000

Chang CH, Qiu J, O'Sullivan D, et al. Metabolic Competition in the Tumor Microenvironment Is a Driver of Cancer Progression. *Cell.* 2015;162(6):1229-1241. doi:10.1016/j.cell.2015.08.016

Chaube B, Malvi P, Singh SV, Mohammad N, Meena AS, Bhat MK. Targeting metabolic

flexibility by simultaneously inhibiting respiratory complex I and lactate generation retards melanoma progression. *Oncotarget*. 2015;6(35):37281-37299. doi:10.18632/oncotarget.6134

Chen DS, Mellman I. Elements of cancer immunity and the cancer-immune set point. *Nature*. 2017;541(7637):321-330. doi:10.1038/nature21349

Chen L, Shi Y, Yuan J, et al. HIF-1 alpha overexpression correlates with poor overall survival and disease-free survival in gastric cancer patients post-gastrectomy. *PLoS One*. 2014;9(3):e90678. Published 2014 Mar 10. doi:10.1371/journal.pone.0090678

Chen P, Bonaldo P. Role of macrophage polarization in tumor angiogenesis and vessel normalization: implications for new anticancer therapies. *Int Rev Cell Mol Biol*. 2013;301:1-35. doi:10.1016/B978-0-12-407704-1.00001-4

Chen P, Zuo H, Xiong H, et al. Gpr132 sensing of lactate mediates tumor-macrophage interplay to promote breast cancer metastasis. *Proc Natl Acad Sci U S A*. 2017;114(3):580-585. doi:10.1073/pnas.1614035114

Cheong JH, Park ES, Liang J, et al. Dual inhibition of tumor energy pathway by 2-deoxyglucose and metformin is effective against a broad spectrum of preclinical cancer models. *Mol Cancer Ther*. 2011;10(12):2350-2362. doi:10.1158/1535-7163.MCT-11-0497

Chisolm DA, Savic D, Moore AJ, et al. CCCTC-Binding Factor Translates Interleukin 2- and α -Ketoglutarate-Sensitive Metabolic Changes in T Cells into Context-Dependent Gene Programs. *Immunity*. 2017;47(2):251-267.e7. doi:10.1016/j.immuni.2017.07.015

Clear AJ, Lee AM, Calaminici M, et al. Increased angiogenic sprouting in poor prognosis FL is associated with elevated numbers of CD163+ macrophages within the immediate sprouting microenvironment. *Blood*. 2010;115(24):5053-5056. doi:10.1182/blood-2009-11-253260

Colegio OR, Chu NQ, Szabo AL, et al. Functional polarization of tumour-associated macrophages by tumour-derived lactic acid. *Nature*. 2014;513(7519):559-563. doi:10.1038/nature13490

Conciatori F, Bazzichetto C, Falcone I, et al. Role of mTOR Signaling in Tumor Microenvironment: An Overview. *Int J Mol Sci*. 2018;19(8):2453. Published 2018 Aug 19. doi:10.3390/ijms19082453

D'Alessandro S, Magnavacca A, Perego F, et al. Effect of Hypoxia on Gene Expression in Cell Populations Involved in Wound Healing. *Biomed Res Int.* 2019;2019:2626374. Published 2019 Aug 22. doi:10.1155/2019/2626374

De Palma M, Biziato D, Petrova TV. Microenvironmental regulation of tumour angiogenesis. *Nat Rev Cancer.* 2017;17(8):457-474. doi:10.1038/nrc.2017.51

DeBerardinis RJ, Lum JJ, Hatzivassiliou G, Thompson CB. The biology of cancer: metabolic reprogramming fuels cell growth and proliferation. *Cell Metab.* 2008;7(1):11-20. doi:10.1016/j.cmet.2007.10.002

Dirat B, Ader I, Golzio M, et al. Inhibition of the GTPase Rac1 mediates the antimigratory effects of metformin in prostate cancer cells. *Mol Cancer Ther.* 2015;14(2):586-596. doi:10.1158/1535-7163.MCT-14-0102

Du R, Lu KV, Petritsch C, et al. HIF1alpha induces the recruitment of bone marrow-derived vascular modulatory cells to regulate tumor angiogenesis and invasion. *Cancer Cell.* 2008;13(3):206-220. doi:10.1016/j.ccr.2008.01.034

Eikawa S, Nishida M, Mizukami S, Yamazaki C, Nakayama E, Usono H. Immune-mediated antitumor effect by type 2 diabetes drug, metformin. *Proc Natl Acad Sci U S A.* 2015;112(6):1809-1814. doi:10.1073/pnas.1417636112

Elango S, Venugopal S, Thangaraj K, Viswanadha VP. Novel mutations in ATPase 8, ND1 and ND5 genes associated with peripheral neuropathy of diabetes. *Diabetes Res Clin Pract.* 2014;103(3):e49-e52. doi:10.1016/j.diabres.2013.12.015

Ellinghaus P, Heisler I, Unterschemmann K, et al. BAY 87-2243, a highly potent and selective inhibitor of hypoxia-induced gene activation has antitumor activities by inhibition of mitochondrial complex I. *Cancer Med.* 2013;2(5):611-624. doi:10.1002/cam4.112

Faubert B, Boily G, Izreig S, et al. AMPK is a negative regulator of the Warburg effect and suppresses tumor growth *in vivo*. *Cell Metab.* 2013;17(1):113-124. doi:10.1016/j.cmet.2012.12.001

Feizi A, Gatto F, Uhlen M, Nielsen J. Human protein secretory pathway genes are expressed in

a tissue-specific pattern to match processing demands of the secretome. *NPJ Syst Biol Appl*. 2017;3:22. Published 2017 Aug 18. doi:10.1038/s41540-017-0021-4

Fendt SM, Bell EL, Keibler MA, et al. Reductive glutamine metabolism is a function of the α -ketoglutarate to citrate ratio in cells. *Nat Commun*. 2013;4:2236. doi:10.1038/ncomms3236

Fingerle-Rowson G, Petrenko O. MIF coordinates the cell cycle with DNA damage checkpoints. Lessons from knockout mouse models. *Cell Div*. 2007;2:22. Published 2007 Jul 19. doi:10.1186/1747-1028-2-22

Fischer K, Hoffmann P, Voelkl S, et al. Inhibitory effect of tumor cell-derived lactic acid on human T cells. *Blood*. 2007;109(9):3812-3819. doi:10.1182/blood-2006-07-035972

Fu H, Luo F, Yang L, Wu W, Liu X. Hypoxia stimulates the expression of macrophage migration inhibitory factor in human vascular smooth muscle cells via HIF-1 α dependent pathway. *BMC Cell Biol*. 2010;11:66. Published 2010 Aug 20. doi:10.1186/1471-2121-11-66

Fu XT, Dai Z, Song K, et al. Macrophage-secreted IL-8 induces epithelial-mesenchymal transition in hepatocellular carcinoma cells by activating the JAK2/STAT3/Snail pathway. *Int J Oncol*. 2015;46(2):587-596. doi:10.3892/ijo.2014.2761

Fukumura D, Xu L, Chen Y, Gohongi T, Seed B, Jain RK. Hypoxia and acidosis independently up-regulate vascular endothelial growth factor transcription in brain tumors *in vivo*. *Cancer Res*. 2001;61(16):6020-6024.

Gasparre G, Kurelac I, Capristo M, et al. A mutation threshold distinguishes the antitumorigenic effects of the mitochondrial gene MTND1, an oncojanus function. *Cancer Res*. 2011;71(19):6220-6229. doi:10.1158/0008-5472.CAN-11-1042

Gasparre G, Porcelli AM, Lenaz G, Romeo G. Relevance of mitochondrial genetics and metabolism in cancer development. *Cold Spring Harb Perspect Biol*. 2013;5(2):a011411. Published 2013 Feb 1. doi:10.1101/cshperspect.a011411

Gaude E, Frezza C. Defects in mitochondrial metabolism and cancer. *Cancer Metab*. 2014;2:10. Published 2014 Jul 17. doi:10.1186/2049-3002-2-10

Gaude E, Schmidt C, Gammage PA, et al. NADH Shuttling Couples Cytosolic Reductive Carboxylation of Glutamine with Glycolysis in Cells with Mitochondrial Dysfunction. *Mol Cell*. 2018;69(4):581-593.e7. doi:10.1016/j.molcel.2018.01.034

Giachin G, Bouverot R, Acajjaoui S, Pantalone S, Soler-López M. Dynamics of Human Mitochondrial Complex I Assembly: Implications for Neurodegenerative Diseases. *Front Mol Biosci*. 2016;3:43. Published 2016 Aug 22. doi:10.3389/fmolb.2016.00043

Gilles C, Bassuk JA, Pulyaeva H, Sage EH, Foidart JM, Thompson EW. SPARC/osteonectin induces matrix metalloproteinase 2 activation in human breast cancer cell lines. *Cancer Res*. 1998;58(23):5529-5536.

Gillespie DL, Whang K, Ragel BT, Flynn JR, Kelly DA, Jensen RL. Silencing of hypoxia inducible factor-1alpha by RNA interference attenuates human glioma cell growth *in vivo* [published correction appears in *Clin Cancer Res*. 2008 Jan 1;14(1):326]. *Clin Cancer Res*. 2007;13(8):2441-2448. doi:10.1158/1078-0432.CCR-06-2692

Gong J, Kelekar G, Shen J, Shen J, Kaur S, Mita M. The expanding role of metformin in cancer: an update on antitumor mechanisms and clinical development. *Target Oncol*. 2016;11(4):447-467. doi:10.1007/s11523-016-0423-z

Hagen T, Taylor CT, Lam F, Moncada S. Redistribution of intracellular oxygen in hypoxia by nitric oxide: effect on HIF1alpha. *Science*. 2003;302(5652):1975-1978. doi:10.1126/science.1088805

Hanahan D, Weinberg RA. Hallmarks of cancer: the next generation. *Cell*. 2011;144(5):646-674. doi:10.1016/j.cell.2011.02.013

Hanahan D, Weinberg RA. The hallmarks of cancer. *Cell*. 2000;100(1):57-70. doi:10.1016/s0092-8674(00)81683-9

Harel M, Ortenberg R, Varanasi SK, et al. Proteomics of Melanoma Response to Immunotherapy Reveals Mitochondrial Dependence. *Cell*. 2019;179(1):236-250.e18. doi:10.1016/j.cell.2019.08.012

Heidelberger C, Chaudhuri NK, Danneberg P, et al. Fluorinated pyrimidines, a new class of tumour-inhibitory compounds. *Nature*. 1957;179(4561):663-666. doi:10.1038/179663a0

- Henze AT, Mazzone M. The impact of hypoxia on tumor-associated macrophages. *J Clin Invest.* 2016;126(10):3672-3679. doi:10.1172/JCI84427
- Heuer TS, Ventura R, Mordec K, et al. FASN Inhibition and Taxane Treatment Combine to Enhance Anti-tumor Efficacy in Diverse Xenograft Tumor Models through Disruption of Tubulin Palmitoylation and Microtubule Organization and FASN Inhibition-Mediated Effects on Oncogenic Signaling and Gene Expression. *EBioMedicine.* 2017;16:51-62. doi:10.1016/j.ebiom.2016.12.012
- Higurashi T, Hosono K, Takahashi H, et al. Metformin for chemoprevention of metachronous colorectal adenoma or polyps in post-polypectomy patients without diabetes: a multicentre double-blind, placebo-controlled, randomised phase 3 trial. *Lancet Oncol.* 2016;17(4):475-483. doi:10.1016/S1470-2045(15)00565-3
- Horton TM, Petros JA, Heddi A, et al. Novel mitochondrial DNA deletion found in a renal cell carcinoma. *Genes Chromosomes Cancer.* 1996;15(2):95-101. doi:10.1002/(SICI)1098-2264(199602)15:2<95::AID-GCC3>3.0.CO;2-Z
- Hu J, Ma Y, Ma J, et al. Macrophage-derived SPARC Attenuates M2-mediated Pro-tumour Phenotypes. *J Cancer.* 2020;11(10):2981-2992. Published 2020 Mar 4. doi:10.7150/jca.39651
- Hudson JD, Shoaibi MA, Maestro R, Carnero A, Hannon GJ, Beach DH. A proinflammatory cytokine inhibits p53 tumor suppressor activity. *J Exp Med.* 1999;190(10):1375-1382. doi:10.1084/jem.190.10.1375
- Husain Z, Huang Y, Seth P, Sukhatme VP. Tumor-derived lactate modifies antitumor immune response: effect on myeloid-derived suppressor cells and NK cells. *J Immunol.* 2013;191(3):1486-1495. doi:10.4049/jimmunol.1202702
- Incio J, Suboj P, Chin SM, et al. Metformin Reduces Desmoplasia in Pancreatic Cancer by Reprogramming Stellate Cells and Tumor-Associated Macrophages. *PLoS One.* 2015;10(12):e0141392. Published 2015 Dec 7. doi:10.1371/journal.pone.0141392
- Iommarini L, Calvaruso MA, Kurelac I, Gasparre G, Porcelli AM. Complex I impairment in mitochondrial diseases and cancer: parallel roads leading to different outcomes. *Int J Biochem*

Cell Biol. 2013;45(1):47-63. doi:10.1016/j.biocel.2012.05.016

Iommarini L, Kurelac I, Capristo M, et al. Different mtDNA mutations modify tumor progression in dependence of the degree of respiratory complex I impairment. *Hum Mol Genet.* 2014;23(6):1453-1466. doi:10.1093/hmg/ddt533

Isles HM, Herman KD, Robertson AL, et al. The CXCL12/CXCR4 Signaling Axis Retains Neutrophils at Inflammatory Sites in Zebrafish. *Front Immunol.* 2019;10:1784. Published 2019 Jul 31. doi:10.3389/fimmu.2019.01784

Iwase T, Fu J, Yoshida T, et al. Sustained delivery of a HIF-1 antagonist for ocular neovascularization. *J Control Release.* 2013;172(3):625-633. doi:10.1016/j.jconrel.2013.10.008

Ju R, Guo L, Li J, et al. Carboxyamidotriazole inhibits oxidative phosphorylation in cancer cells and exerts synergistic anti-cancer effect with glycolysis inhibition. *Cancer Lett.* 2016;370(2):232-241. doi:10.1016/j.canlet.2015.10.025

Kaelin WG Jr, Ratcliffe PJ. Oxygen sensing by metazoans: the central role of the HIF hydroxylase pathway. *Mol Cell.* 2008;30(4):393-402. doi:10.1016/j.molcel.2008.04.009

Katt WP, Cerione RA. Glutaminase regulation in cancer cells: a druggable chain of events. *Drug Discov Today.* 2014;19(4):450-457. doi:10.1016/j.drudis.2013.10.008

Keenan MM, Chi JT. Alternative fuels for cancer cells. *Cancer J.* 2015;21(2):49-55. doi:10.1097/PPO.0000000000000104

Kelso A. Cytokines: principles and prospects. *Immunology and Cell Biology.* 1998 Aug;76(4):300-317. DOI: 10.1046/j.1440-1711.1998.00757.x.

Kim AJ, Chang JY, Shi L, Chang RC, Ko ML, Ko GY. The Effects of Metformin on Obesity-Induced Dysfunctional Retinas [published correction appears in *Invest Ophthalmol Vis Sci.* 2017 Jun 1;58(7):3030]. *Invest Ophthalmol Vis Sci.* 2017;58(1):106-118. doi:10.1167/iovs.16-20691

Kim H, Komiyama T, Inomoto C, et al. Mutations in the Mitochondrial ND1 Gene Are Associated with Postoperative Prognosis of Localized Renal Cell Carcinoma. *Int J Mol Sci.*

2016;17(12):2049. Published 2016 Dec 7. doi:10.3390/ijms17122049

Kita Y, Takamura T, Misu H, et al. Metformin prevents and reverses inflammation in a non-diabetic mouse model of nonalcoholic steatohepatitis. *PLoS One*. 2012;7(9):e43056. doi:10.1371/journal.pone.0043056

Kleemann R, Hausser A, Geiger G, et al. Intracellular action of the cytokine MIF to modulate AP-1 activity and the cell cycle through Jab1. *Nature*. 2000;408(6809):211-216. doi:10.1038/35041591

Koopman WJ, Nijtmans LG, Dieteren CE, et al. Mammalian mitochondrial complex I: biogenesis, regulation, and reactive oxygen species generation. *Antioxid Redox Signal*. 2010;12(12):1431-1470. doi:10.1089/ars.2009.2743

Koppenol WH, Bounds PL, Dang CV. Otto Warburg's contributions to current concepts of cancer metabolism [published correction appears in *Nat Rev Cancer*. 2011 Aug;11(8):618]. *Nat Rev Cancer*. 2011;11(5):325-337. doi:10.1038/nrc3038

Kruger P, Saffarzadeh M, Weber ANR, Rieber N, Radsak M, von Bernuth H, et al. Neutrophils: between host Defence, immune modulation, and tissue injury. *PLoS Pathog*. 2015;11:e1004651

Kurelac I, Abarrategi A, Ragazzi M, et al. A Humanized Bone Niche Model Reveals Bone Tissue Preservation Upon Targeting Mitochondrial Complex I in Pseudo-Orthotopic Osteosarcoma. *J Clin Med*. 2019;8(12):2184. Published 2019 Dec 11. doi:10.3390/jcm8122184

Kurelac I, Iommarini L, Vatrinet R, et al. Inducing cancer indolence by targeting mitochondrial Complex I is potentiated by blocking macrophage-mediated adaptive responses. *Nat Commun*. 2019;10(1):903. Published 2019 Feb 22. doi:10.1038/s41467-019-08839-1

Kurelac I, MacKay A, Lambros MB, et al. Somatic complex I disruptive mitochondrial DNA mutations are modifiers of tumorigenesis that correlate with low genomic instability in pituitary adenomas. *Hum Mol Genet*. 2013;22(2):226-238. doi:10.1093/hmg/dds422

Kurelac I, Umesh Ganesh N, Iorio M, Porcelli AM, Gasparre G. The multifaceted effects of metformin on tumor microenvironment. *Semin Cell Dev Biol*. 2020;98:90-97. doi:10.1016/j.semcdb.2019.05.010

Kürschner G, Zhang Q, Clima R, et al. Renal oncocytoma characterized by the defective complex I of the respiratory chain boosts the synthesis of the ROS scavenger glutathione. *Oncotarget*. 2017;8(62):105882-105904. Published 2017 Nov 11. doi:10.18632/oncotarget.22413

Kzhyshkowska J, Workman G, Cardó-Vila M, et al. Novel function of alternatively activated macrophages: stabilin-1-mediated clearance of SPARC. *J Immunol*. 2006;176(10):5825-5832. doi:10.4049/jimmunol.176.10.5825

Lampropoulou V, Sergushichev A, Bambouskova M, et al. Itaconate Links Inhibition of Succinate Dehydrogenase with Macrophage Metabolic Remodeling and Regulation of Inflammation. *Cell Metab*. 2016;24(1):158-166. doi:10.1016/j.cmet.2016.06.004

Lando D, Peet DJ, Gorman JJ, Whelan DA, Whitelaw ML, Bruick RK. FIH-1 is an asparaginyl hydroxylase enzyme that regulates the transcriptional activity of hypoxia-inducible factor. *Genes Dev*. 2002;16(12):1466-1471. doi:10.1101/gad.991402

Lee JY, Lee I, Chang WJ, et al. MCT4 as a potential therapeutic target for metastatic gastric cancer with peritoneal carcinomatosis. *Oncotarget*. 2016;7(28):43492-43503. doi:10.18632/oncotarget.9523

Lee K, Zhang H, Qian DZ, Rey S, Liu JO, Semenza GL. Acriflavine inhibits HIF-1 dimerization, tumor growth, and vascularization. *Proc Natl Acad Sci U S A*. 2009;106(42):17910-17915. doi:10.1073/pnas.0909353106

Leone G, Abela H, Gasparre G, Porcelli AM, Iommarini L. The Oncojanus Paradigm of Respiratory Complex I. *Genes (Basel)*. 2018;9(5):243. Published 2018 May 7. doi:10.3390/genes9050243

Li J, Zhang J, Xie F, Peng J, Wu X. Macrophage migration inhibitory factor promotes Warburg effect via activation of the NF κ B/HIF 1 α pathway in lung cancer. *Int J Mol Med*. 2018;41(2):1062-1068. doi:10.3892/ijmm.2017.3277

Liu PS, Wang H, Li X, et al. α -ketoglutarate orchestrates macrophage activation through metabolic and epigenetic reprogramming. *Nat Immunol*. 2017;18(9):985-994. doi:10.1038/ni.3796

Liu Q, Tong D, Liu G, et al. Metformin Inhibits Prostate Cancer Progression by Targeting Tumor-Associated Inflammatory Infiltration. *Clin Cancer Res*. 2018;24(22):5622-5634.

doi:10.1158/1078-0432.CCR-18-0420

Liu Y, Morgan JB, Coothankandaswamy V, et al. The Caulerpa pigment caulerpin inhibits HIF-1 activation and mitochondrial respiration. *J Nat Prod.* 2009;72(12):2104-2109. doi:10.1021/np9005794

Lue H, Thiele M, Franz J, et al. Macrophage migration inhibitory factor (MIF) promotes cell survival by activation of the Akt pathway and role for CSN5/JAB1 in the control of autocrine MIF activity. *Oncogene.* 2007;26(35):5046-5059. doi:10.1038/sj.onc.1210318

Lunt SY, Vander Heiden MG. Aerobic glycolysis: meeting the metabolic requirements of cell proliferation. *Annu Rev Cell Dev Biol.* 2011;27:441-464. doi:10.1146/annurev-cellbio-092910-154237

Ma EH, Bantug G, Griss T, et al. Serine Is an Essential Metabolite for Effector T Cell Expansion [published correction appears in *Cell Metab.* 2017 Feb 7;25(2):482]. *Cell Metab.* 2017;25(2):345-357. doi:10.1016/j.cmet.2016.12.011

Mantovani A, Sozzani S, Locati M, Allavena P, Sica A. Macrophage polarization: tumor-associated macrophages as a paradigm for polarized M2 mononuclear phagocytes. *Trends Immunol.* 2002;23(11):549-555. doi:10.1016/s1471-4906(02)02302-5

Marin SE, Mesterman R, Robinson B, Rodenburg RJ, Smeitink J, Tarnopolsky MA. Leigh syndrome associated with mitochondrial complex I deficiency due to novel mutations in *NDUFV1* and *NDUFS2*. *Gene.* 2013;516(1):162-167. doi:10.1016/j.gene.2012.12.024

Martinez FO, Sica A, Mantovani A, Locati M. Macrophage activation and polarization. *Front Biosci.* 2008;13:453-461. Published 2008 Jan 1. doi:10.2741/2692

Masgras I, Ciscato F, Brunati AM, et al. Absence of Neurofibromin Induces an Oncogenic Metabolic Switch via Mitochondrial ERK-Mediated Phosphorylation of the Chaperone TRAP1. *Cell Rep.* 2017;18(3):659-672. doi:10.1016/j.celrep.2016.12.056

Masoud GN, Li W. HIF-1 α pathway: role, regulation and intervention for cancer therapy. *Acta Pharm Sin B.* 2015;5(5):378-389. doi:10.1016/j.apsb.2015.05.007

McEwen ML, Sullivan PG, Rabchevsky AG, Springer JE. Targeting mitochondrial func-

tion for the treatment of acute spinal cord injury. *Neurotherapeutics*. 2011;8(2):168-179. doi:10.1007/s13311-011-0031-7

Mitchell RA, Liao H, Chesney J, et al. Macrophage migration inhibitory factor (MIF) sustains macrophage proinflammatory function by inhibiting p53: regulatory role in the innate immune response. *Proc Natl Acad Sci U S A*. 2002;99(1):345-350. doi:10.1073/pnas.012511599

Mu X, Shi W, Xu Y, et al. Tumor-derived lactate induces M2 macrophage polarization via the activation of the ERK/STAT3 signaling pathway in breast cancer. *Cell Cycle*. 2018;17(4):428-438. doi:10.1080/15384101.2018.1444305

Mullen AR, Wheaton WW, Jin ES, et al. Reductive carboxylation supports growth in tumour cells with defective mitochondria. *Nature*. 2011;481(7381):385-388. Published 2011 Nov 20. doi:10.1038/nature10642

Murdoch C, Muthana M, Coffelt SB, Lewis CE. The role of myeloid cells in the promotion of tumour angiogenesis. *Nat Rev Cancer*. 2008;8(8):618-631. doi:10.1038/nrc2444

Nilsson A, Haanstra JR, Engqvist M, et al. Quantitative analysis of amino acid metabolism in liver cancer links glutamate excretion to nucleotide synthesis. *Proc Natl Acad Sci U S A*. 2020;117(19):10294-10304. doi:10.1073/pnas.1919250117

Nomoto S, Yamashita K, Koshikawa K, Nakao A, Sidransky D. Mitochondrial D-loop mutations as clonal markers in multicentric hepatocellular carcinoma and plasma. *Clin Cancer Res*. 2002;8(2):481-487.

Noy R, Pollard JW. Tumor-associated macrophages: from mechanisms to therapy. *Immunity*. 2014 Nov 20;41(5):866]. *Immunity*. 2014;41(1):49-61. doi:10.1016/j.immuni.2014.06.010

Ochoa AC, Zea AH, Hernandez C, Rodriguez PC. Arginase, prostaglandins, and myeloid-derived suppressor cells in renal cell carcinoma. *Clin Cancer Res*. 2007;13(2 Pt 2):721s-726s. doi:10.1158/1078-0432.CCR-06-2197

Oda S, Oda T, Nishi K, et al. Macrophage migration inhibitory factor activates hypoxia-inducible factor in a p53-dependent manner. *PLoS One*. 2008;3(5):e2215. Published 2008 May 21. doi:10.1371/journal.pone.0002215

Ogino S, Nosho K, Meyerhardt JA, et al. Cohort study of fatty acid synthase expression and patient survival in colon cancer. *J Clin Oncol*. 2008;26(35):5713-5720. doi:10.1200/JCO.2008.18.2675

Orecchioni S, Reggiani F, Talarico G, et al. The biguanides metformin and phenformin inhibit angiogenesis, local and metastatic growth of breast cancer by targeting both neoplastic and microenvironment cells. *Int J Cancer*. 2015;136(6):E534-E544. doi:10.1002/ijc.29193

Orimo A, Weinberg RA. Stromal fibroblasts in cancer: a novel tumor-promoting cell type. *Cell Cycle*. 2006;5(15):1597-1601. doi:10.4161/cc.5.15.3112

Ovens MJ, Manoharan C, Wilson MC, Murray CM, Halestrap AP. The inhibition of monocarboxylate transporter 2 (MCT2) by AR-C155858 is modulated by the associated ancillary protein. *Biochem J*. 2010;431(2):217-225. doi:10.1042/BJ20100890

Parker WB. Enzymology of purine and pyrimidine antimetabolites used in the treatment of cancer. *Chem Rev*. 2009;109(7):2880-2893. doi:10.1021/cr900028p

Patricia Yee, Yiju Wei, Soo Yeon Kim, Tong Lu, Cynthia Lawson, Miaolu Tang, Zhijun Liu, Benjamin Anderson, Megan Young, Krishnamoorthy Thamburaj et al. TAMI-23. Neutrophil-Triggered Ferroptosis Promotes Tumor Necrosis In Glioblastoma Progression. *Neuro-Oncology*. 2020. Page ii218, <https://doi.org/10.1093/neuonc/noaa215.912>

Pereira FV, Melo ACL, Low JS, et al. Metformin exerts antitumor activity via induction of multiple death pathways in tumor cells and activation of a protective immune response. *Oncotarget*. 2018;9(40):25808-25825. Published 2018 May 25. doi:10.18632/oncotarget.25380

Petrova V, Annicchiarico-Petruzzelli M, Melino G, Amelio I. The hypoxic tumour microenvironment. *Oncogenesis*. 2018;7(1):10. Published 2018 Jan 24. doi:10.1038/s41389-017-0011-9

Porcelli AM, Ghelli A, Ceccarelli C, et al. The genetic and metabolic signature of oncocytic transformation implicates HIF1alpha destabilization. *Hum Mol Genet*. 2010;19(6):1019-1032. doi:10.1093/hmg/ddp566

Qian BZ, Li J, Zhang H, et al. CCL2 recruits inflammatory monocytes to facilitate breast-tumour metastasis. *Nature*. 2011;475(7355):222-225. Published 2011 Jun 8. doi:10.1038/nature10138

Quivoron, Cyril, et al. AG-221, an oral, selective, first-in-class, potent IDH2-R140Q mutant inhibitor, induces differentiation in a xenotransplant model. *Blood*. 2014; (3735-3735).

Riess C, Shokraie F, Classen CF, et al. Arginine-Depleting Enzymes - An Increasingly Recognized Treatment Strategy for Therapy-Refractory Malignancies. *Cell Physiol Biochem*. 2018;51(2):854-870. doi:10.1159/000495382

Rodenburg RJ. Mitochondrial complex I-linked disease. *Biochim Biophys Acta*. 2016;1857(7):938-945. doi:10.1016/j.bbabi.2016.02.012

Rohle D, Popovici-Muller J, Palaskas N, et al. An inhibitor of mutant IDH1 delays growth and promotes differentiation of glioma cells. *Science*. 2013;340(6132):626-630. doi:10.1126/science.1236062

Rolny C, Mazzone M, Tugues S, et al. HRG inhibits tumor growth and metastasis by inducing macrophage polarization and vessel normalization through downregulation of PlGF. *Cancer Cell*. 2011;19(1):31-44. doi:10.1016/j.ccr.2010.11.009

Romani L, Fallarino F, De Luca A, et al. Defective tryptophan catabolism underlies inflammation in mouse chronic granulomatous disease. *Nature*. 2008;451(7175):211-215. doi:10.1038/nature06471

Romero-Garcia S, Moreno-Altamirano MM, Prado-Garcia H, Sánchez-García FJ. Lactate Contribution to the Tumor Microenvironment: Mechanisms, Effects on Immune Cells and Therapeutic Relevance. *Front Immunol*. 2016;7:52. Published 2016 Feb 16. doi:10.3389/fimmu.2016.00052

Ruas JL, Poellinger L. Hypoxia-dependent activation of HIF into a transcriptional regulator. *Semin Cell Dev Biol*. 2005;16(4-5):514-522. doi:10.1016/j.semcdb.2005.04.001

Rubic T, Lametschwandtner G, Jost S, et al. Triggering the succinate receptor GPR91 on dendritic cells enhances immunity. *Nat Immunol*. 2008;9(11):1261-1269. doi:10.1038/ni.1657

Saha SK, Parachoniak CA, Ghanta KS, et al. Mutant IDH inhibits HNF-4 α to block hepatocyte differentiation and promote biliary cancer [published correction appears in *Nature*. 2015 Dec 3;528(7580):152]. *Nature*. 2014;513(7516):110-114. doi:10.1038/nature13441

Sangaletti S, Di Carlo E, Gariboldi S, et al. Macrophage-derived SPARC bridges tumor cell-extracellular matrix interactions toward metastasis. *Cancer Res.* 2008;68(21):9050-9059. doi:10.1158/0008-5472.CAN-08-1327

Sazanov LA. The mechanism of coupling between electron transfer and proton translocation in respiratory complex I. *J Bioenerg Biomembr.* 2014;46(4):247-253. doi:10.1007/s10863-014-9554-z

Schwab LP, Peacock DL, Majumdar D, et al. Hypoxia-inducible factor 1 α promotes primary tumor growth and tumor-initiating cell activity in breast cancer. *Breast Cancer Res.* 2012;14(1):R6. Published 2012 Jan 7. doi:10.1186/bcr3087

Selak MA, Armour SM, MacKenzie ED, et al. Succinate links TCA cycle dysfunction to oncogenesis by inhibiting HIF-alpha prolyl hydroxylase. *Cancer Cell.* 2005;7(1):77-85. doi:10.1016/j.ccr.2004.11.022

Semenza GL. HIF-1 mediates metabolic responses to intratumoral hypoxia and oncogenic mutations. *J Clin Invest.* 2013;123(9):3664-3671. doi:10.1172/JCI67230

Semerad CL, Liu F, Gregory AD, Stumpf K, Link DC. G-CSF is an essential regulator of neutrophil trafficking from the bone marrow to the blood. *Immunity.* 2002;17(4):413-423. doi:10.1016/s1074-7613(02)00424-7

Shackelford DB, Shaw RJ. The LKB1-AMPK pathway: metabolism and growth control in tumour suppression. *Nat Rev Cancer.* 2009;9(8):563-575. doi:10.1038/nrc2676

Shanshiashvili L, Tsitsilashvili E, Dabrundashvili N, Kalandadze I, Mikeladze D. Metabotropic glutamate receptor 5 may be involved in macrophage plasticity [published correction appears in *Biol Res.* 2017 Mar 27;50(1):13]. *Biol Res.* 2017;50(1):4. Published 2017 Feb 14. doi:10.1186/s40659-017-0110-2

Sharma MD, Hou DY, Liu Y, et al. Indoleamine 2,3-dioxygenase controls conversion of Foxp3+ Tregs to TH17-like cells in tumor-draining lymph nodes. *Blood.* 2009;113(24):6102-6111. doi:10.1182/blood-2008-12-195354

Shaw RJ, Cantley LC. Ras, PI(3)K and mTOR signalling controls tumour cell growth. *Nature*. 2006;441(7092):424-430. doi:10.1038/nature04869

Shay JE, Imtiyaz HZ, Sivanand S, et al. Inhibition of hypoxia-inducible factors limits tumor progression in a mouse model of colorectal cancer. *Carcinogenesis*. 2014;35(5):1067-1077. doi:10.1093/carcin/bgu004

Silva LS, Poschet G, Nonnenmacher Y, et al. Branched-chain ketoacids secreted by glioblastoma cells via MCT1 modulate macrophage phenotype. *EMBO Rep*. 2017;18(12):2172-2185. doi:10.15252/embr.201744154

Smolková K, Bellance N, Scandurra F, et al. Mitochondrial bioenergetic adaptations of breast cancer cells to aglycemia and hypoxia. *J Bioenerg Biomembr*. 2010;42(1):55-67. doi:10.1007/s10863-009-9267-x

Sousa CM, Biancur DE, Wang X, et al. Pancreatic stellate cells support tumour metabolism through autophagic alanine secretion [published correction appears in *Nature*. 2016 Dec 1;540(7631):150]. *Nature*. 2016;536(7617):479-483. doi:10.1038/nature19084

Storz P. Reactive oxygen species in tumor progression. *Front Biosci*. 2005;10:1881-1896. Published 2005 May 1. doi:10.2741/1667

Su CY, Chang YC, Yang CJ, Huang MS, Hsiao M. The opposite prognostic effect of NDUFS1 and NDUFS8 in lung cancer reflects the oncojanus role of mitochondrial complex I. *Sci Rep*. 2016;6:31357. Published 2016 Aug 12. doi:10.1038/srep31357

Sullivan LB, Gui DY, Hosios AM, Bush LN, Freinkman E, Vander Heiden MG. Supporting Aspartate Biosynthesis Is an Essential Function of Respiration in Proliferating Cells. *Cell*. 2015;162(3):552-563. doi:10.1016/j.cell.2015.07.017

Supuran CT. Carbonic Anhydrase Inhibition and the Management of Hypoxic Tumors. *Metabolites*. 2017;7(3):48. Published 2017 Sep 16. doi:10.3390/metabo7030048

Takano T, Lin J.H. C, Arcuino G, Gao Q, Yang J, Nedergaard, M. Glutamate release promotes growth of malignant gliomas. *Nat. Med*. 2001; 7, 1010–1015.

Tal R, Shaish A, Bangio L, Peled M, Breitbart E, Harats D. Activation of C-transactivation domain is essential for optimal HIF-1 alpha-mediated transcriptional and angiogenic effects. *Microvasc Res.* 2008;76(1):1-6. doi:10.1016/j.mvr.2008.03.002

Taylor RW, Turnbull DM. Mitochondrial DNA mutations in human disease. *Nat Rev Genet.* 2005;6(5):389-402. doi:10.1038/nrg1606

Tennant DA, Frezza C, MacKenzie ED, et al. Reactivating HIF prolyl hydroxylases under hypoxia results in metabolic catastrophe and cell death. *Oncogene.* 2009;28(45):4009-4021. doi:10.1038/onc.2009.250

Uehara T, Eikawa S, Nishida M, et al. Metformin induces CD11b⁺-cell-mediated growth inhibition of an osteosarcoma: implications for metabolic reprogramming of myeloid cells and anti-tumor effects. *Int Immunol.* 2019;31(4):187-198. doi:10.1093/intimm/dxy079

Vander Heiden MG, Cantley LC, Thompson CB. Understanding the Warburg effect: the metabolic requirements of cell proliferation. *Science.* 2009;324(5930):1029-1033. doi:10.1126/science.1160809

Vasamsetti SB, Karnewar S, Kanugula AK, Thatipalli AR, Kumar JM, Kotamraju S. Metformin inhibits monocyte-to-macrophage differentiation via AMPK-mediated inhibition of STAT3 activation: potential role in atherosclerosis. *Diabetes.* 2015;64(6):2028-2041

Vatrinet R, Iommarini L, Kurelac I, De Luise M, Gasparre G, Porcelli AM. Targeting respiratory complex I to prevent the Warburg effect. *Int J Biochem Cell Biol.* 2015;63:41-45. doi:10.1016/j.biocel.2015.01.017

Végran F, Boidot R, Michiels C, Sonveaux P, Feron O. Lactate influx through the endothelial cell monocarboxylate transporter MCT1 supports an NF- κ B/IL-8 pathway that drives tumor angiogenesis. *Cancer Res.* 2011;71(7):2550-2560. doi:10.1158/0008-5472.CAN-10-2828

Vettore L, Westbrook RL, Tennant DA. New aspects of amino acid metabolism in cancer. *Br J Cancer.* 2020;122(2):150-156. doi:10.1038/s41416-019-0620-5

Villani LA, Smith BK, Marcinko K, et al. The diabetes medication Canagliflozin reduces cancer cell proliferation by inhibiting mitochondrial complex-I supported respiration. *Mol*

Metab. 2016;5(10):1048-1056. Published 2016 Aug 26. doi:10.1016/j.molmet.2016.08.014

Vitale I, Manic G, Coussens LM, Kroemer G, Galluzzi L. Macrophages and Metabolism in the Tumor Microenvironment. *Cell Metab.* 2019;30(1):36-50. doi:10.1016/j.cmet.2019.06.001

Vogelstein B, Lane D, Levine AJ. Surfing the p53 network. *Nature.* 2000;408(6810):307-310. doi:10.1038/35042675

Wagner AD, Buechner-Stuedel P, Wein A, et al. Gemcitabine, oxaliplatin and weekly high-dose 5-FU as 24-h infusion in chemo-naïve patients with advanced or metastatic pancreatic adenocarcinoma: a multicenter phase II trial of the Arbeitsgemeinschaft Internistische Onkologie (AIO). *Ann Oncol.* 2007;18(1):82-87. doi:10.1093/annonc/mdl340

Wang J, Li G, Wang Y, et al. Suppression of tumor angiogenesis by metformin treatment via a mechanism linked to targeting of HER2/HIF-1 α /VEGF secretion axis. *Oncotarget.* 2015;6(42):44579-44592. doi:10.18632/oncotarget.6373

Wang JC, Sun X, Ma Q, et al. Metformin's antitumor and anti-angiogenic activities are mediated by skewing macrophage polarization [published online ahead of print, 2018 May 4]. *J Cell Mol Med.* 2018;22(8):3825-3836. doi:10.1111/jcmm.13655

Wang N, Liu W, Zheng Y, et al. CXCL1 derived from tumor-associated macrophages promotes breast cancer metastasis via activating NF- κ B/SOX4 signaling. *Cell Death Dis.* 2018;9(9):880. Published 2018 Aug 29. doi:10.1038/s41419-018-0876-3

Warburg O. On the origin of cancer cells. *Science.* 1956;123(3191):309-314. doi:10.1126/science.123.3191.309

Ward PS, Thompson CB. Metabolic reprogramming: a cancer hallmark even Warburg did not anticipate. *Cancer Cell.* 2012;21(3):297-308. doi:10.1016/j.ccr.2012.02.014

Weidemann A, Johnson RS. Biology of HIF-1 α . *Cell Death Differ.* 2008;15(4):621-627. doi:10.1038/cdd.2008.12

Wheaton WW, Weinberg SE, Hamanaka RB, et al. Metformin inhibits mitochondrial complex I of cancer cells to reduce tumorigenesis. *Elife.* 2014;3:e02242. Published 2014 May 13.

doi:10.7554/eLife.02242

Wittig I, Carozzo R, Santorelli FM, Schägger H. Supercomplexes and subcomplexes of mitochondrial oxidative phosphorylation. *Biochim Biophys Acta*. 2006;1757(9-10):1066-1072. doi:10.1016/j.bbabi.2006.05.006

Wu J, Ke X, Wang W, et al. Aloe-emodin suppresses hypoxia-induced retinal angiogenesis via inhibition of HIF-1 α /VEGF pathway. *Int J Biol Sci*. 2016;12(11):1363-1371. Published 2016 Oct 25. doi:10.7150/ijbs.16334

Wu JY, Huang TW, Hsieh YT, et al. Cancer-Derived Succinate Promotes Macrophage Polarization and Cancer Metastasis via Succinate Receptor. *Mol Cell*. 2020;77(2):213-227.e5. doi:10.1016/j.molcel.2019.10.023

Xiao M, Yang H, Xu W, et al. Inhibition of α -KG-dependent histone and DNA demethylases by fumarate and succinate that are accumulated in mutations of FH and SDH tumor suppressors [published correction appears in *Genes Dev*. 2015 Apr 15;29(8):887]. *Genes Dev*. 2012;26(12):1326-1338. doi:10.1101/gad.191056.112

Xu W, Yang H, Liu Y, et al. Oncometabolite 2-hydroxyglutarate is a competitive inhibitor of α -ketoglutarate-dependent dioxygenases. *Cancer Cell*. 2011;19(1):17-30. doi:10.1016/j.ccr.2010.12.014

Xu Z, Han X, Ou D, et al. Targeting PI3K/AKT/mTOR-mediated autophagy for tumor therapy. *Appl Microbiol Biotechnol*. 2020;104(2):575-587. doi:10.1007/s00253-019-10257-8

Yang L, Venneti S, Nagrath D. Glutaminolysis: A Hallmark of Cancer Metabolism. *Annu Rev Biomed Eng*. 2017;19:163-194. doi:10.1146/annurev-bioeng-071516-044546

Yen K, Travins J, Wang F, et al. AG-221, a First-in-Class Therapy Targeting Acute Myeloid Leukemia Harboring Oncogenic IDH2 Mutations. *Cancer Discov*. 2017;7(5):478-493. doi:10.1158/2159-8290.CD-16-1034

Yu Y, Lv F, Lin H, et al. Mitochondrial ND3 G10398A mutation: a biomarker for breast cancer. *Genet Mol Res*. 2015;14(4):17426-17431. Published 2015 Dec 21. doi:10.4238/2015.December.21.12

Yuan JS, Reed A, Chen F, Stewart CN Jr. Statistical analysis of real-time PCR data. *BMC*

Bioinformatics. 2006;7:85. Published 2006 Feb 22. doi:10.1186/1471-2105-7-85

Zasłona Z, O'Neill LAJ. Cytokine-like Roles for Metabolites in Immunity. *Mol Cell*. 2020;78(5):814-823. doi:10.1016/j.molcel.2020.04.002

Zhu C, Kros JM, Cheng C, Mustafa D. The contribution of tumor-associated macrophages in glioma neo-angiogenesis and implications for anti-angiogenic strategies. *Neuro Oncol*. 2017;19(11):1435-1446. doi:10.1093/neuonc/nox081

